JAERI-M
84-036

EVALUATION OF CCTF CORE-II SECOND ACCEPTANCE TEST C2-AC2 (RUN 052)

—INVESTIGATION OF DIFFERENCE IN REFLOODING BEHAVIORS BETWEEN CORE-I AND CORE-II FACILITIES—

March 1984

Tsutomu OKUBO and Yoshio MURAO

日本原子力研究所
Japan Atomic Energy Research Institute

JAERI-Mレポートは，日本原子力研究所が不定期に公刊している研究報告書です。
入手の問合わせは，日本原子力研究所技術情報部情報資料課（〒319-11茨城県那珂郡東海村）あて，お申しこしください。なお，このほかに財団法人原子力弘済会資料センター（〒319-11 茨城県那珂郡東海村日本原子力研究所内）で複写による実費頒布をおこなっております。

JAERI-M reports are issued irregularly.
Inquiries about availability of the reports should be addressed to Information Section, Division of Technical Information, Japan Atomic Energy Research Institute, Tokai-mura, Naka-gun, Ibaraki-ken 319-11, Japan.

編集兼発行　日本原子力研究所
印　　刷　いばらき印刷㈱

JAERI-M 84-036

Evaluation of CCTF Core-II Second Acceptance Test C2-AC2 (Run 052)

—— Investigation of difference in reflooding behaviors between Core-I and Core-II Facilities ——

Tsutomu OKUBO and Yoshio MURAO

Department of Nuclear Safety Research,
Tokai Research Establishment, JAERI

(Received January 31, 1984)

In order to investigate the thermo-hydrodynamic behavior in a PWR during the reflood phase of the LOCA, large scale reflooding tests have been conducted at JAERI using the CCTF Core-I and Core-II facilities. This report presents the investigation on the difference in the thermo-hydrodynamic behavior observed between in the CCTF Core-I and Core-II facilities. For this purpose the test data of the second CCTF Core-II acceptance test C2-AC2 (Run 052) were evaluated by using the data of the Test C1-21 (Run 040) in the Core-I test series. The experimental conditions for these two tests were almost identical.

Comparing the data of those two tests, the following is obtained.

1. The system behavior observed in the Core-II facility was nearly identical to that observed in the Core-I facility.
2. The core behavior observed in the Core-II facility was also nearly identical to that observed in the Core-I facility except for the top quenching behavior.
3. The differences in the top quenching behavior between the two facilities were as follows:

(1) The selective occurrence of top quenching below the open holes of the upper core support plate observed in the Core-I facility

---

The work was performed under contract with the Atomic Energy Bureau of Science and Technology Agency of Japan.

was not observed in the Core-II facility.

(2) Top quenching tended to occur less in the Core-II facility in the region where the initial average linear power density was over 1.69 kW/m.

Keywords: Reactor Safety, PWR, LOCA, Reflood, ECCS, Quenching, CCTF, Thermo-hydrodynamic Behavior

円筒第２次炉心試験・第２回検収試験Ｃ２－ＡＣ２（Run 052）の評価
－第１次および第２次炉心試験装置における再冠水挙動の差の検討－

日本原子力研究所東海研究所安全工学部
大久保　努・村尾　良夫

（1984 年 1 月 31 日受理）

ＰＷＲのＬＯＣＡ時再冠水過程に於ける熱水力挙動を検討するため，円筒第１次および第２次炉心試験装置を用いた大型再冠水試験が原研で行れている。

本報告書では，円筒第１次炉心試験装置と第２次炉心試験装置に於いて観測される熱水力挙動の差を検討した。このため，円筒第２次炉心試験の第２回検収試験Ｃ２－ＡＣ２（Run 052）のデータを，円筒第１次炉心の試験Ｃ１－21（Run 040）のデータを用いて評価した。両試験の実験条件は，ほぼ同一であった。

これら２つの試験のデータを比較して，以下の知見が得られた。

1. 第２次炉心装置でのシステム挙動は，第１次炉心装置でのものとほぼ同様なものであった。
2. 第２次炉心装置での炉心挙動は，トップクエンチ挙動を除けば，第１次炉心装置でのものとほぼ同様なものであった。
3. 両装置でのトップクエンチ挙動の相違は，以下のとおりである。
   (1) 第１次炉心試験で観測された上部炉心板の開孔の下で選択的に起こるトップクエンチは，第２次炉心試験では観測されなかった。
   (2) 第２次炉心試験では，初期平均線出力密度が 1.69 kW／m より大きな領域で，トップクエンチの発生が少ない傾向が見られた。

本報告書は，電源開発促進対策特別会計法に基づき，科学技術庁からの受託によって行った研究の成果である。

Contents

目　　次

Table list

Figure list

1. Introduction

A reflood test program[1] using large scale test facilities has been conducted at the Japan Atomic Energy Research Institute (JAERI). The facilities are the Cylindrical Core Test Facility (CCTF) and the Slab Core Test Facility (SCTF). This report presents the evaluation for the second CCTF Core-II acceptance test C2-AC2 (Run 052).

The CCTF in an experimental facility designed to model a full-height core section, four primary loops and their components of a pressurized water reactor (PWR). This facility is used to provide information on fluid behaviors in the core, downcomer and upper plenum including steam and water carryover phenomena and integral system effects during the refill and reflood phases of a hypothetical loss-of-coolant accident (LOCA) of a PWR.

The objectives of the test program using the CCTF are:

a. Demonstration of capability of emergency core cooling system (ECCS) during refill and reflood periods.
b. Verification of reflood analysis codes.
c. Collection of information to improve the thermo-hydrodynamic models in the analysis codes, such as, (a) multi-dimensional core thermo-hydrodynamics including the radial power distribution effect, fallback effect and spatial oscillatory behavior, (b) flow behavior in the upper plenum and hot legs, (c) behavior of accumulated water at the bottom of the upper plenum including possible counter-current flow and sputtering effect, (d) hydrodynamic behavior of the injected ECC water and the water passing through the steam generator, (e) multi-dimensional thermo-hydrodynamic behavior in the hot annular downcomer, and (f) overall oscillatory behavior in the system.

As the first series of the CCTF tests, twenty-seven CCTF Core-I tests were conducted. This series of tests presented a lot of information[2] on the system thermo-hydrodynamic behavior as well as the core behavior during the refill and reflood phases of a LOCA in a PWR. The CCTF Core-I test series was initiated in March 1979 and terminated in April 1981. Subsequently, as the second series of the CCTF tests, the CCTF Core-II test series was initiated in March 1982. The special purposes of the CCTF Core-II test program are to investigate the effects

of alternative ECCS such as the combined and the downcomer injections as well as to extend the experimental range of the Core-I test series.

Prior to the initiation of the Core-II tests, two acceptance tests were conducted to ensure the performance of the facility. The second acceptance test C2-AC2 (Run 052) was conducted on January 27, 1982. The purpose of the present test was to investigate the differences in the thermo-hydrodynamic behavior between the Core-I and the Core-II facilities. Therefore, the test conditions were set so as to reproduce the Test C1-21 (Run 40)[3] in the Core-I test series. This test was a coupling test with the FLECHT-SET (Full Length Emergency Cooling Heat Transfer - System Effects Test) RUN2714B experiment, and the ECCS water was injected into the lower plenum.

In this report, the comparisons of the data between the present test and the Test C1-21 are presented and discussed. Some selected data of the present test are presented in Appendix B for better understanding of the test. The comparisons of the data between the FLECHT-SET experiment and the corresponding CCTF FLECHT coupling test are presented in reference 3 and are not brought up for discussion in this report.

2. Test Description

2.1 Test Facility

The CCTF Core-II was designed in consideration of the following objectives and criteria:

a. Design objectives

(1) The facility should provide the capability to reasonably simulate the flow conditions in the primary system of a PWR during the refill and reflood phases of a LOCA.

(2) The downcomer design should provide ECC water flow behavior throughout the test which is reasonably representative of that of the PWR downcomer.

b. Design criteria

(1) The reference reactors are the Trojan reactor in the USA and in certain aspects the Ohi reactor in Japan.

(2) The vertical dimensions and locations of system components are kept as close to those of the reference reactors as possible.

(3) The flow areas of the system components are scaled down in proportion to the scaling factor of core flow area.

(4) The facility is equipped with four loops which are composed of three intact loops and one broken loop.

(5) A 200% cold leg large break is simulated in the broken loop.

(6) The ECCS consists of an accumulator system (Acc) and low pressure coolant injection system (LPCI), and the injection locations are the upper plenum and the downcomer as well as the lower plenum and the cold legs.

(7) The maximum allowable pressure of the facility is 588 kPa (6 kg/cm^2 absolute).

(8) The maximum allowable temperature of the simulated fuel rods is 1173 K (900°C).

(9) The maximum allowable temperature of the components in the primary system except the simulated fuel rod assembly is 623 K (350°C)

(10) The reactor vessel contains approximately 2,000 electrically heated rods simulating the fuel rods.

(11) The design of upper plenum internals is based on that of a new 17×17 type fuel assembly.

(12) The flow resistance of each loop is adjusted by an orifice in the pump simulator.

(13) The containment system consists of two tanks.

A bird's-eye view and a schematic diagram of the CCTF are shown in Figs. 2.1 and 2.2, respectively. The scaled dimensions of the components are given in Table 2.1.

The differences in the design of the Core-II facility from the Core-I are:

(1) Axial peaking factor of heater rods

(2) Local peaking factor of heater rods in a bundle

(3) Upper plenum structures (upper plenum internals, plugging devices in end box region and a upper ring)

(4) Vent valves

(5) Alternative ECCS (downcomer injection and upper plenum injection)

(6) Instruments

2.1.1 Pressure Vessel and Internals

The pressure vessel is of a cylindrical type as shown in Fig. 2.3. The height is the same as the reference reactor pressure vessel. The dimension of the radial direction is scaled down in proportion to the core flow area scaling, that is, 1/21.44. The upper ring was newly installed for the installation of the upper plenum ECC water injection lines and the instruments. Four vent valves and two downcomer ECC water injection nozzles, which are called Core Flooding Nozzle (CFN), are also newly equipped in the Core-II facility as shown in Figs. 2.3 and 2.4. Vent valves and CFNs are for the simulation of a Babcock & Wilcox (B&W) type PWR. Downcomer injection nozzles also exist in a couple of recent Japanese PWRs.

The cross section of the pressure vessel is shown in Fig. 2.4 and the dimensions are given in Fig. 2.5. The core consists of thirty-two 8×8 electrically heated rod bundles arranged in a cylindrical configuration and simulates a Westinghouse 15×15 type fuel assemblies.

The downcomer is an annulus of 61.5 mm gap. In determining the gap size, the flow area of the core baffle region was added to that of the downcomer region. Thus, the core baffle flow area is included in the downcomer simulation and is not simulated separately in the vessel inserting stainless steel fillers to prevent fluid flow.

The vessel wall is constructed of carbon steel which is cladded with stainless steel plate. The wall is 90 mm thick to simulate the stored energy as reasonably as possible during ECC water injection.

The design of upper plenum internals is based on that of the new Westinghouse 17 × 17 type fuel assemblies instead of the old type simulated in the Core-I facility. The internals consists of ten control rod guide tubes, ten support columns and twelve open holes as shown in Fig. 2.6. The radius of each internals is scaled down by factor 8/15 from that of an actual reactor. They are illustrated in Fig. 2.7. Flow resistance baffles are inserted into the control rod guide tubes. The baffles consist of two kinds of baffle plates and a shaft. The baffle plates are shown in Fig. 2.8.

End boxes are attached beneath the UCSP. The structure for one heater rod bundle is shown in Fig. 2.9. Plugging devices are installed newly in the Core-II facility as shown in Figs. 2.9 and 2.10 to simulate the flow resistance more correctly.

2.1.2 Heater Rod Assembly

The heater rod assembly simulating the fuel assembly consists of thirty-two 8 × 8 array rod bundle. Each bundle consists of fifty-seven electrically heated rods and seven non-heated rods as shown in Fig. 2.11. The core is usually subdivided into three regions to achieve a desired radial power distribution. This is shown in Fig. 2.4. The high, medium and low power regions are named A, B and C regions, respectively. The local peaking factor of heated rods in a bundle is unity, that is, all heated rods in a bundle have the same power density in the Core-II facility.

A heater rod consists of a nichrome heating element, magnesium oxide (MgO) and boron nitride (BN) insulators, and Inconel-600 sheath. BN is used for only central part of the heated region and MgO for the other part as shown in Fig. 2.12. The heated length and the outer diameter of the heater rods are 3.66 m and 10.7 mm, respectively, which are identical to the corresponding dimensions of actual PWR fuel rods. The sheath wall thickness is 1.0 mm and is thicker than the actual fuel cladding, because of the requirements for thermocouple installation. The heating element is a helical coil with a verying pitch to generate a 17 steps chopped consine axial power profile as shown in Fig. 2.13.

The peaking factor is 1.40, instead of 1.492 for a Core-I rod.

Non-heated rods are either stainless steel pipes or solid bars of 13.8 mm O.D. The pipes are utilized for installation of instruments such as superheated steam probes and thermocouples. The bars are used for supporting the assembly loads.

The heater rods and non-heated rods are held in radial position by grid spacers which are located at six elevations along the axial length as shown in Fig. 2.13. A grid spacer is a lattice structure composed of stainless steel plates of 0.4 mm and 0.8 mm thick and 40 mm high. The rod pitch is 14.3 mm which is the same as that of the reference PWR.

The heater rods penetrate through the bottom plate of the vessel to facilitate lead out of the power cables from the bottom of the vessel. The outer diameter of the rods in the lower plenum is reduced to 8.6 mm. Three phase electric current is used for heating the heater rods and the electrical neutral point is at the top of the rods where they are interconnected to each other.

2.1.3 Primary Loops and ECCS

Primary loops consist of three intact loops and a broken loop. Each loop consists of hot leg and cold leg pipings, a steam generator simulator and a pump simulator. The 200% cold leg large break is simulated in the broken loop. The broken cold leg is connected to two containment tanks through blowdown valves. The primary loop arrangement is shown in Figs. 2.14 and 2.15.

The inner diameter of the piping is scaled down in proportion to the core flow area scaling. The length of each piping section is almost the same as the corresponding section of the reference PWR.

The steam generator simulators are of the U-tube and shell type as shown in Fig. 2.16. The tube length is about 5 m shorter than in the reference PWR. The vertical height of the steam generator simulators is also about 5 m lower than in the reference PWR. The primary coolant passes through the tube side and the secondary coolant is stagnant in the shell side. The steam generator simulators of two loops are housed in a single shell assembly which has two compartment, one simulator for each loop in one compartment. The wall thickness of the U-tube is 2.9 mm compared to 1.27 mm of the reference PWR, because of a higher pressure difference between the primary and secondary sides in the simulator.

The pump simulator consists of the casing and duct simulators and an orifice plate as shown in Fig. 2.17. The loop flow resistance is simulated with the orifice plate. Each orifice plate has a hole with diameter and thickness of 95 mm and 10 mm, respectively.

ECCS consists of an Acc and a LPCI. The injection points are at each cold leg and at the lower plenum. The upper plenum and downcomer injection system was not constructed at that time. The system became available at the time Test C2-AA1 was conducted.

2.1.4 Instrumentation

The instrumentation is divided into two groups. One of them is JAERI-supplied instruments measuring the temperatures, absolute pressures, differential pressures, water levels and flow rates. Thermocouples measure the temperatures of the rod surface, fluid and structure. The absolute pressures are measured in the upper and lower plena, steam generator plena and containment tanks. The differential pressure measurements are carried out at many locations covering almost the whole system. In the ECC water supply tanks and the containment tank 1, the liquid levels are measured. The flow meters measure the ECC water flow rates. Furthermore, flow rates in the downcomer, loop seal pipings and the vent line from the containment tank 2 to the atomosphere are measured with drag disk flow meters, pitot tubes and a ventulli tube, respectively. The total number of the JAERI-supplied instruments is 1317 channels and the signals from these instruments are recorded on a magnetic tape.

The other group of the instrumentation is the USNRC-supplied instruments. They are the advanced instrumentation for the two-phase flow measurement. The kinds and quantities of those are tabulated in Table 2.2. The total number is 540 channels.

2.2 Test Conditions and Procedures

2.2.1 Test Conditions

The summary of the test conditions are presented in Table 2.3. The test conditions were set as closely as possible to those of the Test C1-21. The containment tank pressure was set at 0.15 MPa and the ECC water was injected only into the lower plenum. Since the core differs in the axial and local peaking factors between the Core-I and

Core-II facilities, all the conditions for the core could not be set to be identical between the two tests. In the present test, the peak linear power density was set to be identical. The average linear power density was a little lower in the present test because of the limitation of the total power, *i.e.* the maximum available linear power density is 1.438 kW/m for the Core-II facility. The radial power distribution was steeper in the present test also due to the limitation of the power in the low power region.

2.2.2 Test Procedures

In preparation for the test, the accumulator tank, the LPCI tank, the saturated water tank and the secondary sides of the steam generator simulators were filled with water which was purified with ion exchange resin. After all the components and instruments were inspected for mechanical and electrical leakages, the instruments were checked for zero points and sensitivity.

After these preparatory operation, the primary system was heated with the preheaters to its specified temperature (384 K) and pressurized to a specified pressure (150 kPa) by substituting steam for nitrogen gas in the system. The water in the accumulator tank was electrically heated to its specified temperature (340 K) and pressurized with nitrogen gas to provide sufficient head to drive the injection flow required. The water in the LPCI tank was also heated to its specified temperature (341 K) and was circulated through the circulation line including the LPCI line so as to preheat the line to the same temperature as the water. The water in the saturated water tank was heated up to near saturation temperature (384 K) of the expected primary system pressure (150 kPa). The water in the secondary side of each steam generator simulator was also heated and pressurized to the specified temperature (538 K) and pressure (5.1 MPa).

After establishing the initial conditions of the test, electric power for preheating was turned off and the lower plenum was filled with water from the saturated water tank to a specified level (0.9 m). When the water level in the lower plenum reached the specified level and other initial conditions of the test were stabilized at the allowable tolerance, electric power was applied to the heater rods in the core and the data recording was started. The temperature rise of the rods

were monitored by using a computer. When a specified initial clad temperature (775 K) was reached, Acc injection (0.11 m^3/s) into the lower plenum was initiated. The system pressure was maintained at the specified initial pressure (150 kPa) throughout the test by controlling the outlet valve of containment tank 2. Decay of power input to the rods was programed to begin when the water reached bottom of the heated region of the core. The specified initial clad temperature (775 K) of the heater rods for initiation of coolant injection was predetermined by interpolation between the clad temperature (381 K) after preheating and the clad temperature (866 K) assumed for the time of bottom of core recovery (BOCREC). The specified power decay was obtained by normalizing the decay curve of the ANS standard $\times 1.2 + {}^{238}U$ capture decay $\times 1.1$ at 30 seconds after shutdown.

At a specified time (16 s) after the initiation of Acc injection, the valves in Acc injection line and LPCI circulation line were closed and the valve in LPCI injection line was opened. These actions transferred ECC injection from Acc mode to LPCI mode. A specified LPCI flow rate (11.1×10^{-3} m^3/s) was maintained constantly until the ECC injection was turned off.

The generated steam and the entrained water flowed via broken and intact loops to the containment tanks. The steam was then vented to the atmosphere to maintain the pressure in the containment tanks constant.

When all thermocouples on the surface of heater rods indicated quenching of the rods, the power supply to heater rods and the ECC water injection were turned off terminating the test.

Table 2.1 CCTF component scaled dimensions

COMPONENT		PWR	JAERI	RATIO
PRESSURE VESSEL				
VESSEL INSIDE DIAMETER	(mm)	4394 (173")	1084	
VESSEL THICKNESS	(mm)	216 (8 1/2")	90	
CORE BARREL OUTSIDE DIAMETER	(mm)	3974	961	
CORE BARREL INSIDE DIAMETER	(mm)	3760	929	
THERMAL SHIELD OUTSIDE DIAMETER	(mm)	4170		
THERMAL SHIELD INSIDE DIAMETER	(mm)	4030		
DOWNCOMER LENGTH	(mm)	4849	4849	1/1
DOWNCOMER GAP	(mm)	114.3	61.5	
DOWNCOMER(+ BUFFLE) FLOW AREA	(m^2)	4.23	0.197	1/21.44
LOWER PLENUM VOLUME	(m^3)	29.6	1.38	1/21.44
UPPER PLENUM VOLUME	(m^3)	43.6	2.04	1/21.44
FUEL (HEATER ROD) ASSEMBLY				
NUMBER OF BUNDLES	(—)	193	32	
ROD ARRAY	(—)	15 × 15	8 × 8	
ROD HEATED LENGTH	(mm)	3660	3660	1/1
ROD PITCH	(mm)	14.3	14.3	1/1
FUEL ROD OUTSIDE DIAMETER	(mm)	10.72	10.7	1/1
THIMBLE TUBE DLAMETER	(mm)	13.87	13.8	1/1
INSTRUMENT TUBE DIAMETER	(mm)	13.87	13.8	1/1
NUMBER OF HEATER RODS	(—)	39372	1824	1/21.58
NUMBER OF NON-HEATED RODS	(—)	4053	224	1/18.09
CORE FLOW AREA	(m^2)	5.29	0.25	1/21.2
CORE FLUID VOLUME	(m^3)	17.95	0.915	1/19.6
PRIMARY LOOP				
HOT LEG INSIDE DIAMETER	(mm)	736.6 (29")	155.2	1/4.75
HOT LEG FLOW AREA	(m^2)	0.426	0.019	1/22.54
HOT LEG LENGTH	(mm)	3940	3940	1/1
PUMP SUCTION INSIDE DIAMETER	(mm)	787.4 (31")	155.2	1/5.07
PUMP SUCTION FLOW AREA	(m^2)	0.487	0.019	1/25.77
PUMP SUCTION LENGTH	(mm)	7950	7950	1/1

Table 2.1 (Cont'd)

COMPONENT		PWR	JAERI	RATIO
COLD LEG INSIDE DIAMETER	(mm)	698.5 (27.5")	155.2	1/4.50
COLD LEG FLOW AREA	(m^2)	0.383	0.019	1/20.26
COLD LEG LENGTH	(mm)	5600	5600	1/1
STEAM GENERATOR SIMULATOR				
NUMBER OF TUBES	(—)	3388	158	1/21.44
TUBE LENGTH (AVERAGE)	(m)	20.5	15.2	1/1.35
TUBE OUTSIDE DIAMETER	(mm)	22.225 (0.875")	25.4	
TUBE INSIDE DIAMETER	(mm)	19.7 (0.05")	19.6	1/1
TUBE WALL THICKNESS	(mm)	1.27	2.9	
HEAT TRANSFER AREA	(m^2)	4784 (51500 ft^2)	192	1/24.92
TUBE FLOW AREA	(m^2)	1.03	0.048	1/21.44
INLET PLENUM VOLUME	(m^3)	4.25	0.198	1/21.44
OUTLET PLENUM VOLUME	(m^3)	4.25	0.198	1/21.44
PRIMARY SIDE VOLUME	(m^3)	30.50 (1077 ft^3)	1.2	1/25.41
SECONDARY SIDE VOLUME	(m^3)	157.33 (5556 ft^3)	2.5	1/62.93
CONTAINMENT TANK - I	(m^3)		30	
CONTAINMENT TANK - II	(m^3)		50	
STORAGE TANK	(m^3)		25	
ACC. TANK	(m^3)		5	
SATURATED WATER TANK	(m^3)		3.5	
ELEVATION				
BOTTOM OF HEATED REGION IN CORE	(mm)	0	0	
TOP OF HEATED REGION IN CORE	(mm)	3660	3660	0
TOP OF DOWNCOMER	(mm)	4849	4849	0
BOTTOM OF DOWNCOMER	(mm)	0	0	0
CENTERLINE OF COLD LEG	(mm)	5198	4927	- 271
BOTTOM OF COLD LEG (INSIDE)	(mm)	4849	4849	0
CENTERLINE OF LOOP SEAL LOWER END	(mm)	2056	2047	- 9
BOTTOM OF LOOP SEAL LOWER END	(mm)	1662	1959	+ 297

Table 2.1 (Cont'd)

COMPONENT		PWR	JAERI	RATIO
CENTER OF HOT LEG	(mm)	5198	4927	- 271
BOTTOM OF HOT LEG (INSIDE)	(mm)	4830	4849	+ 19
BOTTOM OF UPPER CORE PLATE	(mm)	3957	3957	0
TOP OF LOWER CORE PLATE	(mm)	- 108	- 50	+ 58
BOTTOM OF TUBE SHEET OF STEAM GENERATOR SIMULATOR	(mm)	7308	7307	- 1
LOWER END OF STEAM GENERATOR SIMULATOR PLENUM	(mm)	5713	5712	- 1
TOP OF TUBES OF STEAM GENERATOR SIMULATOR (avg)	(mm)	17952.7	14820	

Table 2.2 Instruments provided by USNRC

Instrument	Number of sets	Number of sensors
DC FDG	18	162
DC VOP	1	1
DC drag disk	4	8
Core velocimeter	4	4
Core flag probe	12	24
Core LLD	6	96
LP LLD	3	15
End box turbine meter	8	8
UP turbine meter	4	4
UP FDG	11	110
UP film probe	2	4
UP prong probe	2	4
UP VOP	1	1
VV turbine meter	2	2
VV string probe	2	2
HL film probe	2	4
HL VOP	1	1
Reference probe	1	1
Spool piece	8	89
Total	92	540

Note

DC : Downcomer, FDG: Fluid distribution grid,
VOP: Video optical probe, LLD: Liquid level detector,
LP : Lower plenum, UP : Upper plenum,
VV : Vent valve

Table 2.3 Summary of test conditions

1. Test type: FLECHT-SET coupling (lower plenum injection) test
2. Test No.: C2-AC2 (Run 052)
3. Test data: January 27, 1982
4. Power: Total; 9.59 MW, Linear; 1.44 kW/m
5. Radial power distribution:

   A : B : C

   2.176 : 1.689 : 1.068 kW/m
6. Pressure (MPa):

   Upper plenum; 0.209 ∿ 0.258

   Containment ; 0.170
7. Temperature (K):

   Downcomer wall; 383, Vessel internals; 373

   Primary piping; 383, Lower plenum liquid; 373

   ECC liquid; 341, Steam generator secondary; 539
8. ECC injection type: Lower plenum injection
9. Pump K-factor: 15
10. ECC injection rates and duration:

    Acc; 0.1075 m^3/s from 46.8 to 70.8 s (at half maximum)

    LPCI; 11.1×10^{-3} m^3/s from 63.0 to 956.0 s

    ECC injection to lower plenum; from 46.2 to 956.0 s
11. Initial water level in lower plenum: 0.9 m
12. Power decay: ANS × 1.2 + Actinide × 1.1 (30 s after scram)
13. Peak clad temperature at BOCREC: 867 K

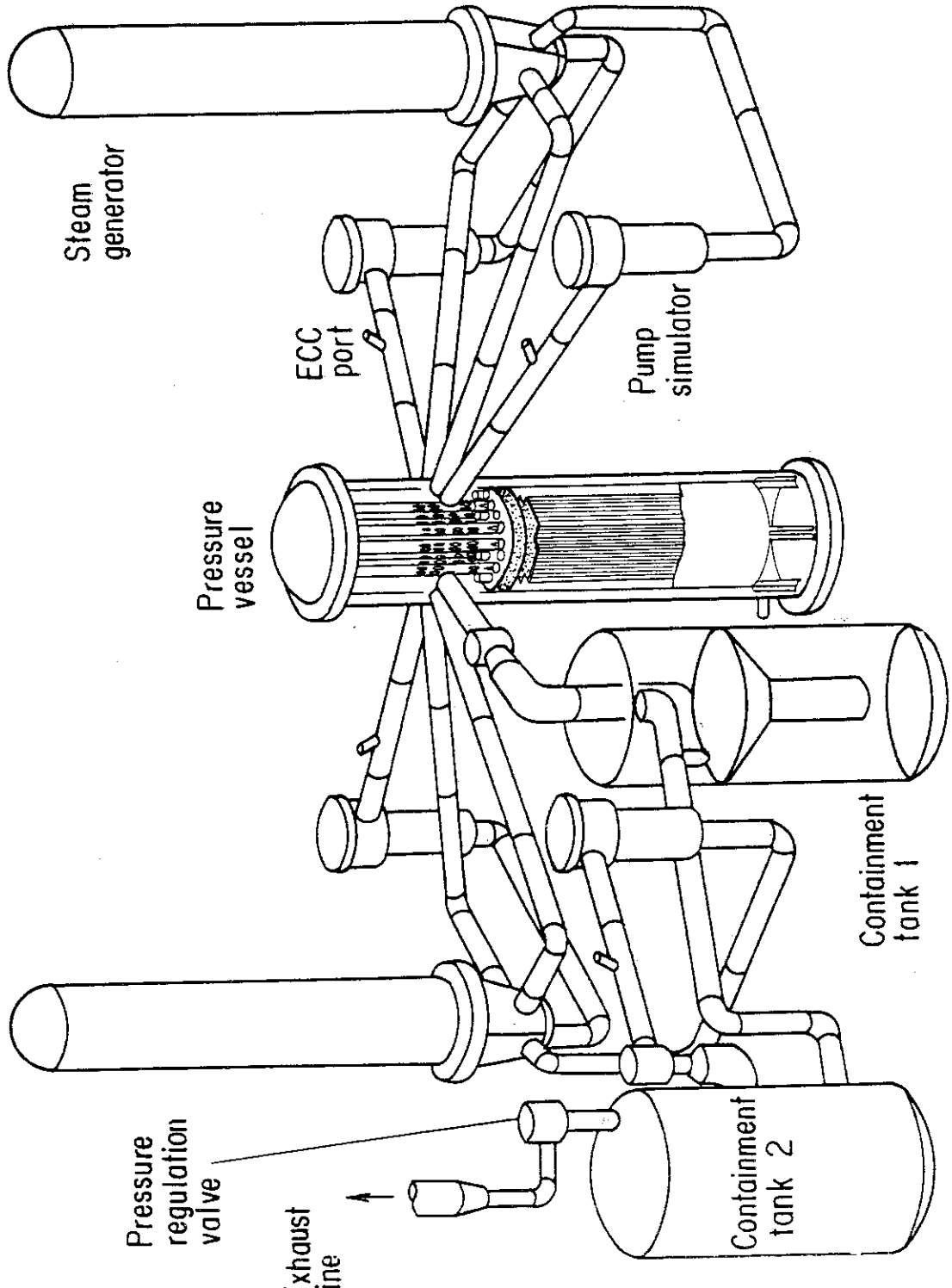

Fig. 2.1 Brid's-eye view of CCTF

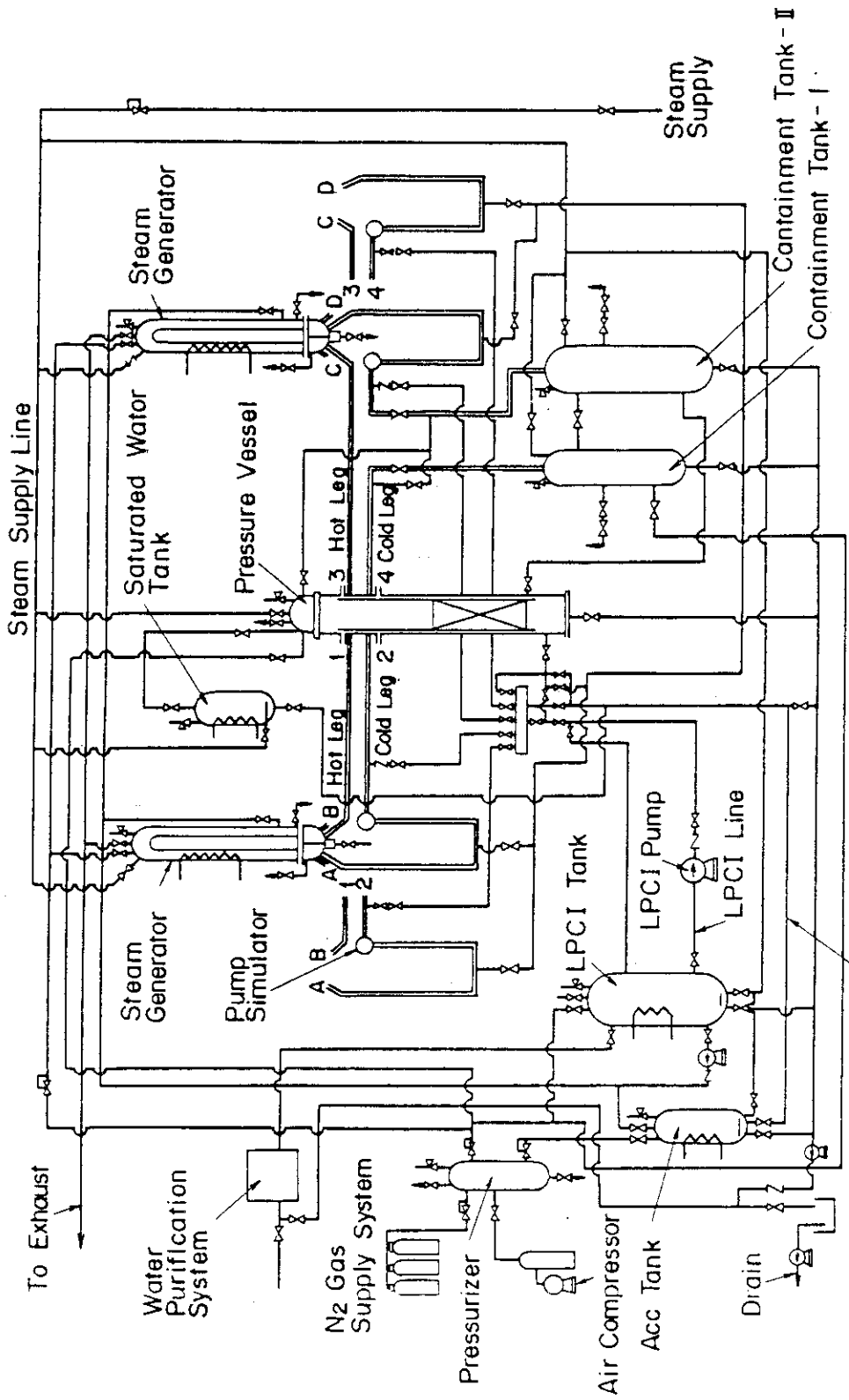

Fig. 2.2 Schematic diagram of CCTF

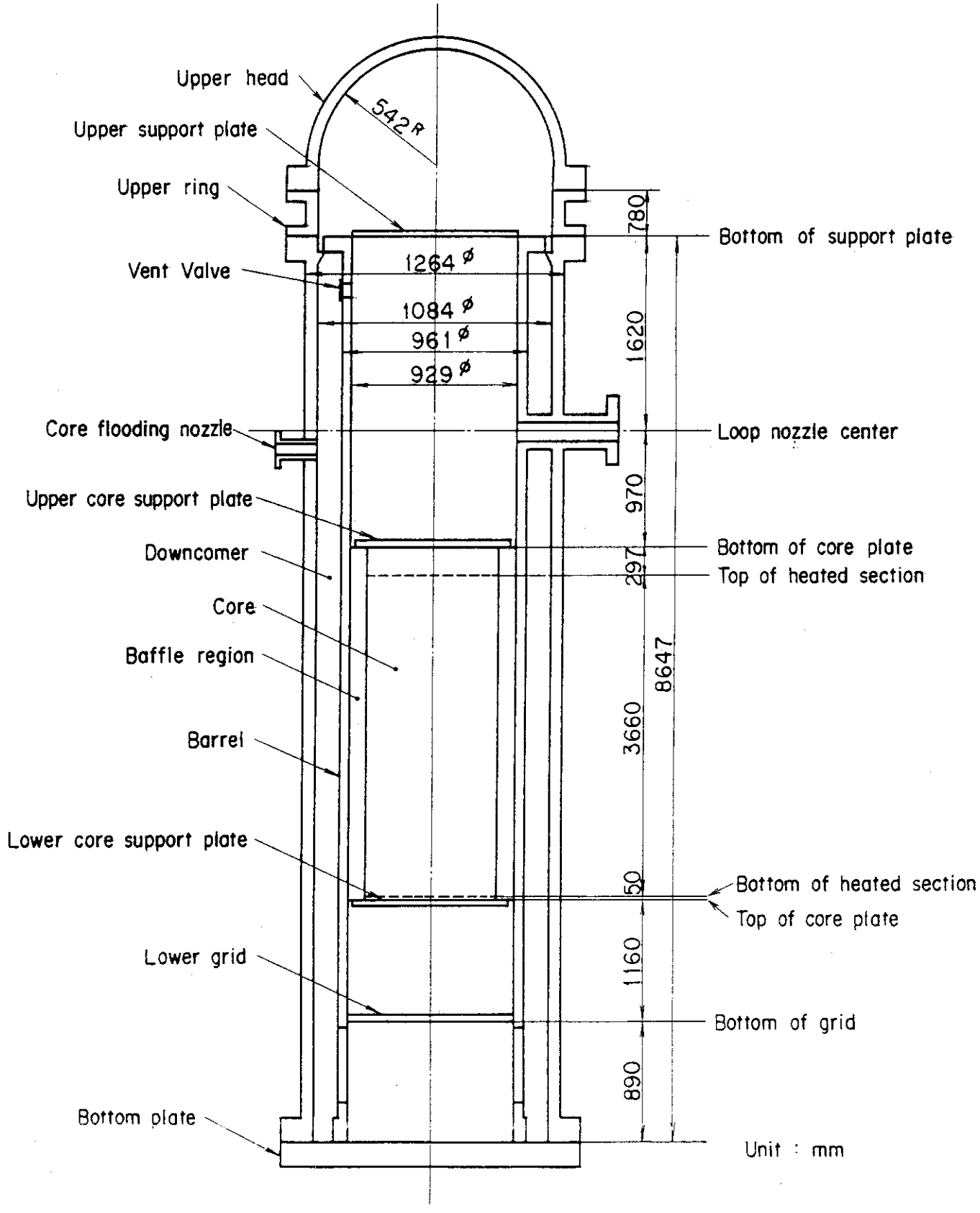

Fig. 2.3 CCTF Core-II pressure vessel

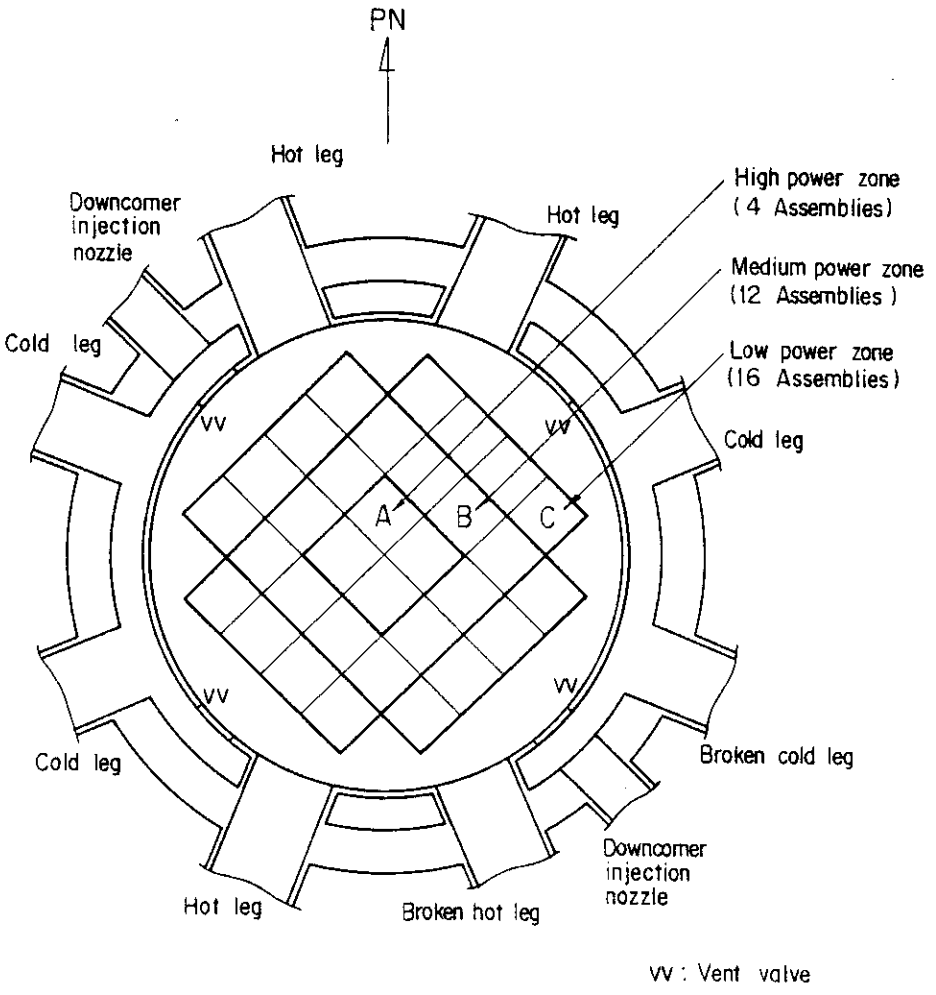

Fig. 2.4 Cross section of CCTF Core-II pressure vessel

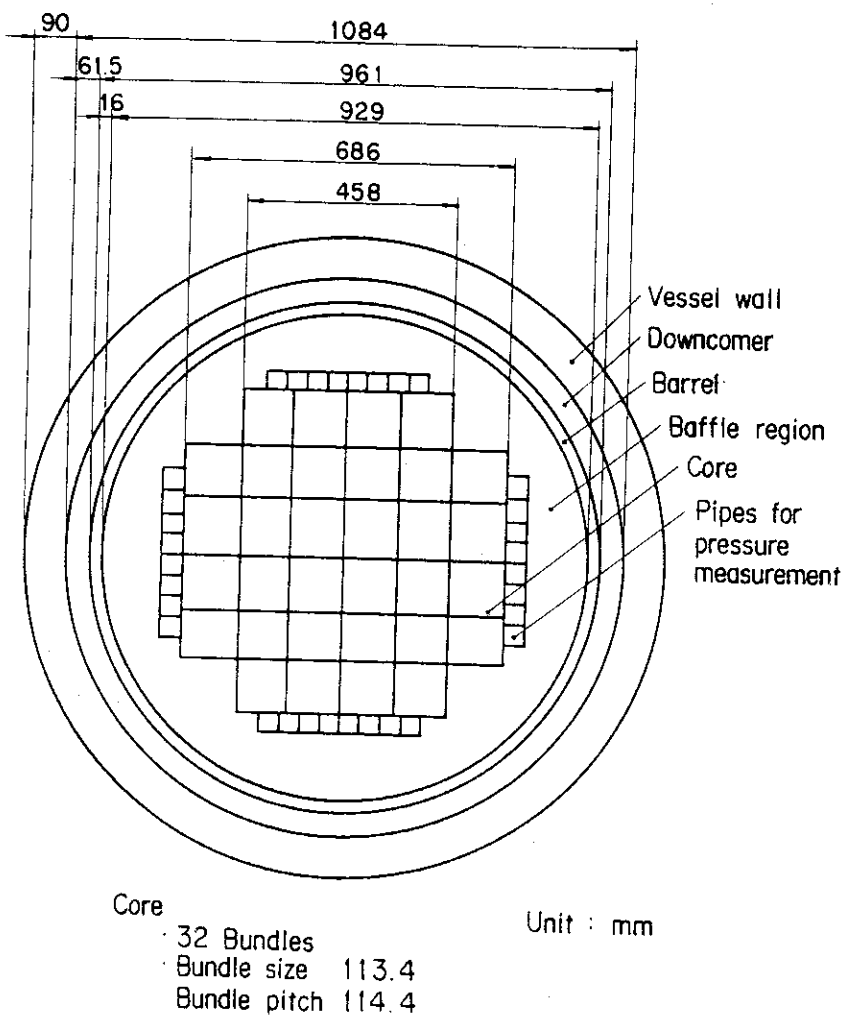

Fig. 2.5 Dimension of CCTF Core-II pressure vessel cross section

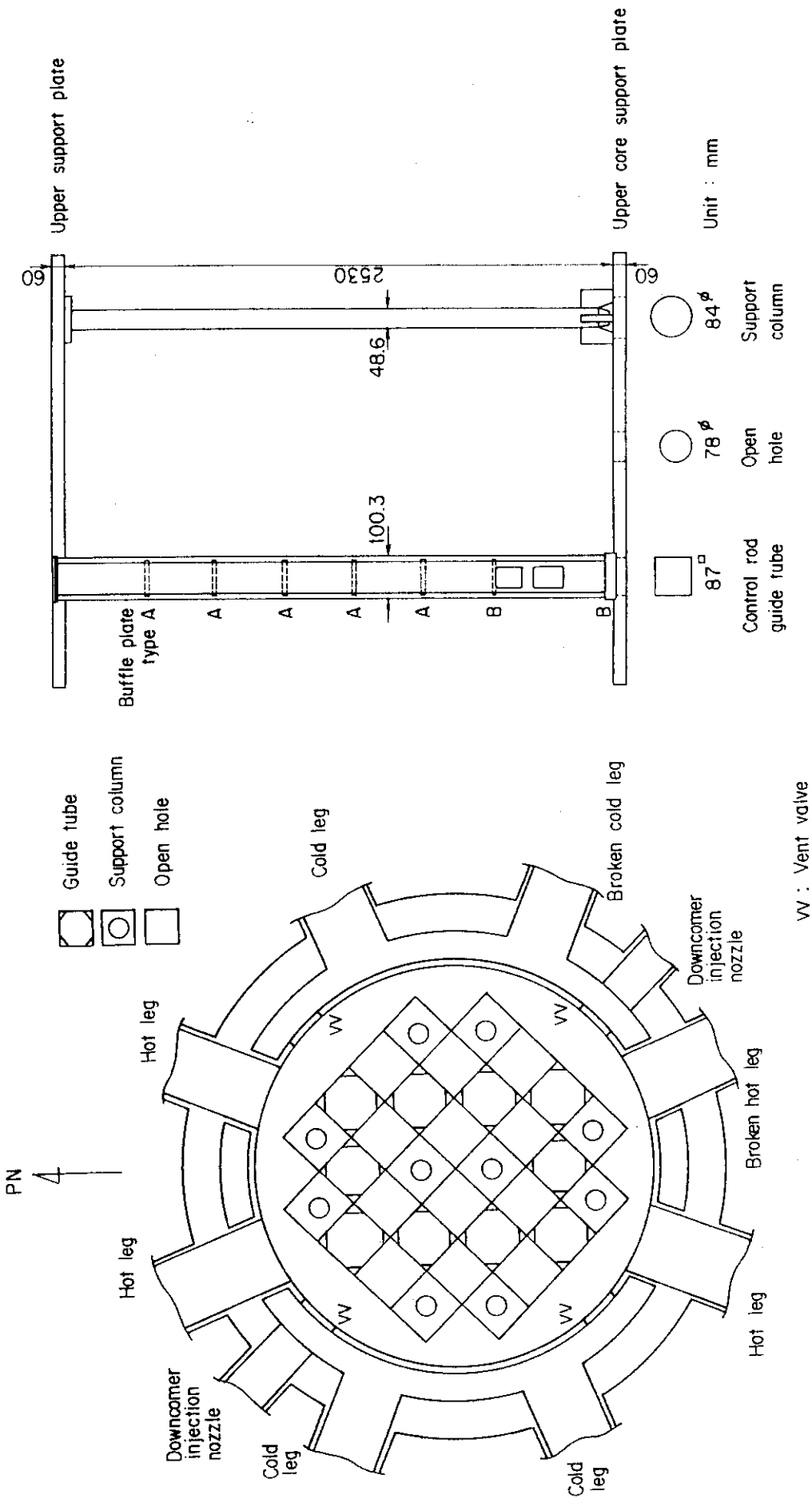

Fig. 2.6 Arrangement of upper plenum internals

Fig. 2.7 Upper plenum internals

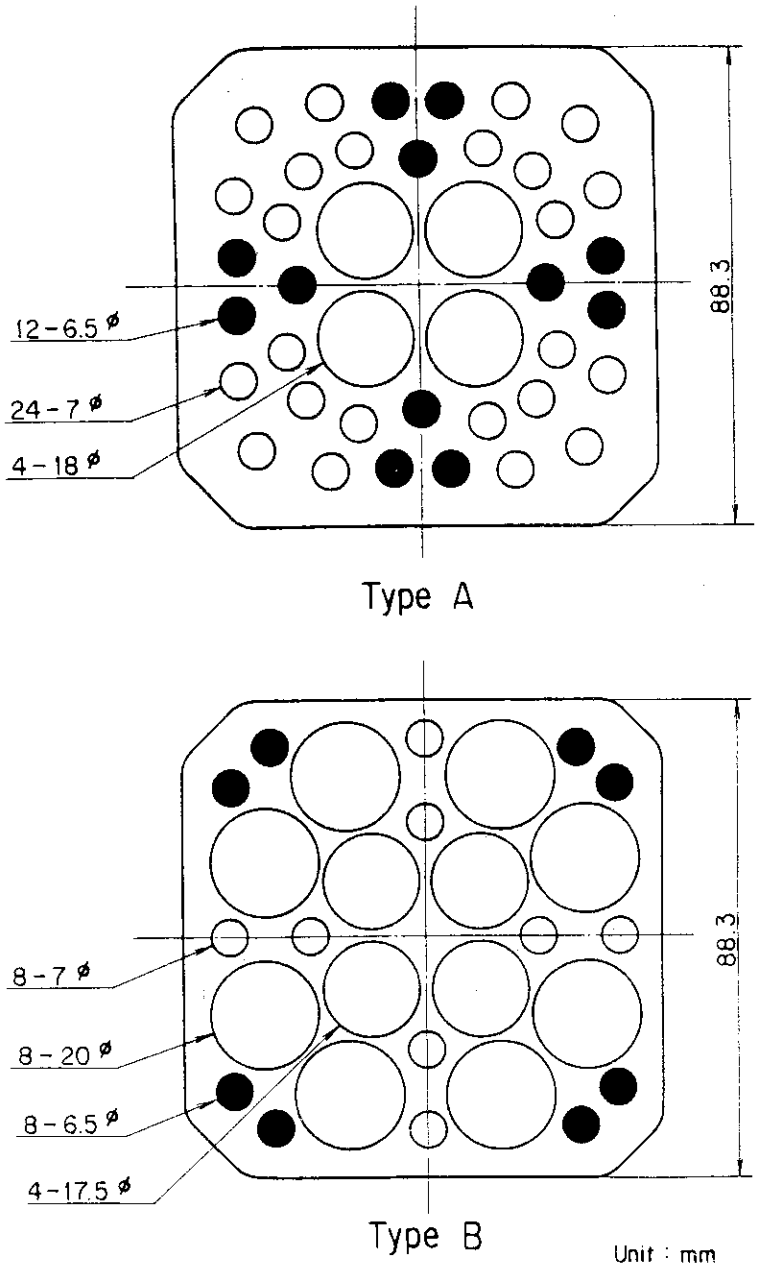

Fig. 2.8 Buffle plantes in control rod guide tube

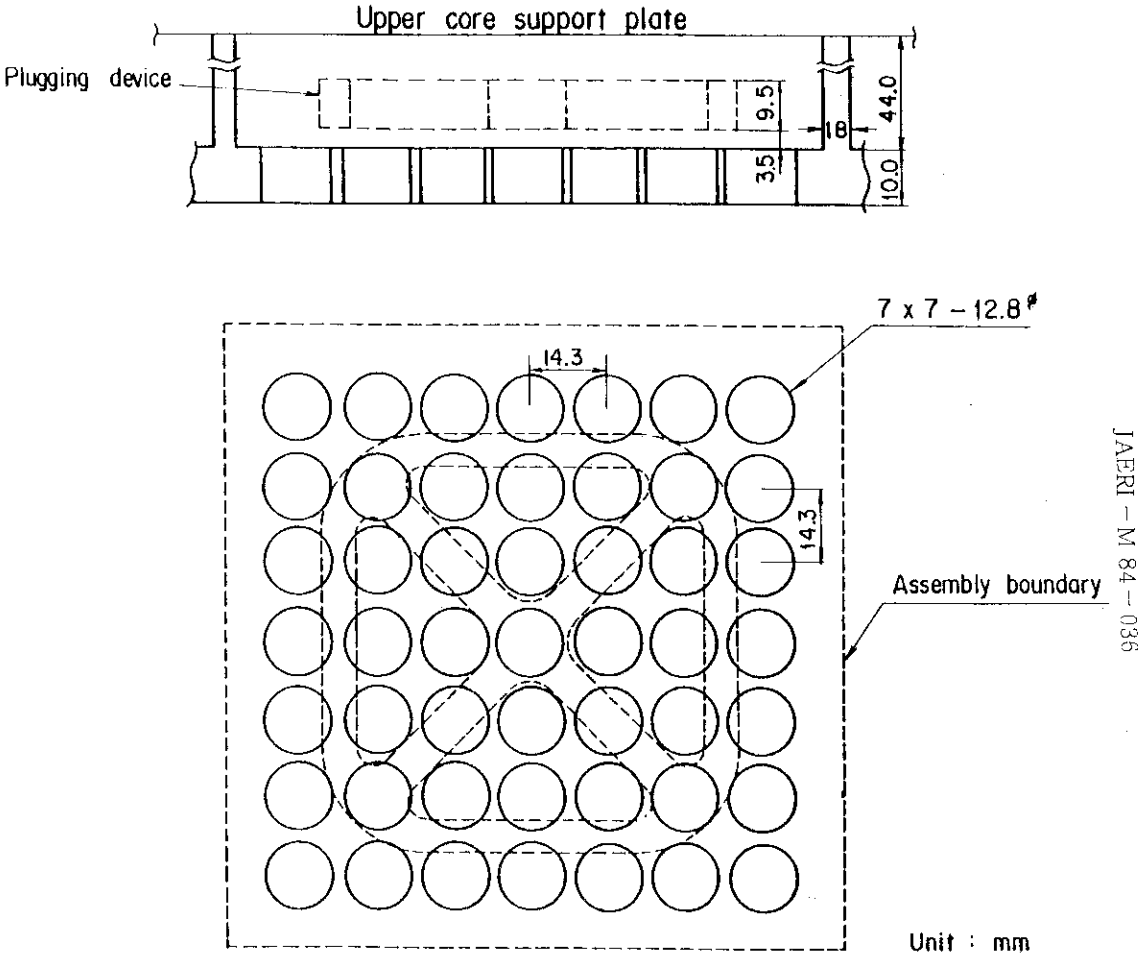

Fig. 2.9 End box

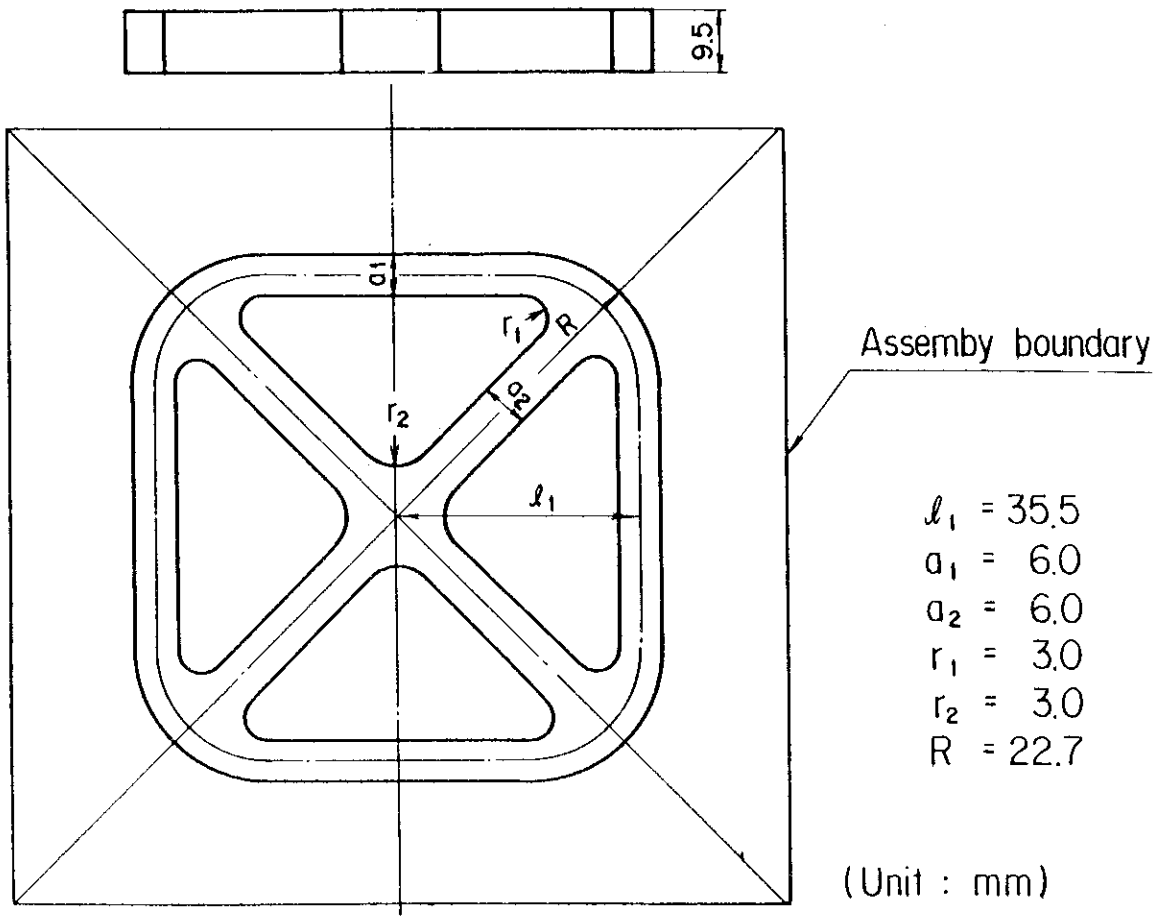

Fig. 2.10 Dimensions of plugging device

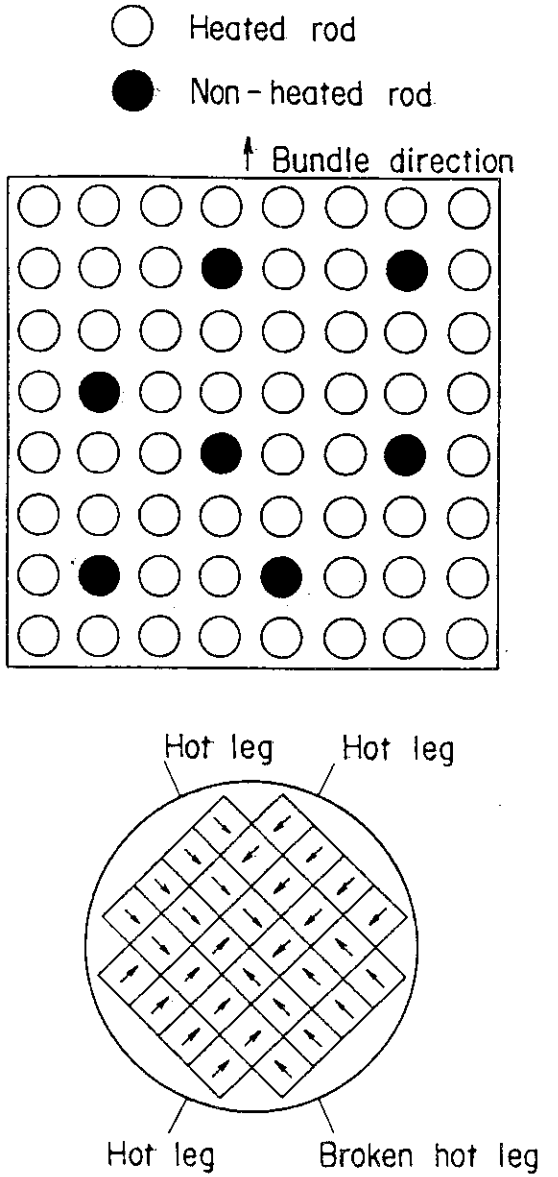

Fig. 2.11 Arrangement of non-heated rods and bundle direction

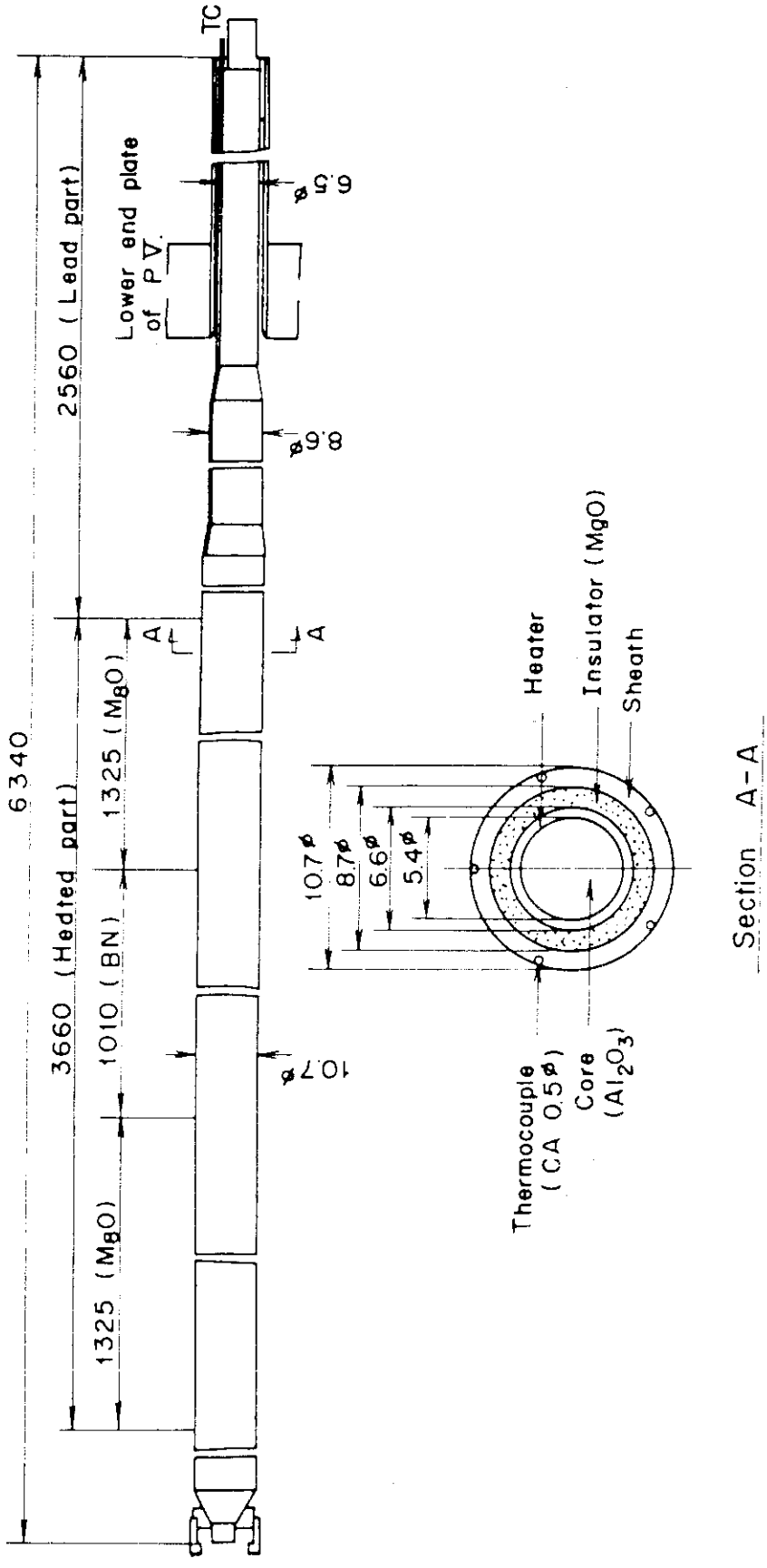

Fig. 2.12 Heater rod

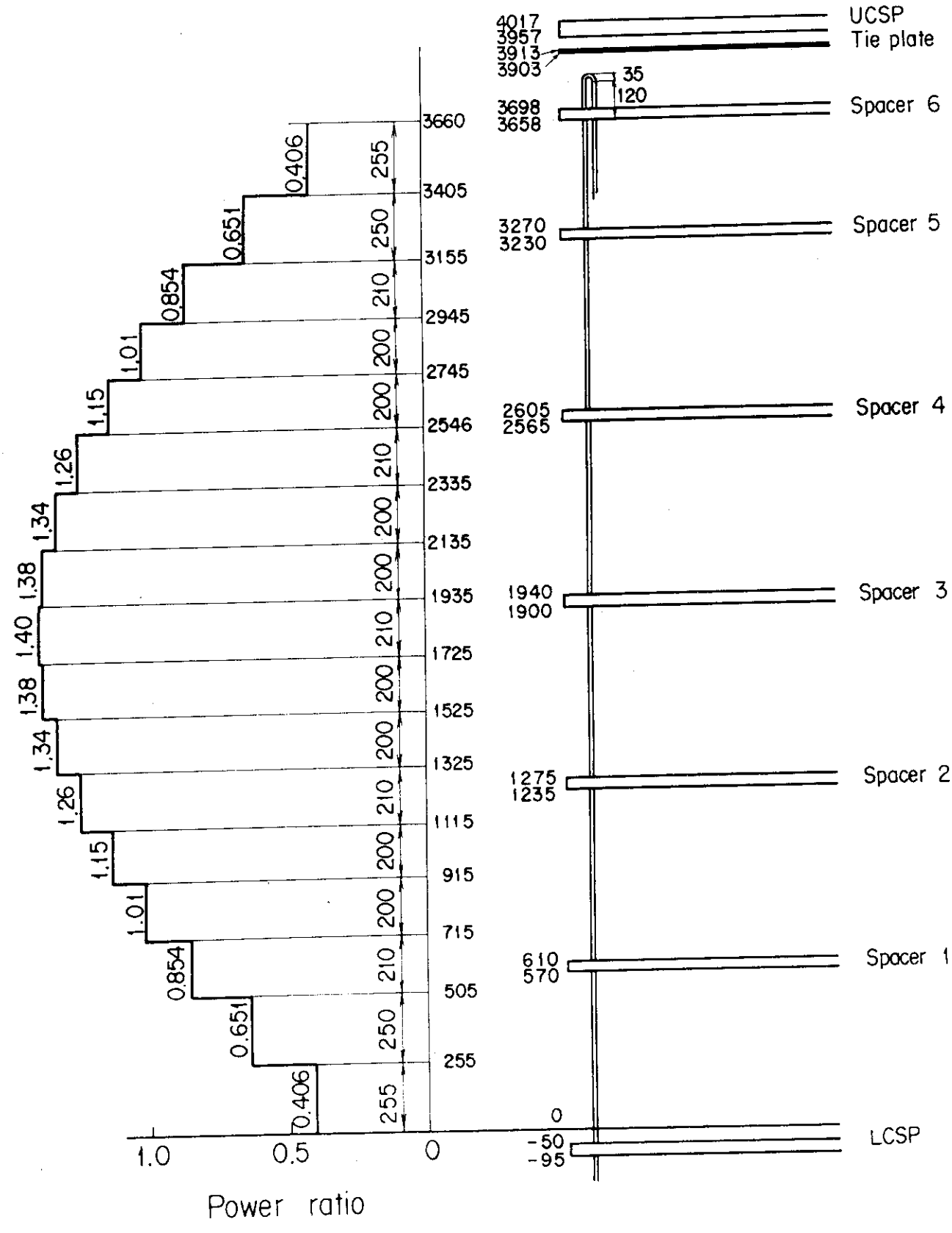

Fig. 2.13 Axial power profile of CCTF Core-II heater rod

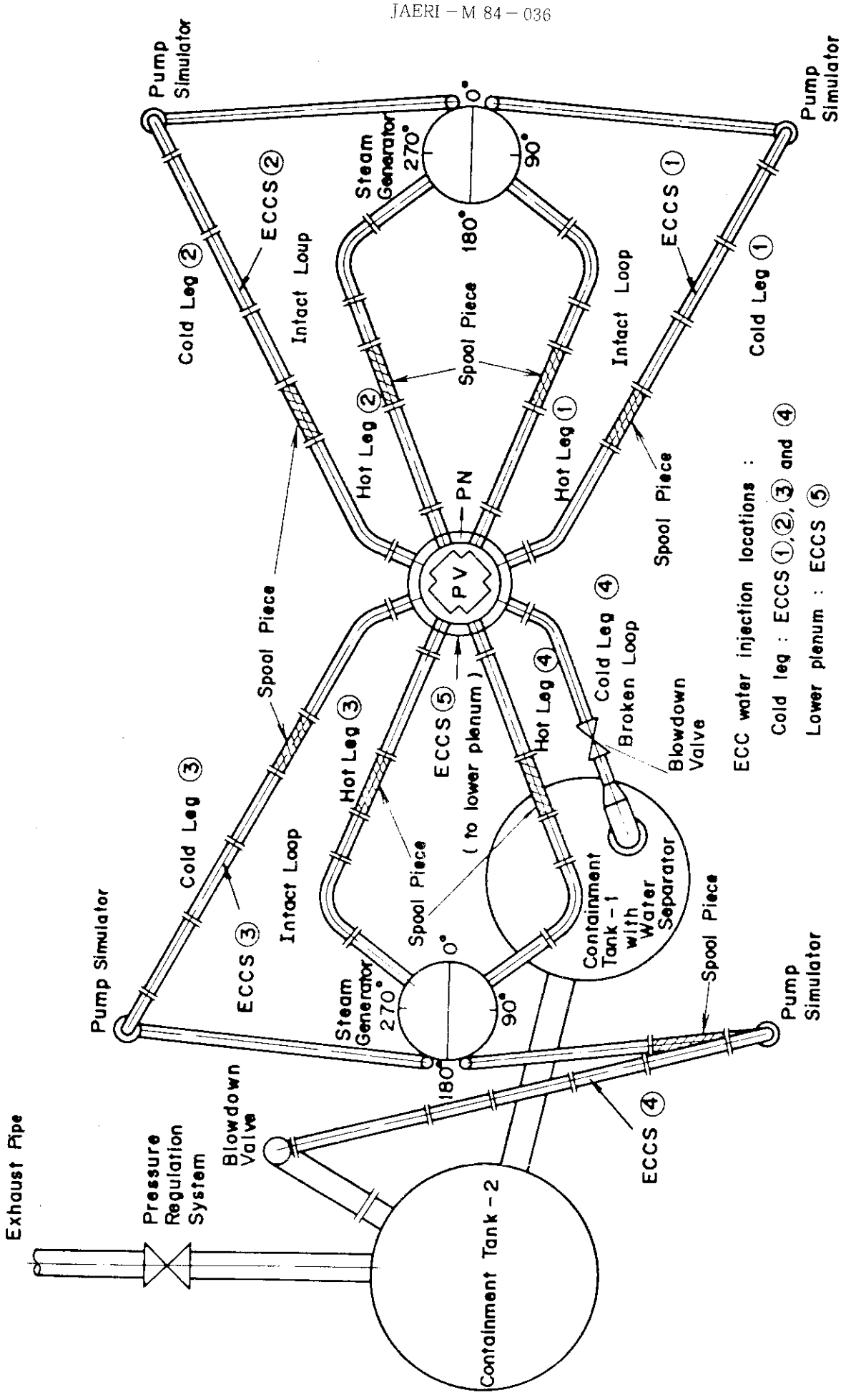

Fig. 2.14 Top view of primary loop pipings

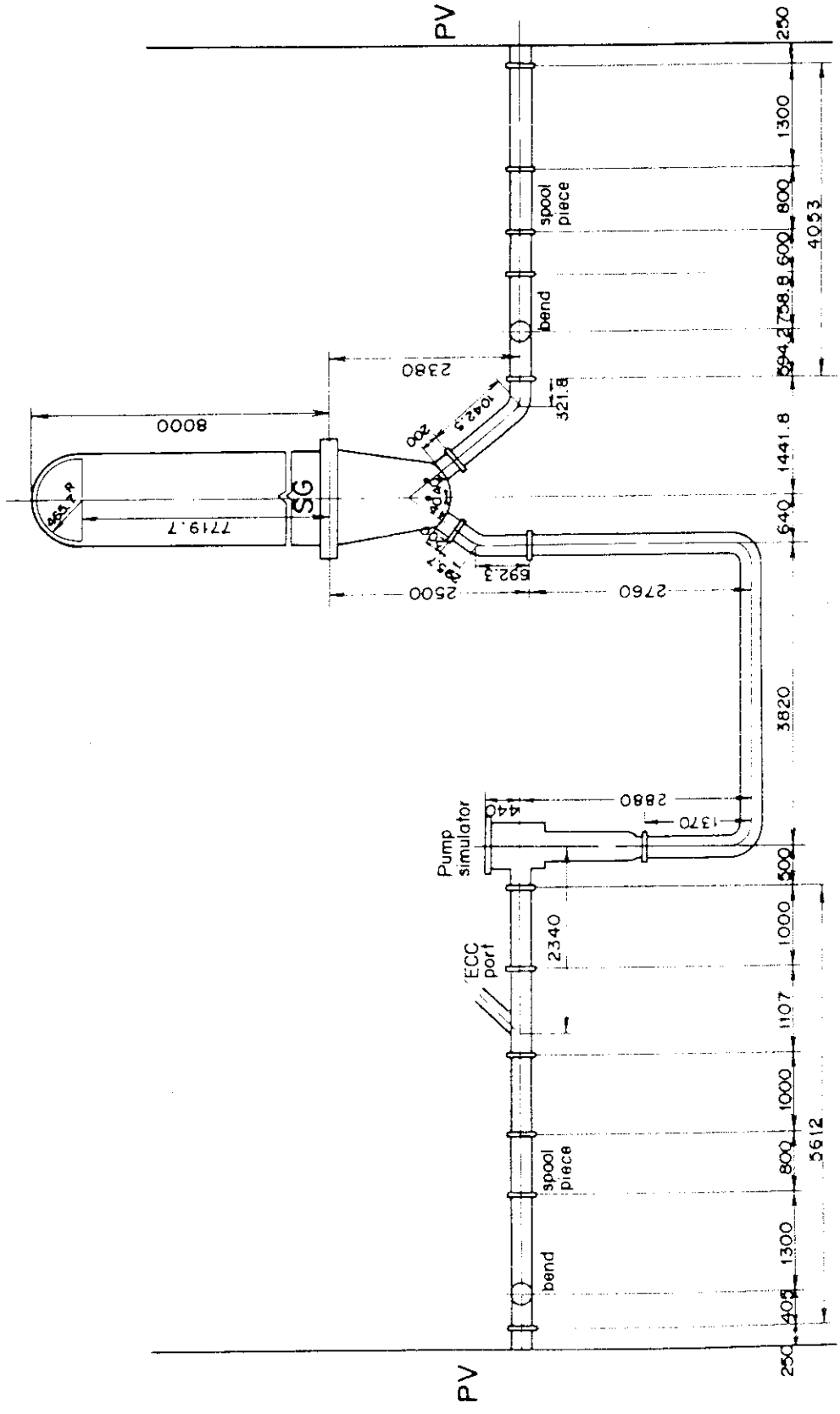

Fig. 2.15 Dimensions of primary loop

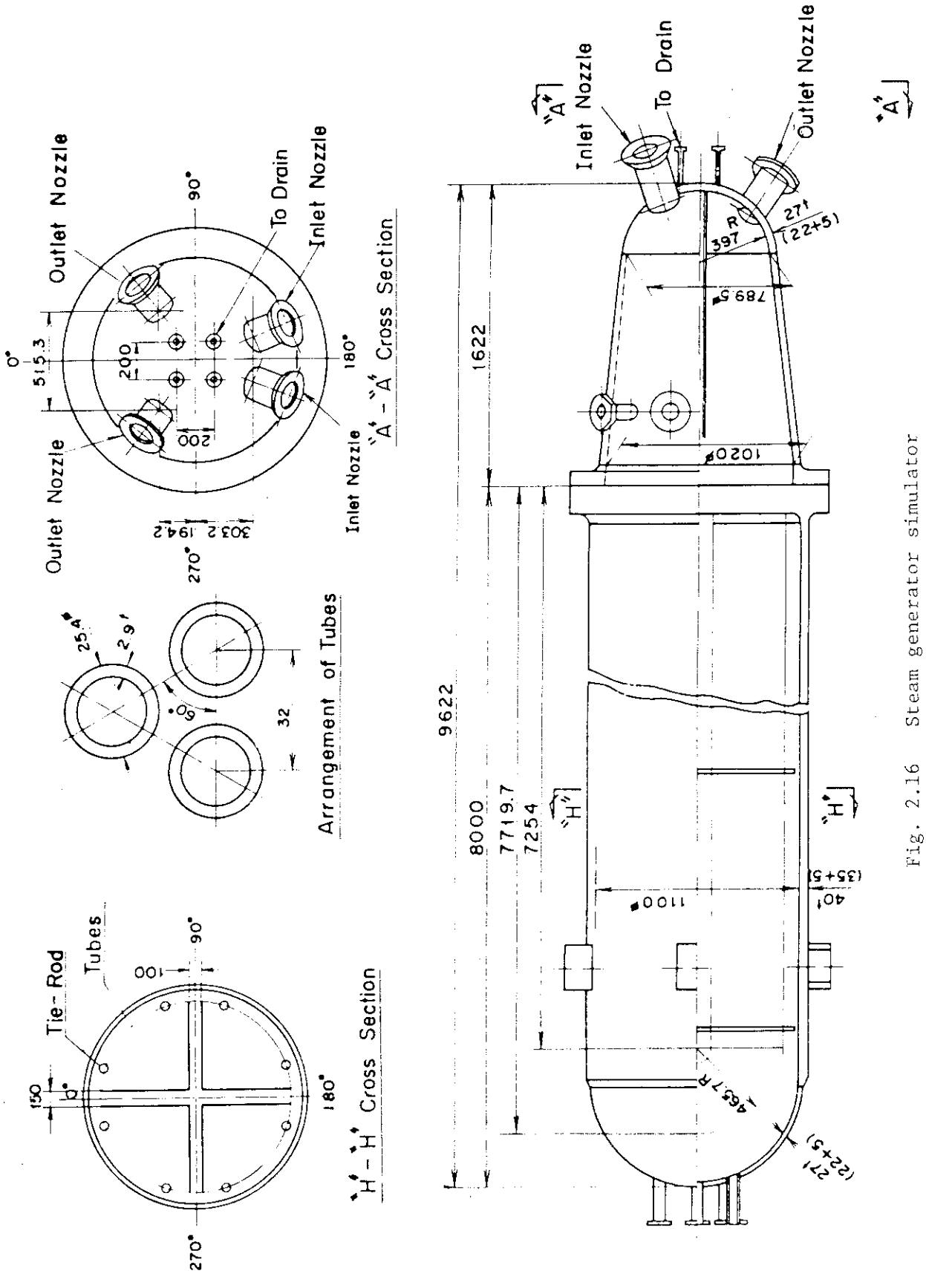

Fig. 2.16 Steam generator simulator

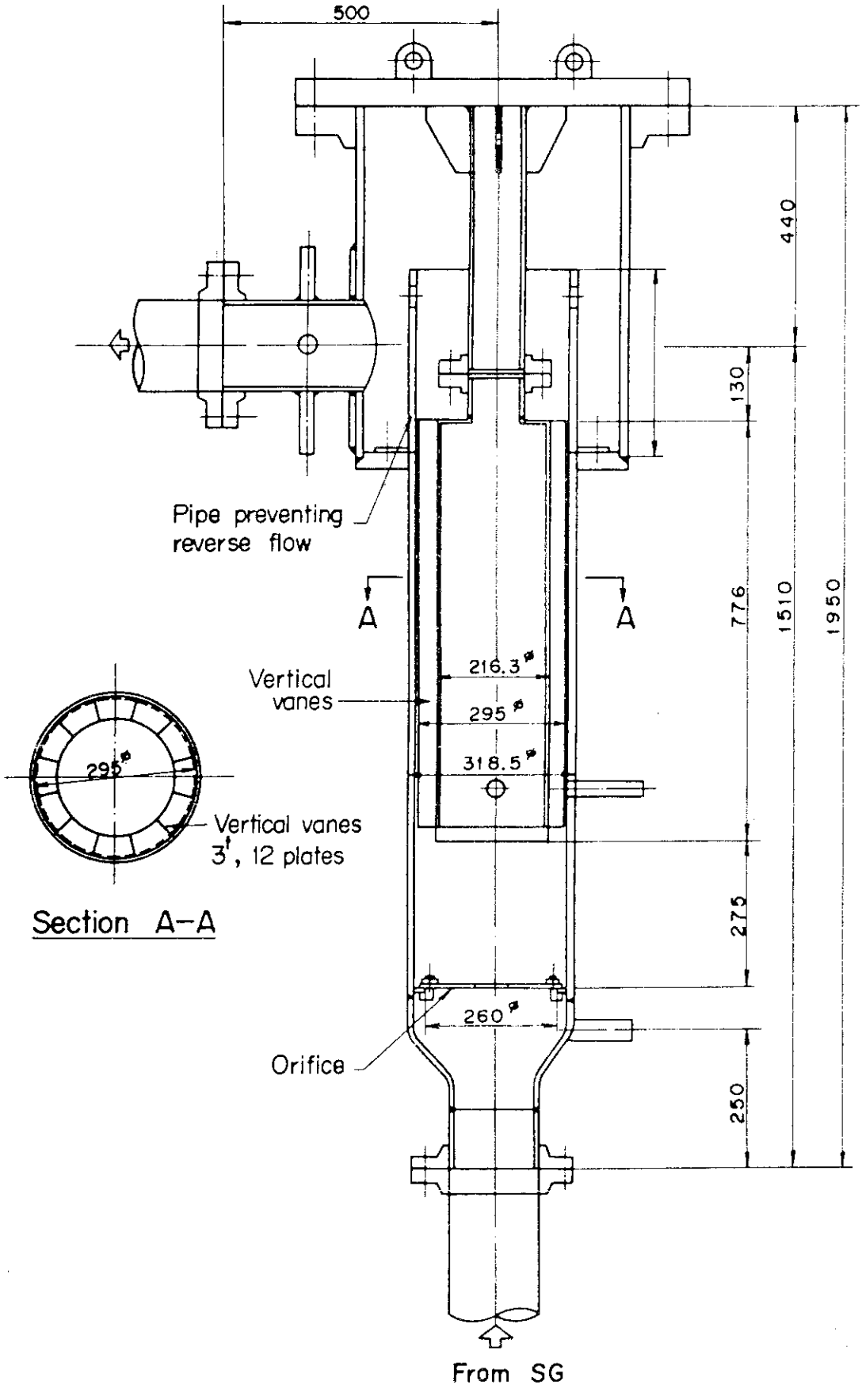

Fig. 2.17 Pump simulator

3. Test Results and Discussion

In the following, the system behavior and the core behavior are presented and discussed separately. The comparison of several measured test conditions between the present test and the Test C1-21 is given in Table 3.1. The chronologies of events are compared in Table 3.2. For better understanding of the test results, selected data are presented in Appendix with the additional information.

3.1 System Behavior

The differential pressures through the intact and broken loops are compared in Figs. 3.1 and 3.2, respectively. These differential pressures experienced relatively large oscillations (about 10 kPa in magnitude) after the time the downcomer water reached the overflow level. Therefore, the mean values and the ranges of oscillations are given in these figures. The amplitudes of the oscillations are almost the same in both tests. The frequencies have also been found to be the same and are 0.5 Hz.

The mean value of the present test is smaller by about 2 kPa for the intact loop, whereas it is larger by about 3 kPa for the broken loop. Although the mean values are a little different between both tests, the differences are small and the histories are similar except for the early period. The differences during the early period are discussed in the last part of this section.

In order to examine the similarity of the behavior in each section of the primary loop between both tests, the differences of pressures from the pressure at the containment tank 2 are compared at some locations in Fig. 3.3 at 150 s. Figure 3.3 indicates that the differential pressures at each section of the primary loop are nearly identical between both tests. The slight increase of the differential pressure between the containment tank 1 and 2 in the present test is caused by the orifice plate which was newly installed in the piping between those two tanks.

The downcomer differential pressures (mean values) are compared in Fig. 3.4. Except for the early period they are identical and stay at the value which corresponds to the overflow level. The downcomer differential pressures also experienced the large oscillation as shown in Fig. B.19 in Appendix B. The amplitude of the oscillation is 4 kPa

at most and is almost identical to that for the Test C1-21. The frequency is 0.5 Hz and is the same as that for the Test C1-21.

The oscillation of the downcomer differential pressure has been found to be in phase with those of the core and the primary loop differential pressures. This fact was the same in the Test C1-21. Although the cause of the oscillation has not been clarified yet, the overflowing behavior of the downcomer water seems to have a close relation.

The core differential pressure data have been judged unreliable and are not available in the present test (see Figs. B.17 and B.19 in Appendix B). However, they are inferred to be nearly identical to those obtained in the Test C1-21 since the differential pressures in the intact loop (ΔP_I) and the downcomer (ΔP_D) are nearly identical to those of the Test C1-21. This is because the core differential pressure (ΔP_C) is expressed as

$$\Delta P_C \approx \Delta P_D - \Delta P_I$$

based on the momentum balance in the system.

The upper plenum differential pressures between the tops of the UCSP and upper plenum are compared in Fig. 3.5. These data show the water accumulation above the UCSP and indicate the value for the present test is generally smaller than for the Test C1-21. However, the difference is small and is 0.6 kPa at most. At present, it cannot be concluded that the difference is caused by the difference in the structure of the upper plenum internals, because the total core power and the radial power distribution were also different to some extent between the two tests, and hence, these might change the steam flow rate in the upper plenum resulting in the difference in the water accumulation there.

During the early period, considerable differences are found in the downcomer and the intact and broken loop differential pressures as shown in Figs. 3.4, 3.1 and 3.2, respectively. These differences were caused by the differences in the Acc injection rate and duration. The Acc injection rates are compared in Fig. 3.6. From this figure it is found that the Acc injection rate is higher and the duration is longer in the present test. This larger amount of Acc water injected in the present test caused the rapider water filling in the downcomer, as shown in Fig. 3.4. This is inferred to cause the higher core flooding rate, and hence, the higher mass flow rate in the primary loop resulting in

the higher differential pressures in the early period shown in Figs. 3.1 and 3.2.

As the summary of the system behavior, it can be pointed out that the system behavior observed in the Core-II facility is nearly identical to that observed in the Core-I facility.

3.2 Core Behavior

Since the core differential pressures have been judged unreliable in the present test, only the rod surface temperature information is compared in the following.

In order to determine which temperature data to be compared between the Core-II and the Core-I tests, the initial linear power densities of heater rods are compared in Table 3.3. For the temperature history comparison, the sections which locate at the same elevation and have the same power density, *i.e.* the data of the thermocouples with Tag-IDs of TE32Y17 (Core-II) and TE32X13 (Core-I) were selected based on the information in Table 3.3 and compared in Fig. 3.7. Both thermocouples measure the temperatures at the midplane level. The linear power densities there are the same and 3.05 kW/m. For the quench envelope comparison, on the other hand, the rods which have the same power density were selected. Therefore, based on Table 3.3, the data of the rods in B region (Core-II) and Y rods in B region (Core-I) were selected and compared in Fig. 3.8. The linear power densities are not exactly the same and are 1.689 and 1.632 for the Core-II and Core-I, respectively, as listed in Table 3.3.

Figure 3.7 indicates that the temperature history of the present test is not identical to that of the Test C1-21. This might be caused by the small differences in the initial clad temperature, the amount of Acc water and the axial power distribution of heater rod between those tests. However, the difference in the temperature history is not significant and the shapes of the history curves are similar.

In Fig. 3.8 the mean value $\bar{t}_q$ and the standard deviation σ_{n-1} of the quench times for all rods in the specified region are plotted. The data sources for this figure are listed in Table 3.4. It should be noted that the number of the thermocouple locations is more in the Core-II facility, especially in the upper part of the core. In contrast, for the concerned rods in the Core-I facility, there is only one elevation

(3.05 m) above the 2.44 m elevation. As shown in Fig. 3.8, both quench envelopes are nearly identical in the region below 2.44 m elevation. At the 3.05 m elevation, however, the quench times are shorter and deviate more for the Test C1-21 (Core-I). These data suggest that top quenching tends to occur more in the Core-I test than in the Core-II test. The definition of top quenching is that the quench time at the concerned elevation is shorter than that at the next lower elevation. In the Test C1-21, the percentage of top quenching for the concerned rods (Y rods in B region) at 3.05 m elevation was 44 percent, whereas it was 16 percent in the present test.

As described above, top quenching behavior is different between the Core-I and Core-II tests in B region. In order to examine whether this tendency can be observed over all regions of the core, the top quenched rods are illustrated in Figs. 3.9(a) and (b) for the Test C1-21 and the present test, respectively. From Fig. 3.9(a) it is found that top quenching occurred in the bundles just below or near the open holes of the UCSP in the Test C1-21. In contrast, for the present test, top quenching is found to occur without the special relation with the open holes, as shown in Fig. 3.9(b). The reasons for this difference in the top quenching behavior might be the differences in the upper plenum structures between those facilities. In the Core-II facility, the number of open holes is larger and the structure of the support column is closer to the open hole at the UCSP section (Fig. 2.7). Also, in the Core-II facility, the plugging devices are equipped beneath every upper plenum internal (Fig. 2.9). These changes in the Core-II facility seem to equalize the hydraulic behavior around the UCSP mitigating the dependence of the top quenching behavior on the open hole which was observed in the Core-I facility. These results and discussion indicate that the top quenching behavior is significantly influenced by the geometry of the upper plenum internals.

Another characteristic observed for top quenching is that in the present test the occurrence of top quenching is only a few and less in A and B region but it occurs at almost all locations in C region. As listed in Table 3.1, the linear power density for C region is relatively low (1.07 kW/m) in the present test and this seems to be the reason of the occurrence of top quenching observed in almost all locations in C region. In the Test C1-21, the linear power density of Z rod in C region was 1.205 kW/m and the top quenching occurred only a few locations

except for the locations just below or near the open holes. These results and discussion indicate that the top quenching behavior is also significantly influenced by the power of the rod and the top quenching tends to occur on the low power rods.

As the summary of the core behavior, it can be pointed out that the core behavior observed in the Core-II facility is nearly identical to that observed in the Core-I facility except for the top quenching behavior.

Table 3.1 Comparison of test conditions

Item	Present test	Test C1-21
System pressure (MPa)	0.170	0.176
Average linear power (kW/m)	1.44	1.49
Radial power distribution (kW/m)	A B C 2.18:1.69:1.07	A B C 1.87:1.61:1.27
Acc injection rate (m^3/s)	0.108	0.100
Acc duration (s)	18	17.5
LPCI injection rate (m^3/s)	0.011	0.011
ECC water temperature (K)	340	340
Initial peak clad temperature (K)	867	867

Table 3.2 Comparison of chronologies of events

	Time (s)	
Event	Present test	Test C1-21
Test initiated (Heater rods power on) (Data recording initiated)	0.0	0.0
Acc injection initiated	46.2	49.5
Bottom of core recovery (BOCREC)	55.0	59.0
Power decay initiated	56.0	60.0
LPCI initiated	63.0	67.5
Acc injection ended	72.8	76.2
All heater rod quenched	600.0	540.0
Power off	766.0	620.0
LPCI ended	956.0	711.0
Test ended (Data recording ended)	1054.0	930.0

Table 3.3 Comparison of initial linear power densities per rod

1. Present test (Core-II)

Power region	A	B	C
	2.176	1.689	1.068

Axial peaking factor = 1.40

2. Test C1-21 (Core-I)

Power region / Rod type	A	B	C
X	2.045	1.796	1.395
Y	1.859	1.632	1.268
Z	1.766	1.551	1.205

Axial peaking factor = 1.492

* Unit: kW/m·rod

Table 3.4 Statistical data of quench times

(a) Rods in B region for present test

Elevation (m)	Number of data: n	Mean value: $\bar{t}_q$ (s)	Standard deviation: σ_{n-1} (s)
0.128	12	2.1	0.7
0.380	24	8.1	2.1
0.815	12	19.5	3.6
1.015	24	45.0	6.0
1.425	12	120.0	5.4
1.830	24	222.0	9.8
2.035	12	270.0	6.0
2.440	24	360.0	9.6
2.845	1	459.3	——
3.050	25	409.8	82.2
3.340	1	22.8	——
3.560	13	26.1	7.5

(b) Y rods in B region for Test C1-21

Elevation (m)	Number of data: n	Mean value: $\bar{t}_q$ (s)	Standard deviation: σ_{n-1} (s)
0.380	16	5.9	0.3
1.015	16	61.9	4.4
1.830	16	228.4	14.4
2.440	16	348.9	29.1
3.050	16	336.7	111.0

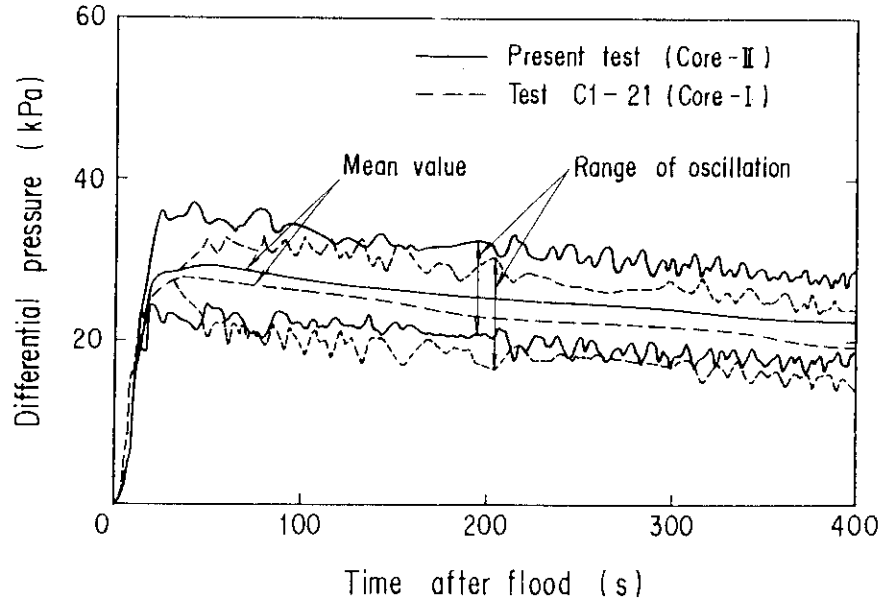

Fig. 3.1 Comparison of intact loop differential pressures (mean value and oscillation range)

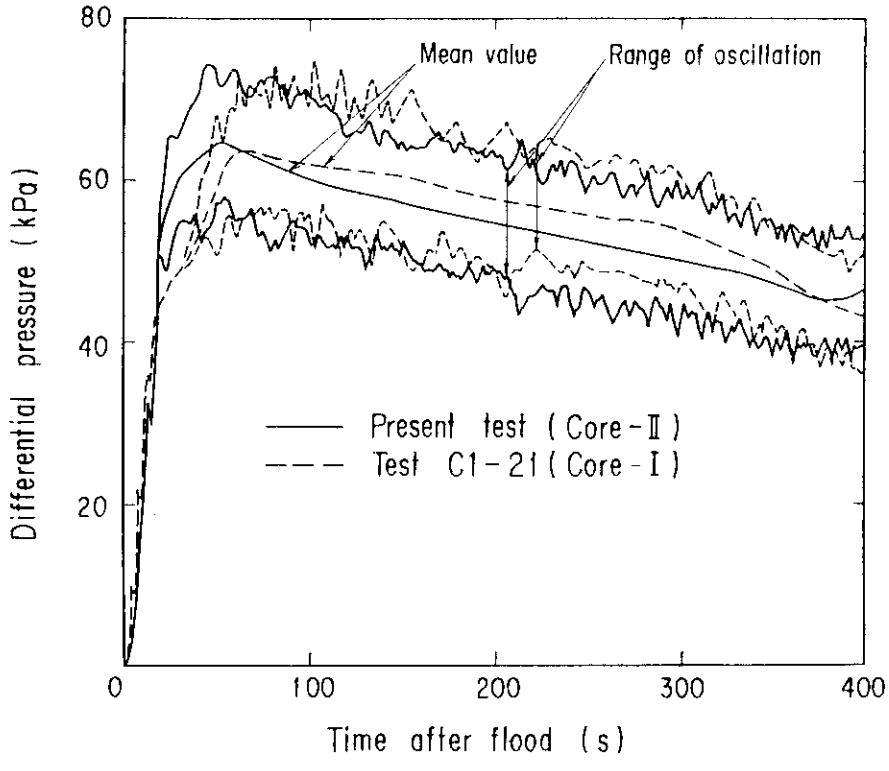

Fig. 3.2 Comparison of broken loop differential pressures (mean value and oscillation range)

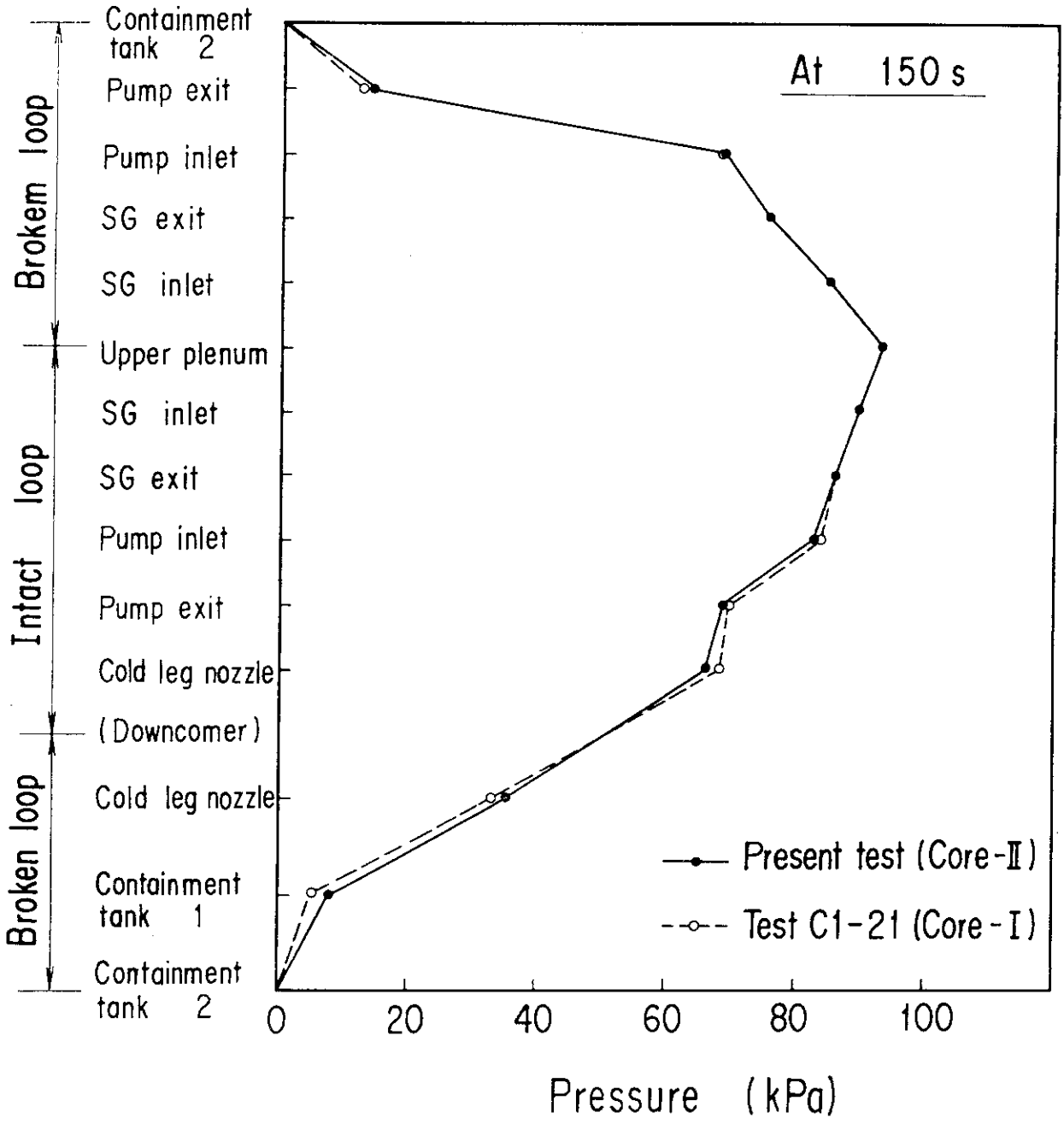

Fig. 3.3 Comparison of differences of pressure from the containment tank 2 pressure

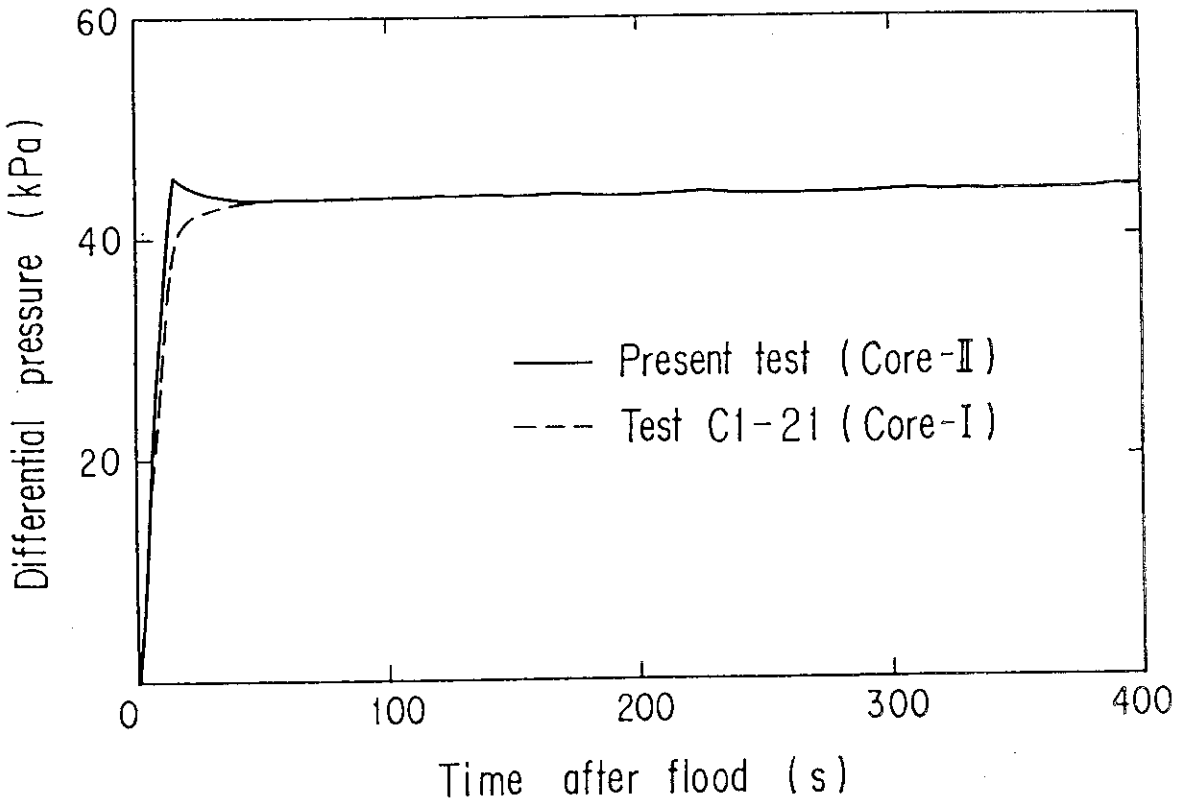

Fig. 3.4 Comparison of downcomer differential pressures (mean value)

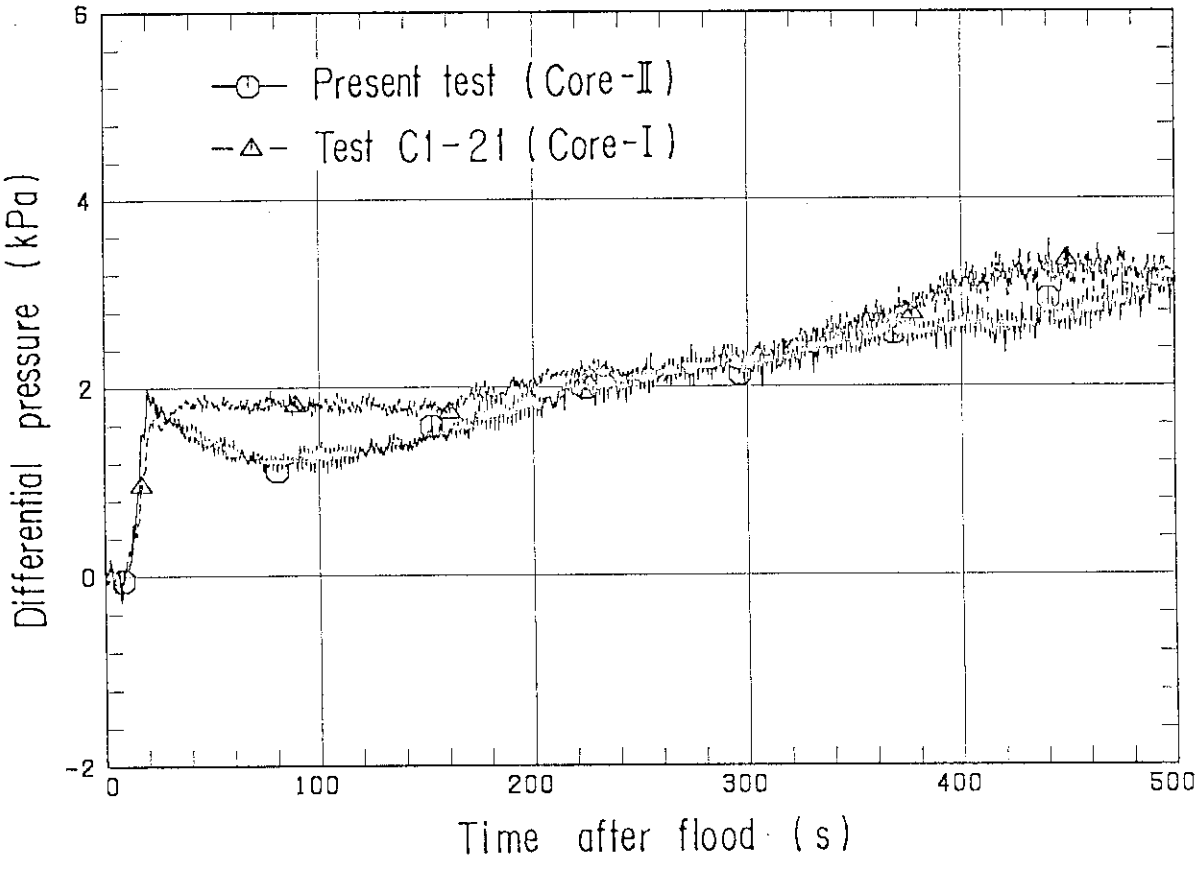

Fig. 3.5 Comparison of upper plenum differential pressures

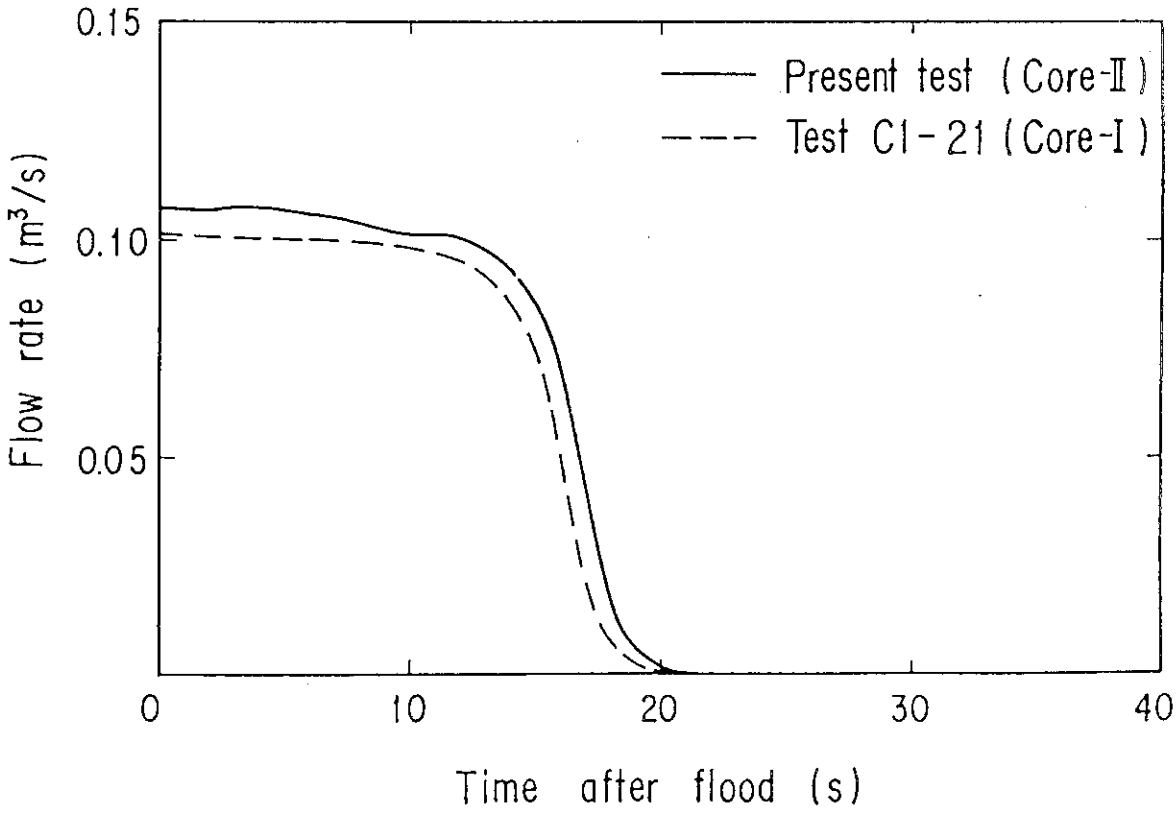

Fig. 3.6　Comparison of Acc injection rates

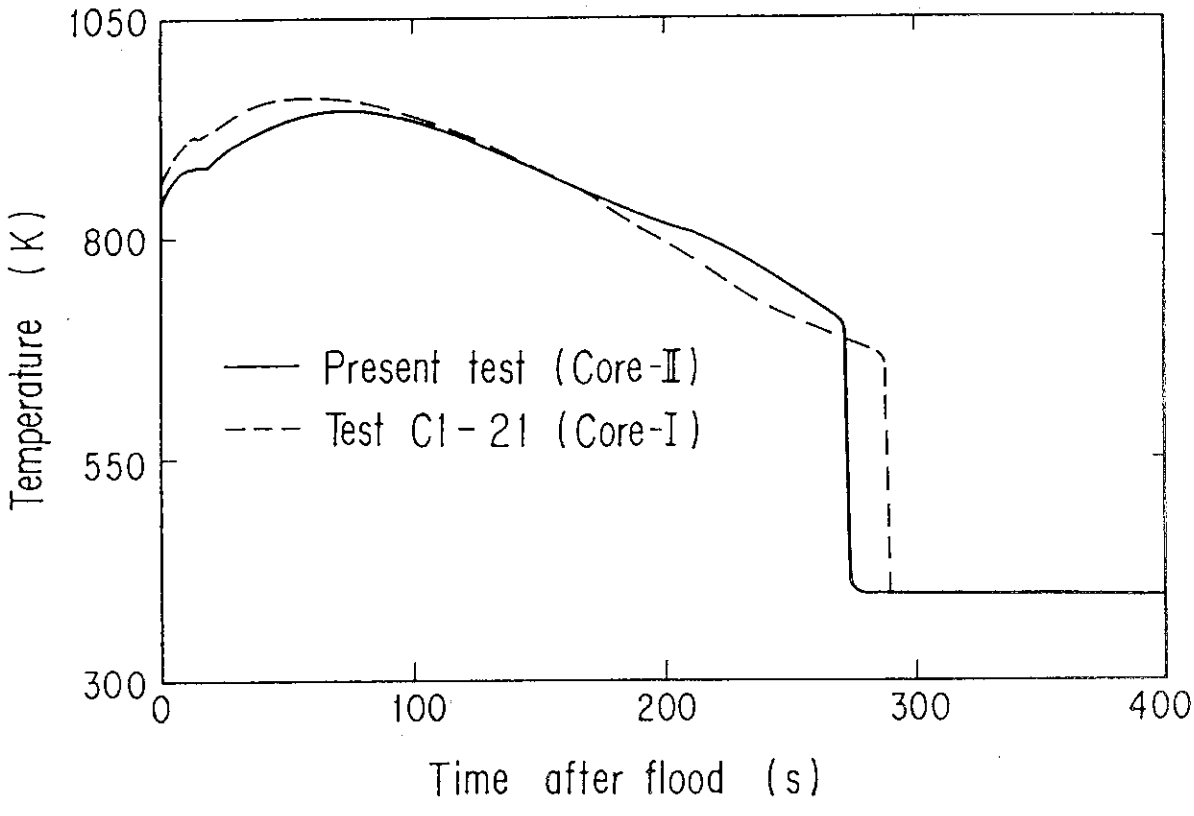

Fig. 3.7　Comparison of rod temperature histories of maximum power rods at midplane level

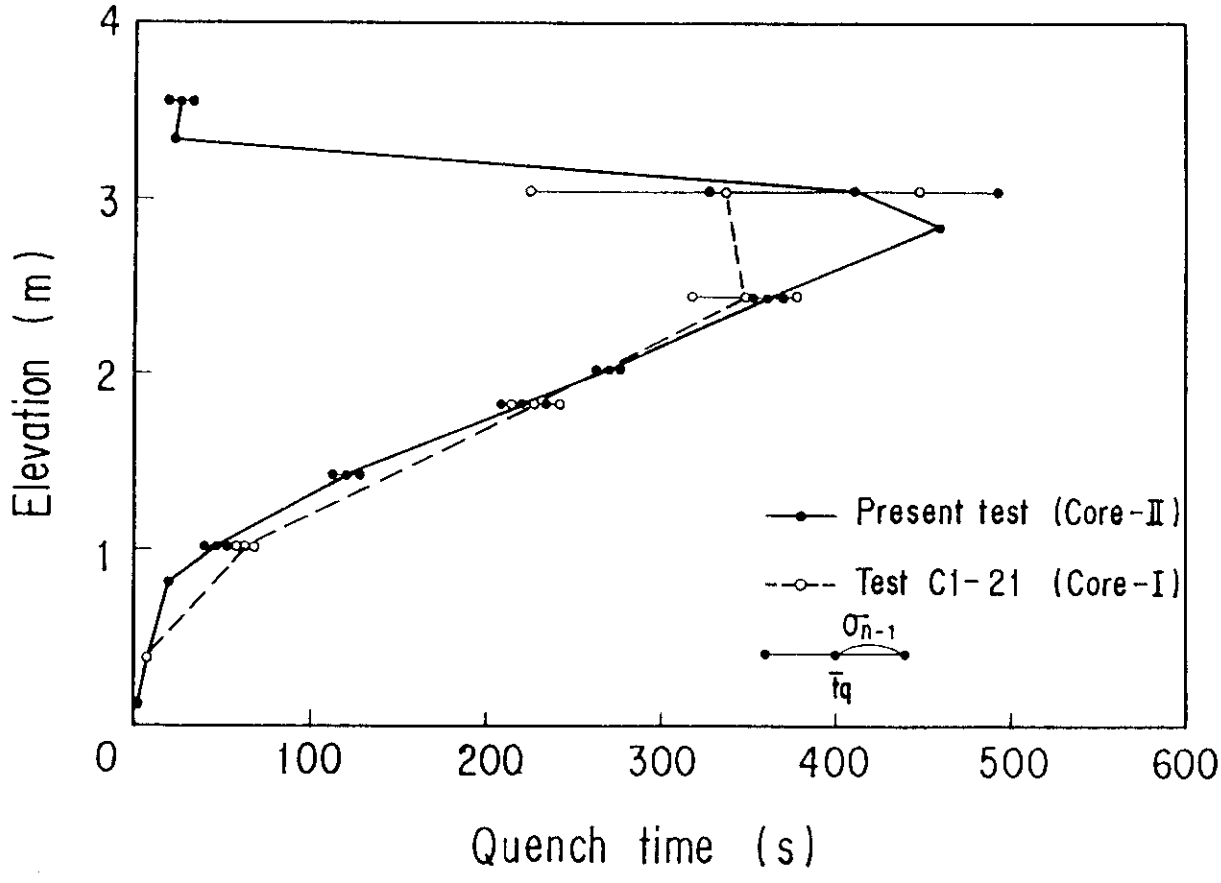

Fig. 3.8 Comparison of quench envelopes in medium power regions (mean value and standard deviation)

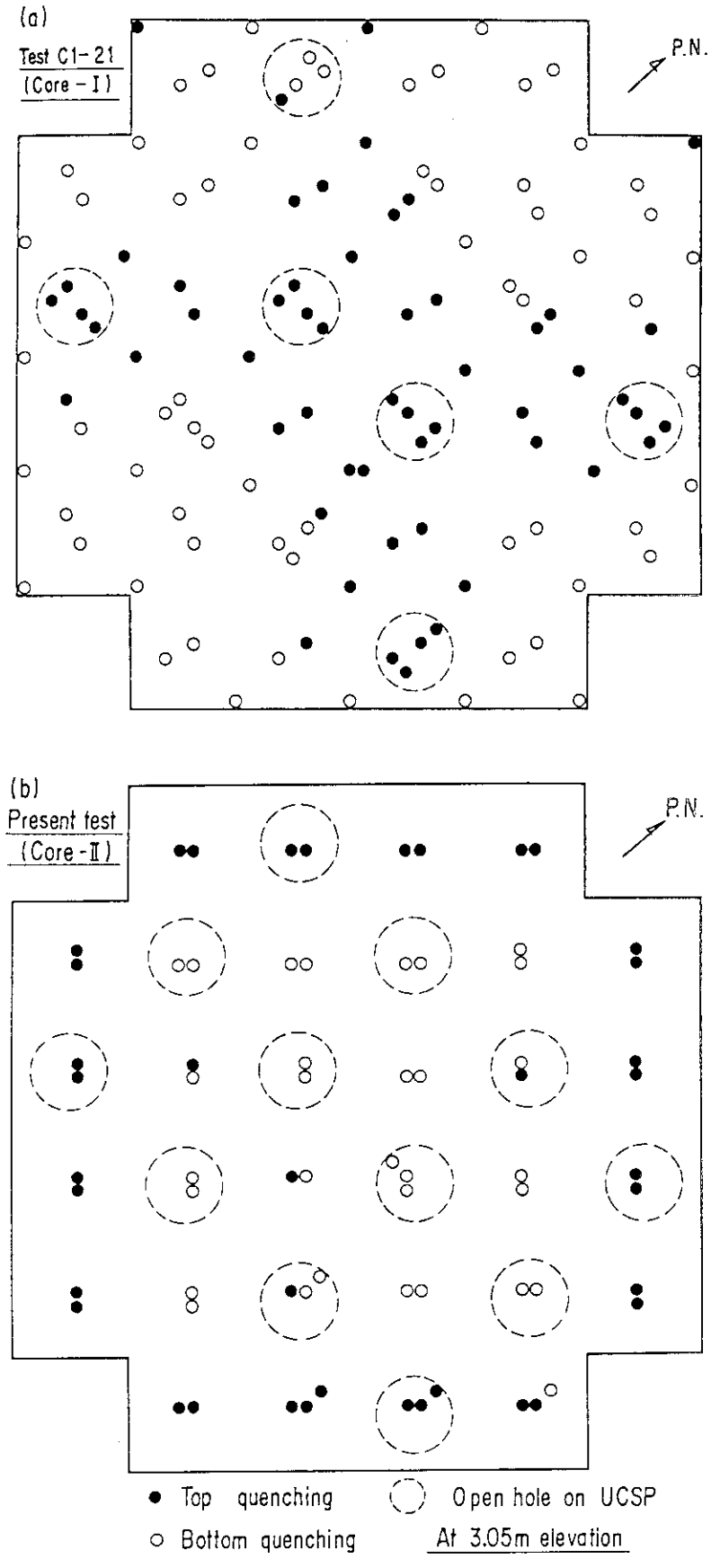

Fig. 3.9 Top quenched rods at 3.05 m elevation for Test C1-21 (a) and present test (b)

4. Conclusions

The data of the CCTF Core-II acceptance test C2-AC2 have been evaluated in order to clarify the differences in thermo-hydrodynamic behavior between the Core-I and the Core-II facilities. The conclusions are as follows:

1. The system behavior observed in the Core-II facility was nearly identical to that observed in the Core-I facility.
2. The core behavior observed in the Core-II facility was also nearly identical to that observed in the Core-I facility except for the top quenching.
3. The differences in the top quenching behavior between the two facilities were as follows:
   (1) The selective occurrence of top quenching below the open holes of the UCSP observed in the Core-I facility was not observed in the Core-II facility.
   (2) Top quenching tended to occur less in the Core-II facility in the region where the initial average linear power density was over 1.69 kW/m.

Acknowledgements

The authors are grateful to Dr. M. Nozawa, Deputy director General of Tokai Research Establishment of JAERI, Dr. S. Katsuragi, Director of Nuclear Safety Research Center, Dr. M. Hirata, Director of Department of Nuclear Safety Research and Dr. K. Hirano, Deputy Director of Department of Nuclear Safety Research, for their hearty suggestions and encouragement.

They would like to express their appreciation to the members of their analysis group, especially, Messrs. T. Iguchi, T. Sudoh, K. Okabe, J. Sugimoto, Dr. H. Akimoto, Messrs. H. Adachi, M. Sobajima, M. Osakabe, A. Ohnuki and Y. Abe, and to Dr. P.J. Schally and Mr. C.E. Winsel, resident engineers from FRG and USNRC, respectively.

They are deeply indebted to Messrs. Y. Fukaya, T. Ohyama, T. Wakabayashi, Y. Niitsuma, K. Nakajima, T. Chiba, J. Matsumoto, K. Komori and H. Sonobe for their contribution to the test conduction.

They also would like to express their thanks to the 2D/3D project members of USA and FRG for valuable suggestions.

References

1. Hirano, K. and Murao, Y.; "Large scale reflood test", J. At. Energy Soc. Japan, (in Japanese), 22 [10], 681 (1980).
2. For instance: Murao, Y. *et al.*; "Findings in CCTF Core-I Test", NUREG/CP-0041, Vol.1, 275 (1983).
3. Murao, Y. *et al.*; "Evaluation Report on CCTF Core-I Reflood Tests C1-16 (Run 25), C1-21 (Run 40) and C1-22 (Run 41) —— Comparison of Results between FLECHT Coupling Tests and FLECHT-SET Tests ——", JAERI-M 83-065 (1983).

Acknowledgements

The authors are grateful to Dr. M. Nozawa, Deputy director General of Tokai Research Establishment of JAERI, Dr. S. Katsuragi, Director of Nuclear Safety Research Center, Dr. M. Hirata, Director of Department of Nuclear Safety Research and Dr. K. Hirano, Deputy Director of Department of Nuclear Safety Research, for their hearty suggestions and encouragement.

They would like to express their appreciation to the members of their analysis group, especially, Messrs. T. Iguchi, T. Sudoh, K. Okabe, J. Sugimoto, Dr. H. Akimoto, Messrs. H. Adachi, M. Sobajima, M. Osakabe, A. Ohnuki and Y. Abe, and to Dr. P.J. Schally and Mr. C.E. Winsel, resident engineers from FRG and USNRC, respectively.

They are deeply indebted to Messrs. Y. Fukaya, T. Ohyama, T. Wakabayashi, Y. Niitsuma, K. Nakajima, T. Chiba, J. Matsumoto, K. Komori and H. Sonobe for their contribution to the test conduction.

They also would like to express their thanks to the 2D/3D project members of USA and FRG for valuable suggestions.

References

1. Hirano, K. and Murao, Y.; "Large scale reflood test", J. At. Energy Soc. Japan, (in Japanese), 22 [10], 681 (1980).
2. For instance: Murao, Y. *et al.*; "Findings in CCTF Core-I Test", NUREG/CP-0041, Vol.1, 275 (1983).
3. Murao, Y. *et al.*; "Evaluation Report on CCTF Core-I Reflood Tests C1-16 (Run 25), C1-21 (Run 40) and C1-22 (Run 41) —— Comparison of Results between FLECHT Coupling Tests and FLECHT-SET Tests ——", JAERI-M 83-065 (1983).

Appendix

Appendix A

Definitions of Tag IDs

Figure List

1. Definition of Tag. ID for clad surface temperatures and heat fransfer coefficients

Notation : TEnnYlm (temperature)

HTEmmYlm (heat transfer coefficient)

nn : Bundle number (see Fig. A.1)

m : Elevation number

	Elevation (m)	Axial power factor
3	0.38	0.651
5	1.015	1.147
7	1.83	1.40
9	2.44	1.256
A	3.05	0.854

2. Definition of power zone and boundle number

See Fig. A.1

3. Definition of Tag. ID for void fraction

See Fig. A.2

4. Definition of Tag. ID for average linear power of heater rod in each power unit zone

See Fig. A.3

5. Definition of Tag. ID for differential pressure through downcomer, upper plenum, core and lower plenum

See Fig. A.4

6. Definition of Tag. ID for differential pressure through intact and broken loop and broken cold leg nozzle

See Fig. A.5

7. Definition of Tag. ID for fluid temperature in inlet and outlet plenum and secondary side of steam generator

See Fig. A.6

8. Definition of Tag. ID for ECC water injection rate, ECC water temperature and vented steam flow rate

See Fig. A.7

9. Definition of initial temperature, turnaround temperature quench temperature, temperature rise, turnaround time and quench time. (See Fig. A.8

T_i : Initial temperature (Clad surface temperature at reflood initiation)

T_t : Turnaround temperature (Maximum clad surface temperature in each temperature history)

ΔT_r : Temperature rise ($= T_t - T_i$)

T_q : Quench temperature (Clad surface temperature at quenching)

10. Definition of quenching

See Fig. A.8

Quench time t_t is determined as

$$t_t = i \times \Delta t - \text{(reflood initiation time)}$$

In above equation, i is determined by the following criteria.

(1) Clad surface temperature is high, compared with the saturation temperature.

$$T_i > T_{sat} + \Delta T_1$$

(2) Decreasing rate of clad surface temperature is large.

$$\frac{T_{i+1} - T_i}{\Delta t} < - C_{st}$$

(3) Clad surface temperature falls around the saturation temperature.

$$T_{i+k_1} \leq T_{sat} + \Delta T_1$$

(4) If the determined i is inadequate, the value i is manually re-determined.

Δt : Data sampling period (s)

T_i : Clad surface temperature (K)

T_{sat} : Saturation temperature at the pressure in upper plenum (K)

ΔT_1 : Temperature discrepancy (K)
Default value = 50.0

C_{st} : Decreasing rate of clad surface temperature (K/S)
Default value = 25.0

k_1 : Number of referred data (-)
Default value = 6

11. Definition of Tag. ID for core inlet mass flow rate, time-integral core inlet mass flow rate and carry-over rate fraction

(1) Core inlet mass flow rate : $\dot{m}_F$
Notation : MLCRI□ (□ = N, 1 or 11)

(2) Time-intefral core inlet mass flow rate : $\int \dot{m}_F dt$
Notation : IMLCRI□ (□ = N, 1 or 11)

(3) Carry-over rate fraction : $(\dot{m}_F - \dot{m}_{CR})/\dot{m}_F$
Natation : CRF□ (□ = N, 1 or 11)

where $\dot{m}_F$: Core inlet mass flow rate (See item 12)

$\dot{m}_{CR}$: Water accumulation rate in core

Suffix	$\dot{m}_F$ base on
N	Eq.(A.2)
1	Eq.(A.1) with K=15
11	Eq.(A.1) with K=20

12. Evaluation of core inlet mass flow rate

The reflood phenomena is a relatively slow transient and a steady state condition can be applied. In a steady state condition, based on the mass balance relations of the system, the core flooding mass flow rates $\dot{m}_F$s can be written as follows:

By using the data measured at the downstream of the core inlet, $\dot{m}_F$ is derived as,

$$\dot{m}_F = \dot{m}_C + \dot{m}_U + \dot{m}_B + \Sigma \dot{m}_I \quad , \qquad (A.1)$$

where $\dot{m}_C$ and $\dot{m}_U$ are the mass accumulation rates in the core and the upper plenum respectively. The $\dot{m}_B$ and $\dot{m}_I$ are the mass flow rates in the broken loop and the intact loop, respectively.

By using the data measured at the upstream of the core inlet, $\dot{m}_F$ is derived as,

$$\dot{m}_F = \Sigma \dot{m}_{DL} - \dot{m}_D - \dot{m}_O + \dot{m}_{ECC/LP} \quad , \tag{A.2}$$

where $\dot{m}_{DL}$ and $\dot{m}_O$ are the mass flow rates of the water flowing into and overflowing from the downcomer, $\dot{m}_{ECC/LP}$ and $\dot{m}_D$ are the mass flow rate of the ECC water injected into the lower plenum and the water accumulation rate in the dowmcomer respectively.

The $\dot{m}_I$s and $\dot{m}_B$ can be obtained from the pressure drops at the pump simulators with orifices by assuming the K-factor of the orifice is constant. The values of $\dot{m}_C$, $\dot{m}_D$ and $\dot{m}_U$ can be evaluated with the differential pressure ΔP_C, ΔP_D and ΔP_U, respectively, as follows:

$$\dot{m}_n = d(\Delta P_n S_n/g)/dt \quad (n : C, D, U) \quad , \tag{A.3}$$

where g is the gravitational acceleration and S_n is the cross sectional area. The value of $\dot{m}_O$ can be obtained from the liquid level X in the Containment tank 1 as,

$$\dot{m}_O = d(X\rho_\ell S_o)/dt \quad , \tag{A.4}$$

where ρ_ℓ is the liquid density and S_o is the cross sectional area of the containment tank 1.

The value of $\dot{m}_{DL}$, $\dot{m}_{DV}$ and h, which are liquid flow rate, steam flow rate and enthalpy of two phase mixture downstream each ECC port respectively, are obtained from the following mass and energy balance relations at each ECC port under the assumption of thermal equilibrium:

$$\dot{m}_{DV} + \dot{m}_{DL} = \dot{m}_{ECC} + \dot{m}_I \quad , \tag{A.5}$$

$$(\dot{m}_{DV} + \dot{m}_{DL})i = \dot{m}_{ECC}h_{ECC} + \dot{m}_I h_I \quad , \tag{A.6}$$

$$\text{if} \quad h_g \geq h \geq h_\ell \ , \ (\dot{m}_{DV} + \dot{m}_{DL})h = \dot{m}_{DV}h_g + \dot{m}_{DL}h_\ell$$

$$\text{if} \quad h \geq h_g \quad , \ \dot{m}_{DL} = 0 \quad , \tag{A.7}$$

$$\text{if} \quad h \geq h_\ell \quad , \ \dot{m}_{DV} = 0$$

where h is enthalpy of fluid and h_ℓ and h_g are enthalpies of liquid and steam at the saturation temperature, respectively.

The fluid temperatures can be measured with thermocouples immersed in the fluid and the enthalpies h_I and h_{ECC} can be estimated.

Mass balance calculations were performed with Eqs. (A.1) and (A.2). The K-factor of the orifice in the pump simulator was evaluated in the following two ways.

The K-factor of 20 was obtained with the steam and water single phase calibration tests using the flow meter and spool piece data. The K-factor of 15 was obtained with the Pitot tube measurement in a typical reflood condition assuming the flat velocity profile in the pipings. In the differentiation, higher frequency components of the data tends to be amplified more. Therefore, in the differentiation of the differential pressure data, the smoothing procedure was used to suppress the high frequency components of the data.

In the Acc injection period, the calculated $\dot{m}_F$s with Eqs. (A.1) and (A.2) are significantly different from each other. This discrepancy may be caused by inaccuracy of the mass flow rate injected into the system and by the unaccounting of the storage of water in the cold leg pipe. The former might be introduced from the slow time response of the flow meter (time constant 1 second) and the change of the gas volume in the injection line. In this period, especially before the steam generation from the core becomes noticeable, the mass flow rate, $\dot{m}_F$, calculated with Eq. (A.1) is probably reasonable, since the calculation uses the increasing rates of the masses in the core and the upper plenum and their accuracy is good enough for our estimation.

In the LPCI injection period, the calculated $\dot{m}_F$s are slightly different from each other. Judging from the time-integral values of both $\dot{m}_F$s, their average values are nearly proportional. The discrepancy was inferred to be caused by the disregard of the bypass of steam and liquid from the upper plenum without going through the hot legs in the calculation with Eq. (A.1). And additionally the discrepancy was caused by the disregard of the steam generation in the downcomer due to the hot wall of the pressure vessel in the calculation with Eq. (A.2). It was estimated that the disregard of the downcomer steam generation causes the error of 0.25 kg/s on predicted $\dot{m}_F$. The estimation was made by comparing the results of the tests with hot and cold downcomer conditions.

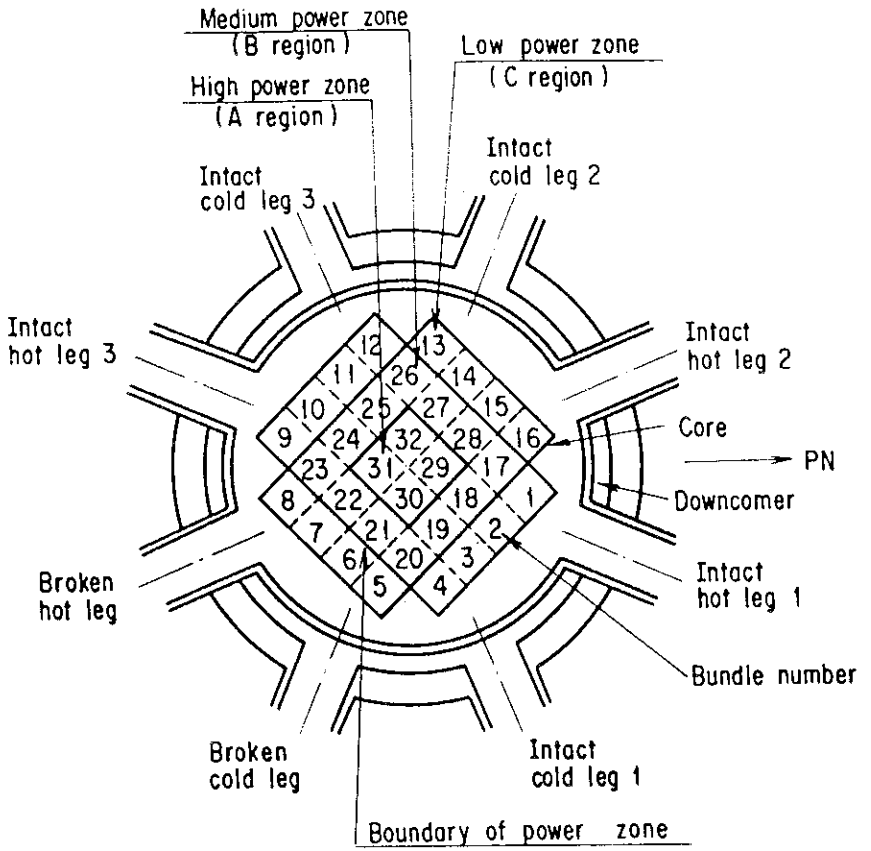

Fig. A. 1 Definition of power zones and bundle numbers

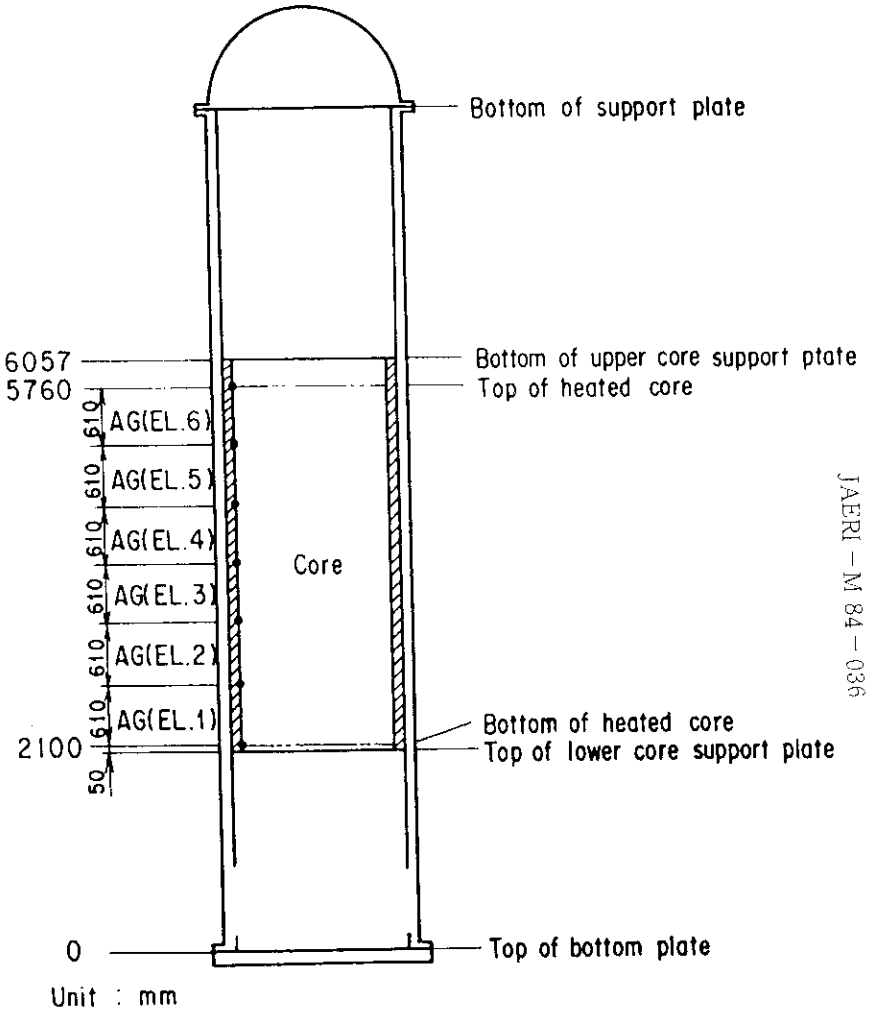

Fig. A. 2 Definition of Tag ID for void fraction (AG(EL. 1) ~ AG(EL. 6))

JAERI — M 84 — 036

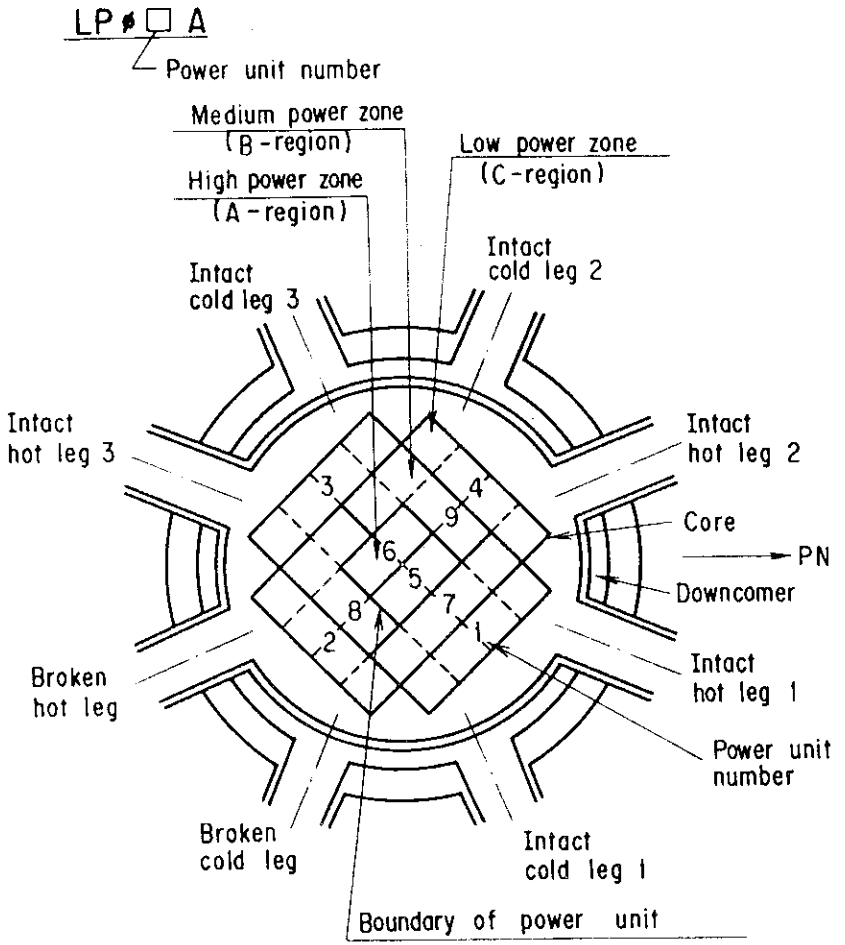

Fig. A. 3 Definition of Tag. ID for average linear power of heater rod in each power unit zone
(LP01A ~ LP09A)

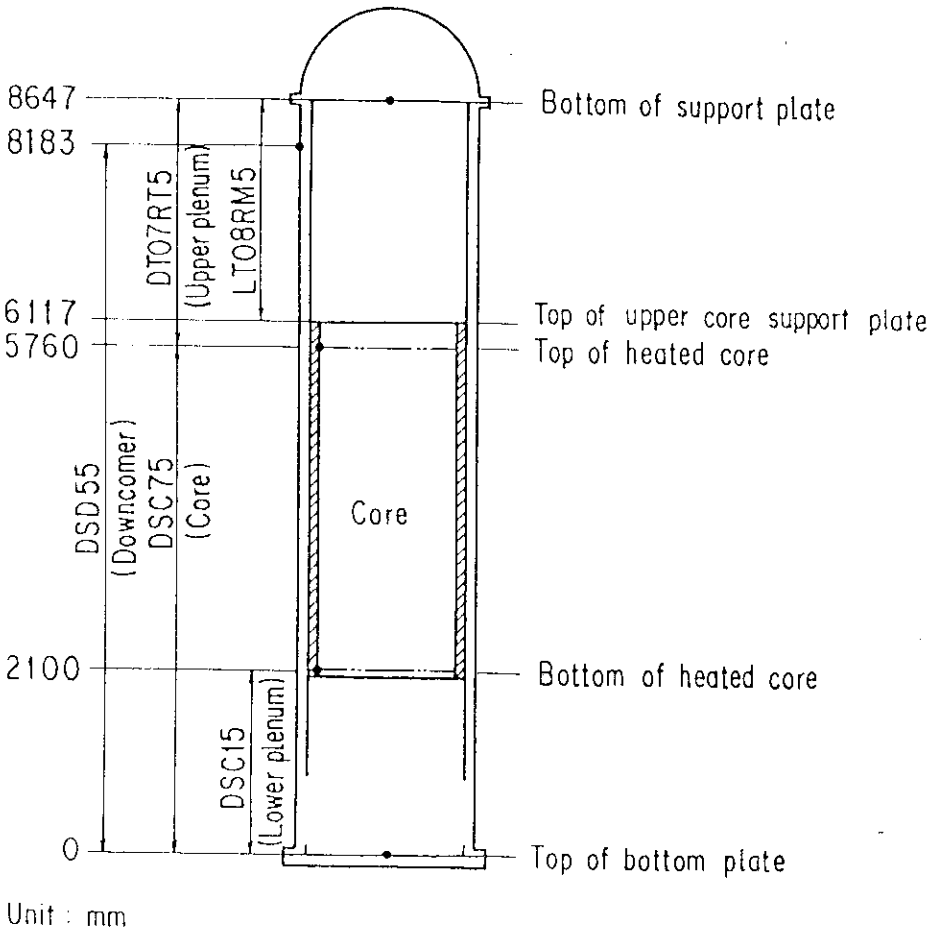

Fig. A. 4 Definition of Tag. ID for differential pressure through downcomer, upper plenum, core, and lower plenum
(DSD55, DT07RT5, LT08RM5, DSC75, DSC15)

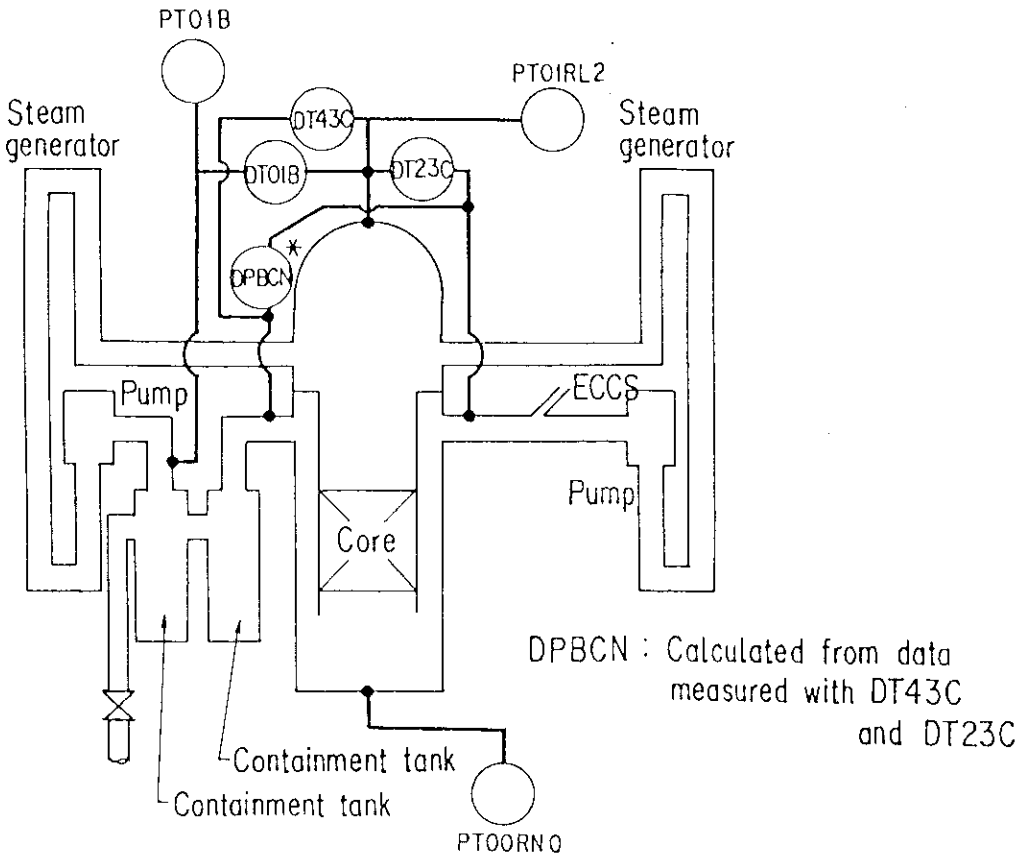

Fig. A. 5 Definition of Tag. ID for pressures in upper and lower plena and containment tank 2 (PT01RL2, PT00RN0, PT01B) and for differential pressure through intact and broken loop and broken cold leg nozzle (DT23C, DT01B, DPBCN)

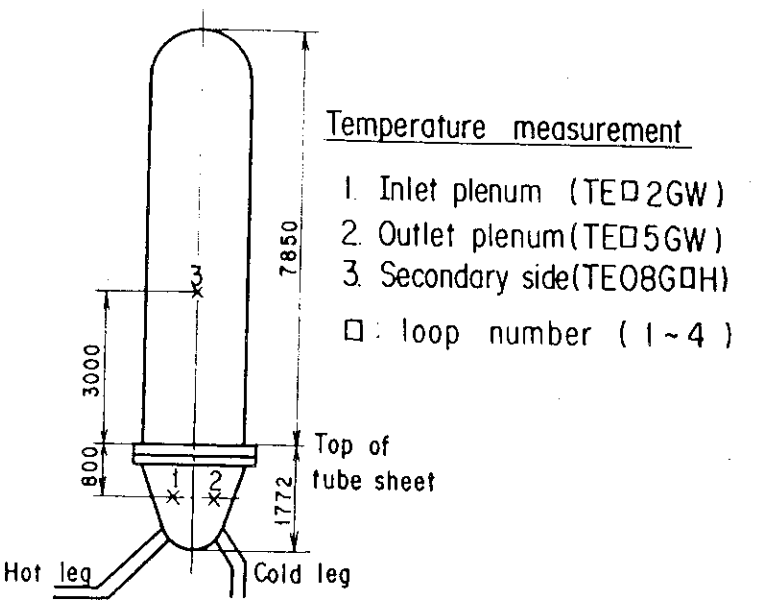

Fig. A. 6 Definition of Tag. ID for fluid temperature in inlet and outlet plenum and secondary of steam generator (TE□2GW, TE□5GW, TE08G□H)

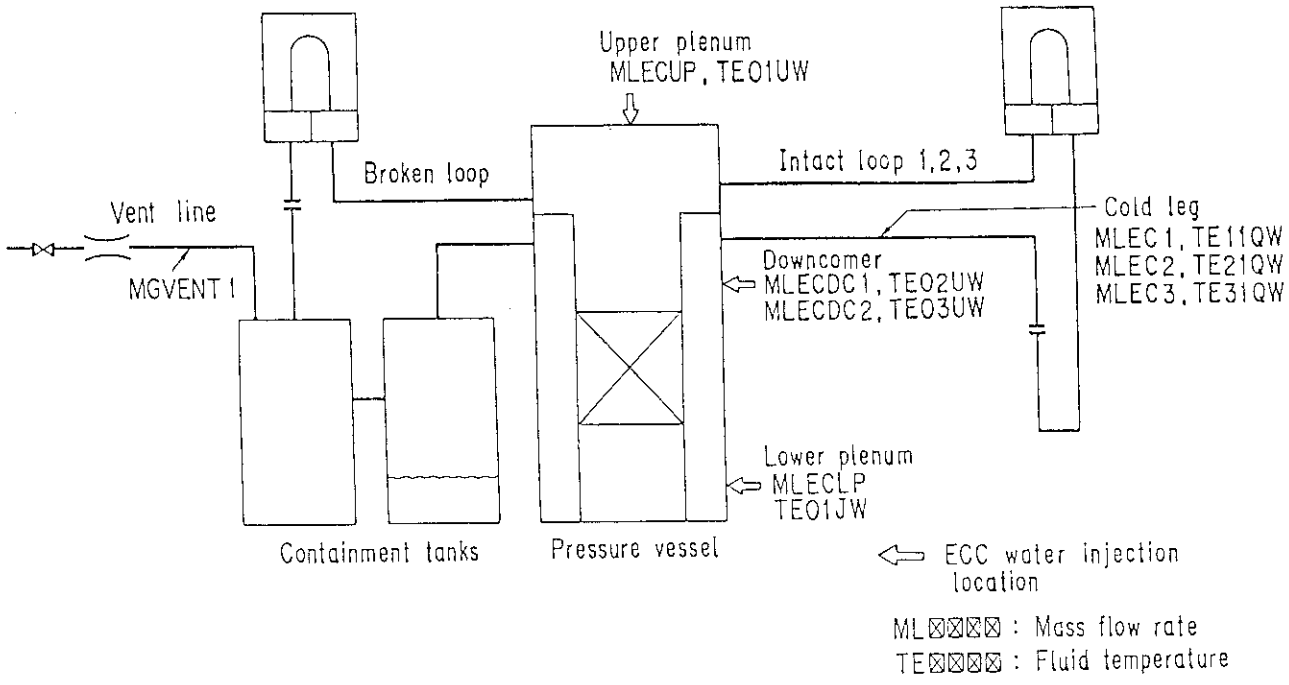

Fig. A. 7 Definition of Tag. ID for ECC water injection rate, ECC water temperature and vented steam flow rate

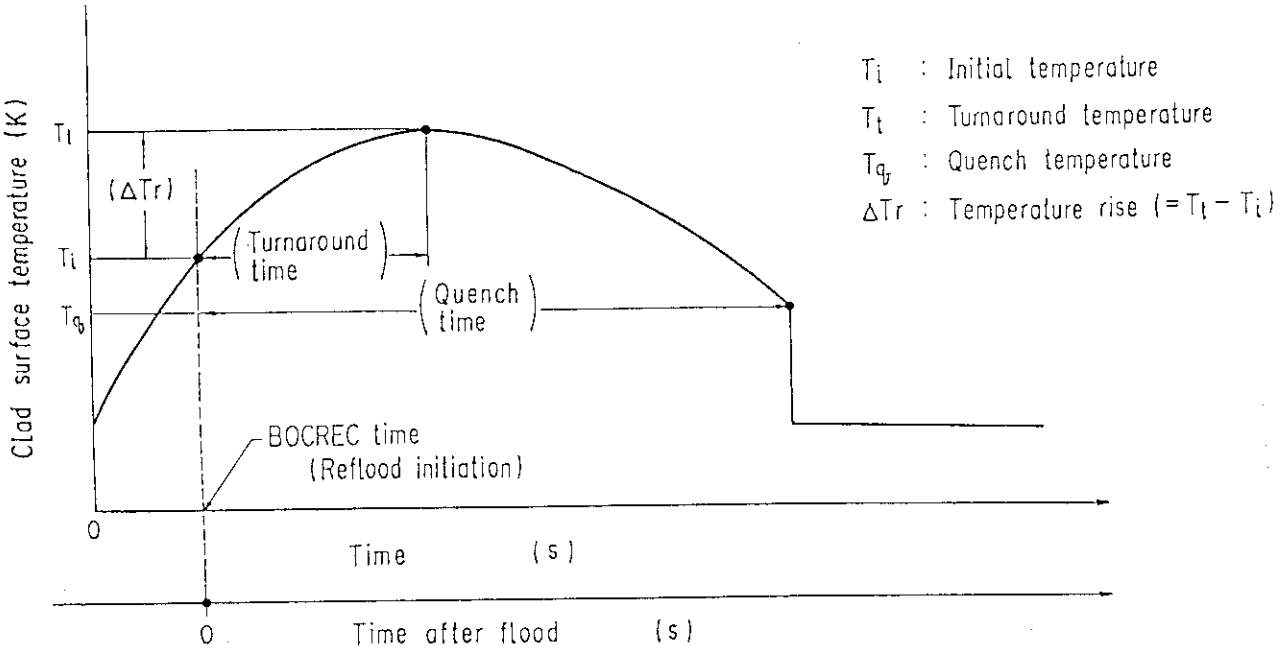

Fig. A. 8 Definition of initial temperature, turnaround temperature, quench temperature, temperature rise, turnaround time and quench time

Appendix B

Selected data of CCTF Test C2-AC2 (Run 52)

Figure List

Fig. B.25 Time-integral mass flooded into core evaluated with Eqs. (A.1) and (A.2).

Fig. B.26 Carry-over rate fraction.

Fig. B.27 Core inlet subcooling.

Fig. B.28 Exhausted mass flow rate from containment tank 2.

Note:

In the Test C2-AC2, the core differential pressure measurement was not successful, and hence, the core differential pressure data are judged to be unreliable. Therefore, the reduced data obtained by using the core differential pressures are also unreliable. The data judged unreliable are, however, presented in this Appendix. The figure Nos. and Tag IDs of these data are listed below.

Figure No.	Tag ID
B.17	AG(EL.1), AG(EL.2), AG(EL.3)
	AG(EL.4), AG(EL.5), AG(EL.6)
B.18	DT07RT5
B.19	DSC75, DSC15
B.24	MLCRI1, MLCRI11
B.25	IMLCRI1, IMLCRI11
B.26	CRF1, DRF11

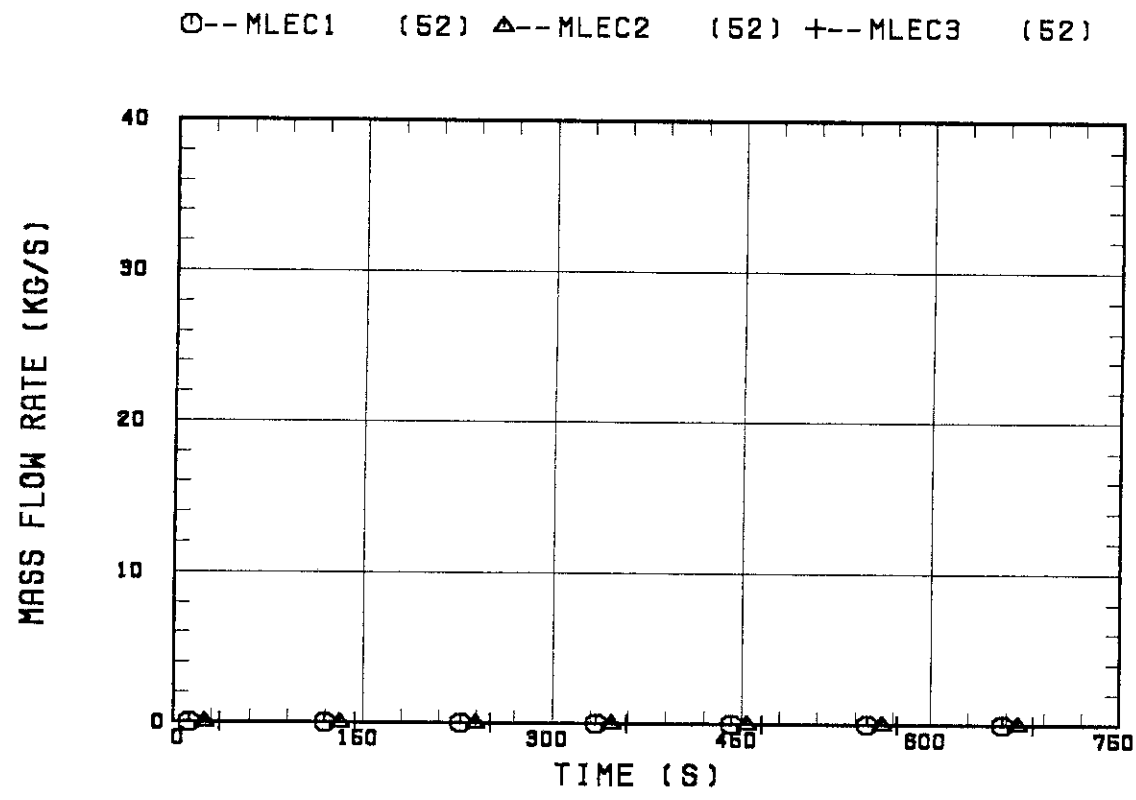

Fig. B.1 ECC water injection rates into the primary system.

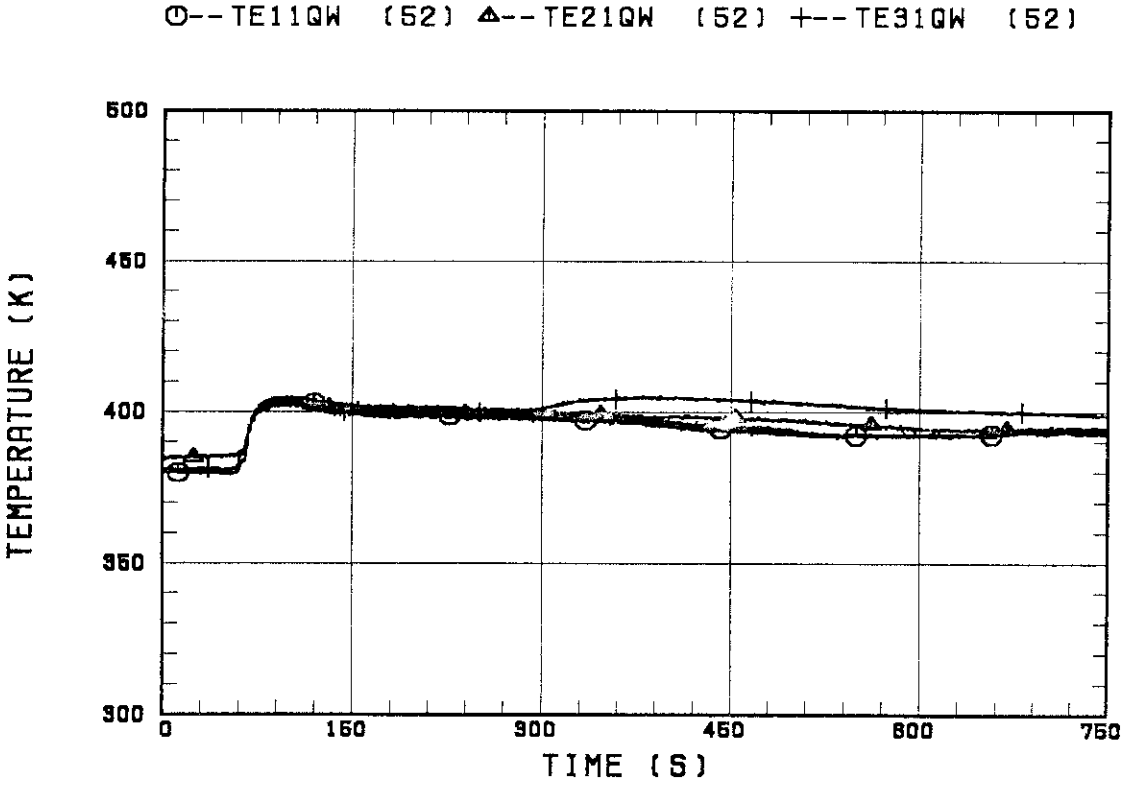

Fig. B.2 ECC water temperature.

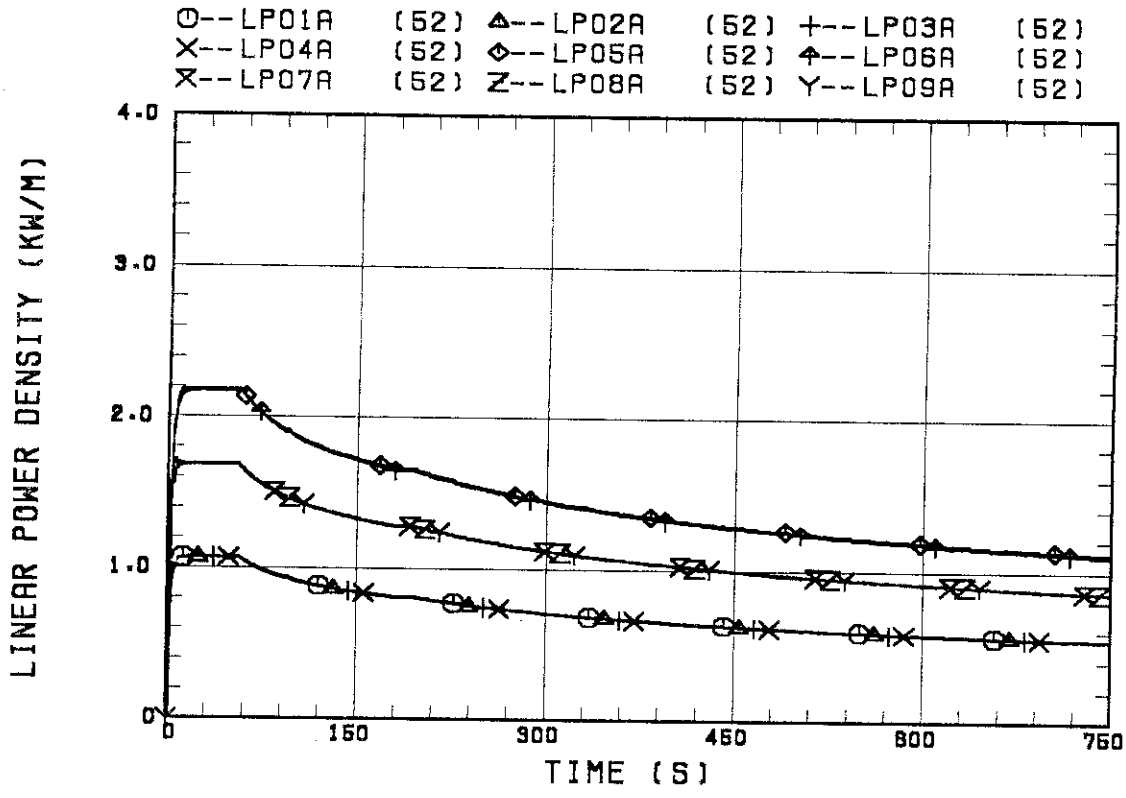

Fig. B.3 Average linear power of heater rod in each power unit zone.

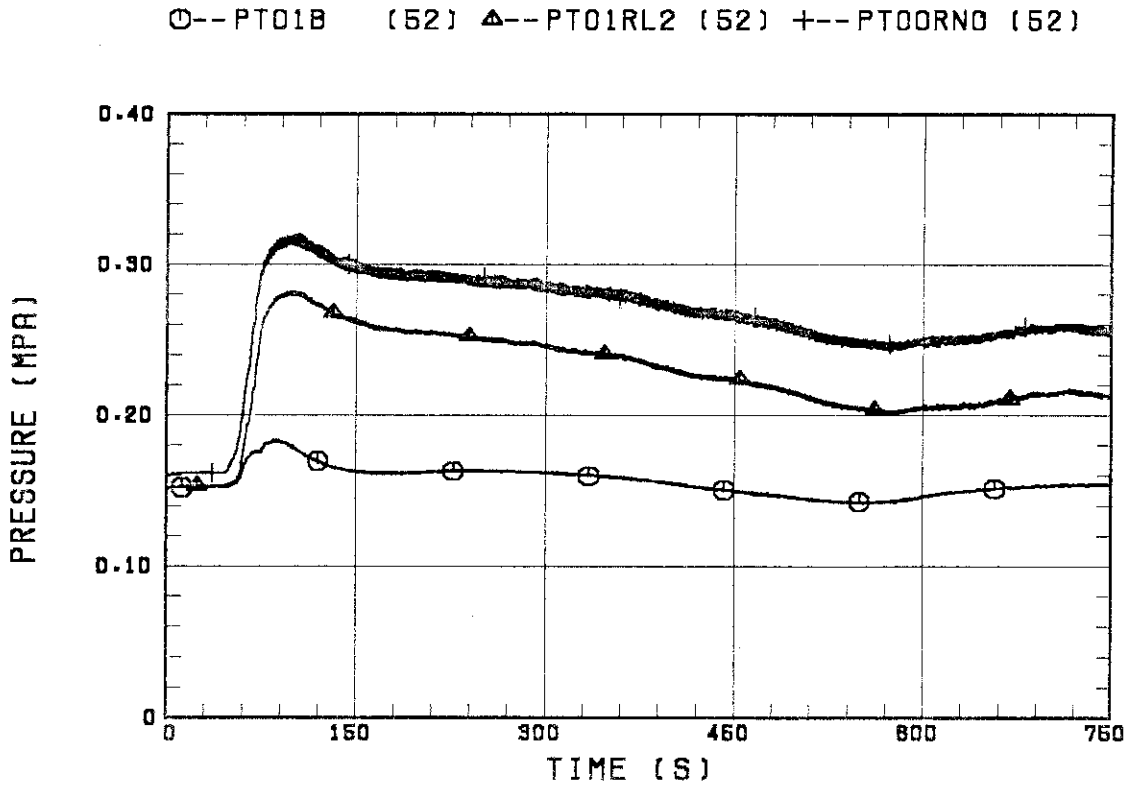

Fig. B.4 Pressure history in containment tank 2, upper plenum and lower plenum.

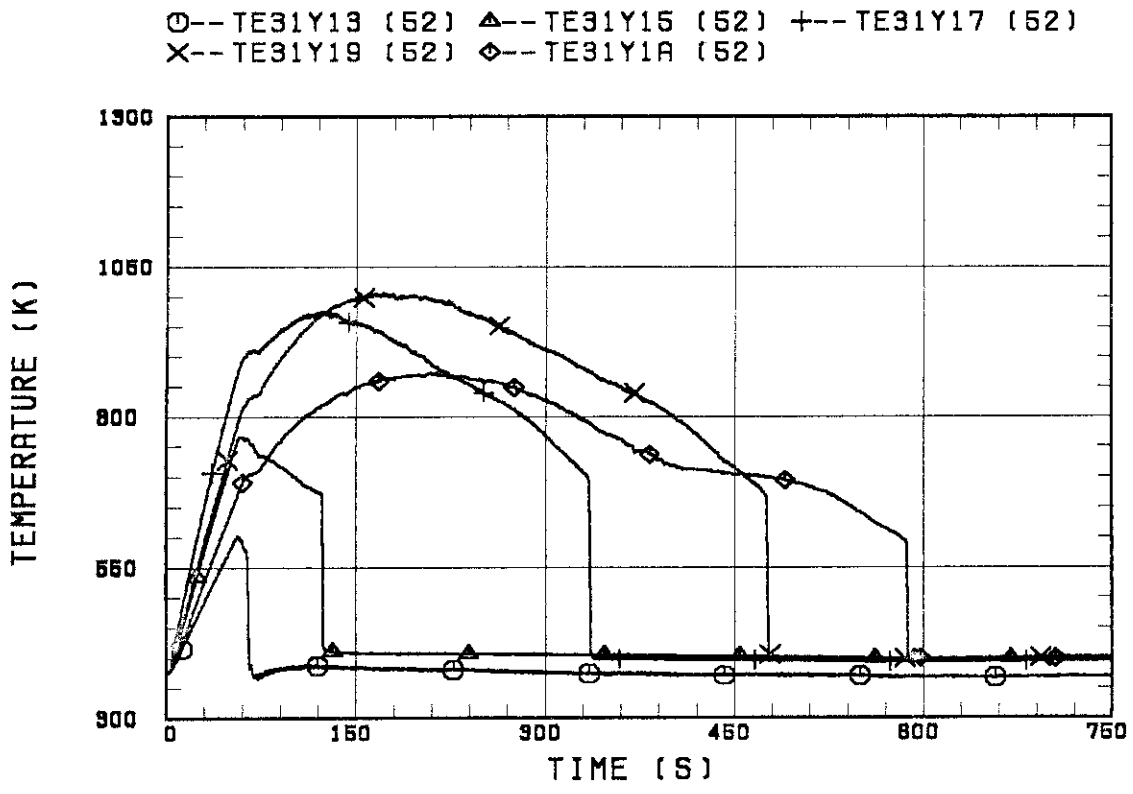

Fig. B.5 Clad surface temperature at various elevations along a heater rod in high power region (A region).

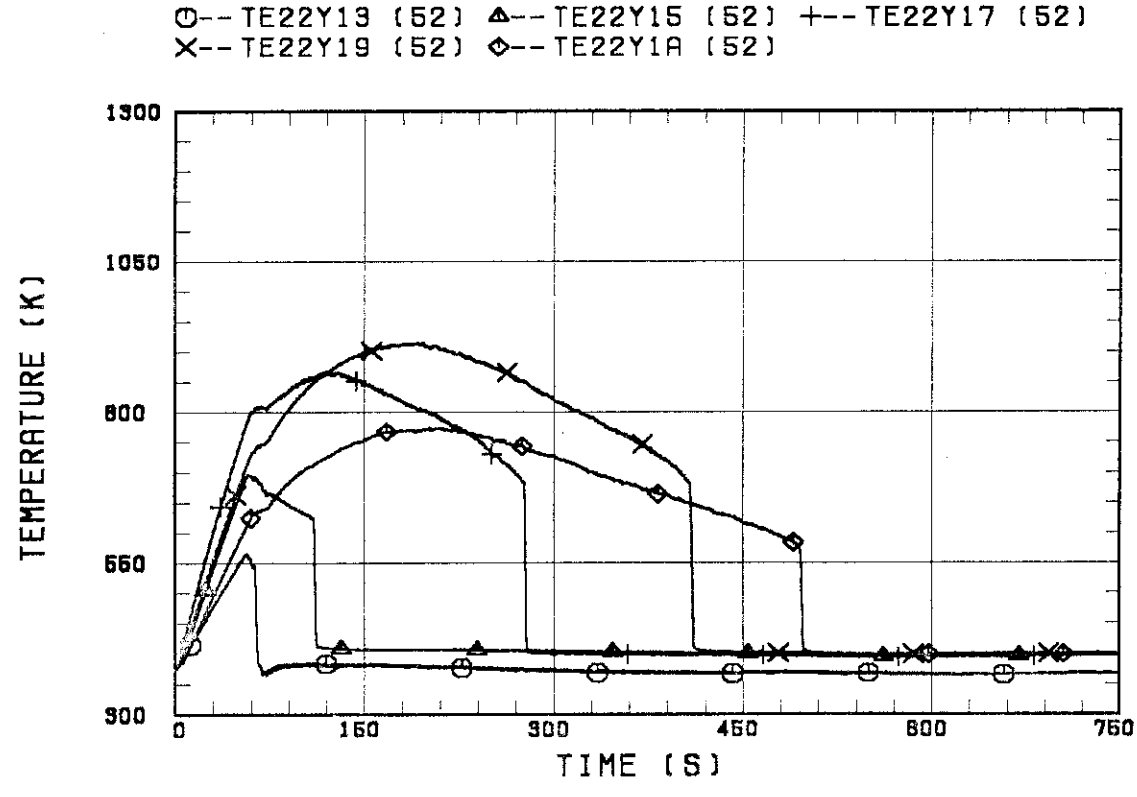

Fig. B.6 Clad surface temperature at various elevations along a heater rod in medium power region (B region).

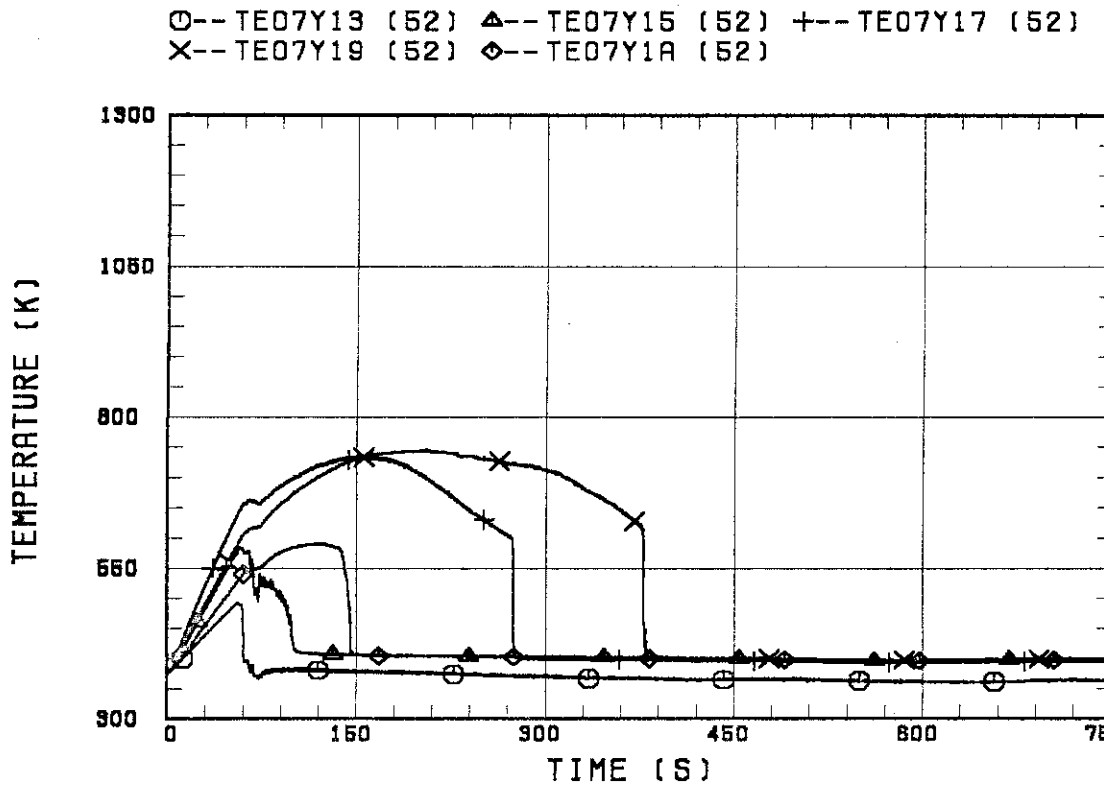

Fig. B.7 Clad surface temperature at various elevations along a heater rod in low power region (C region).

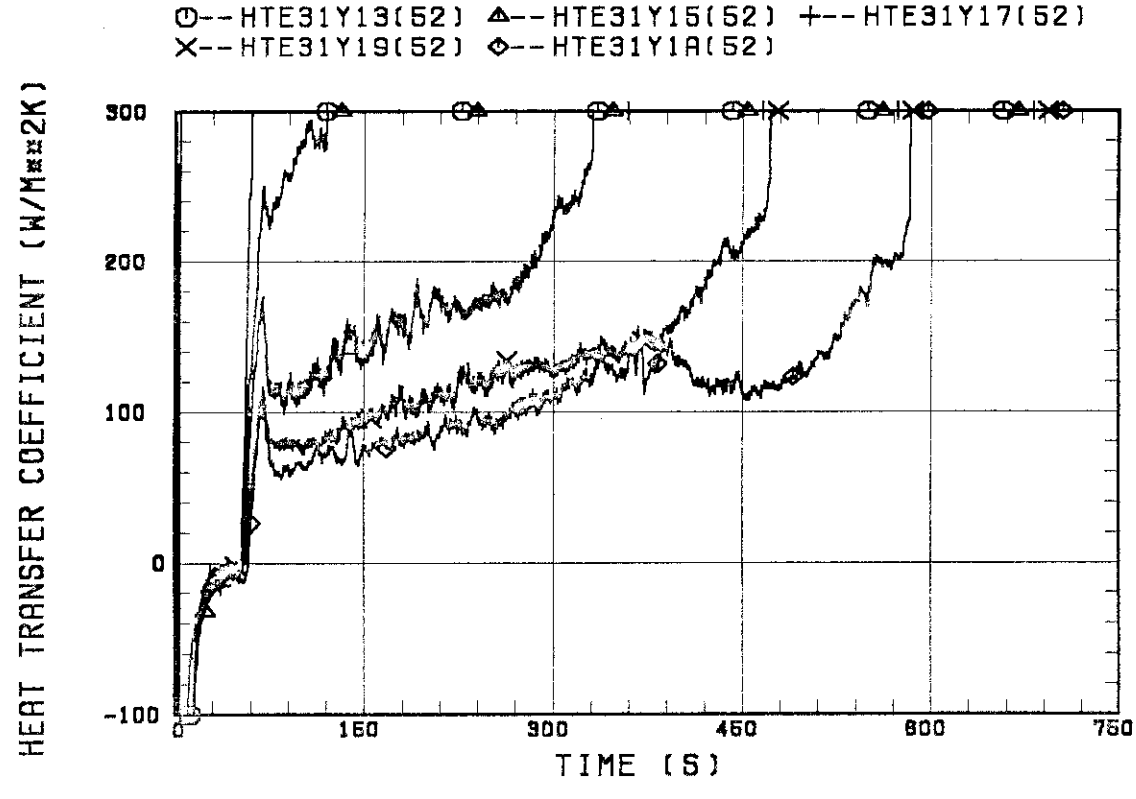

Fig. B.8 Heat transfer coefficient at various elevations along a heater rod in high power region (A region).

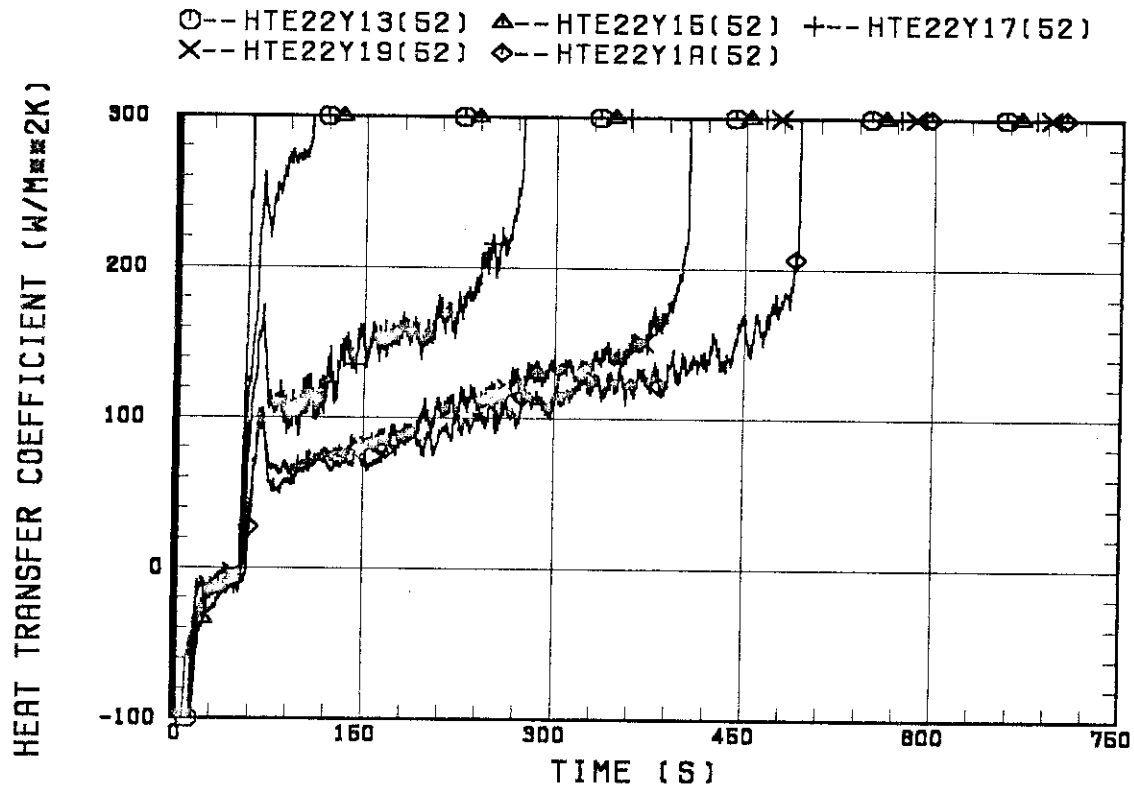

Fig. B.9 Heat transfer coefficient at various elevations along a heater rod in medium power region (B region).

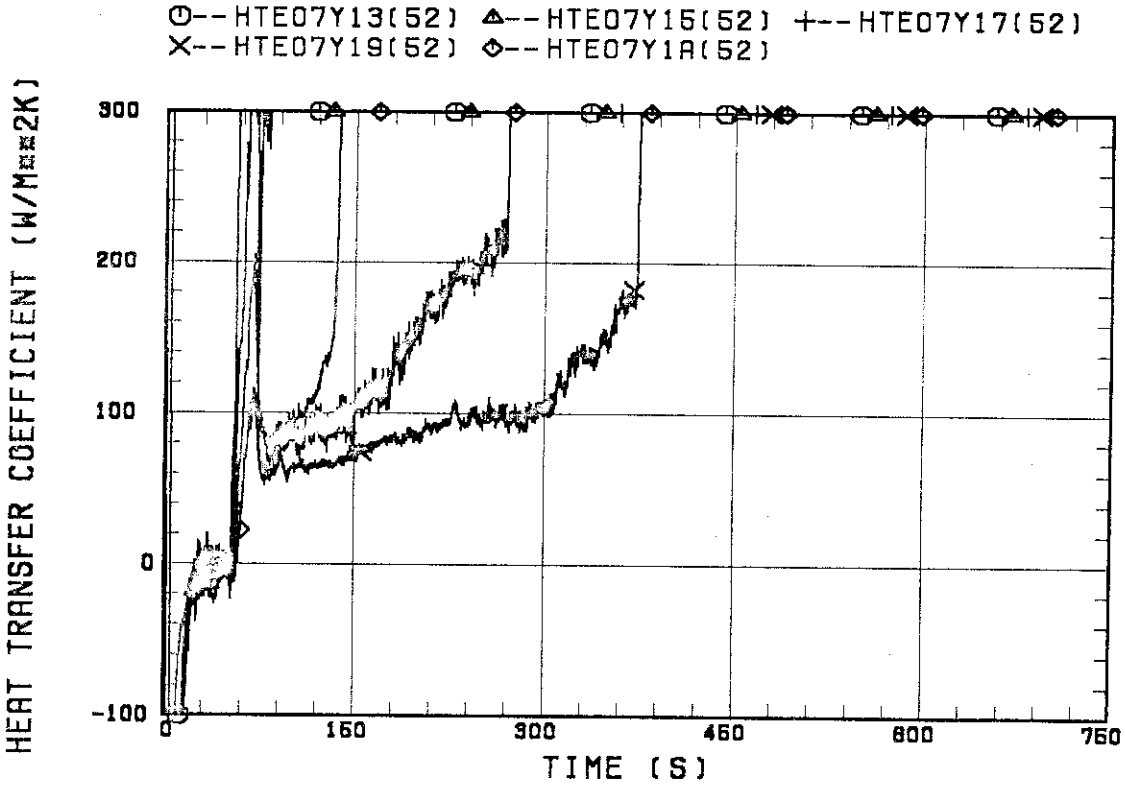

Fig. B.10 Heat transfer coefficient at various elevations along a heater rod in low power region (C region).

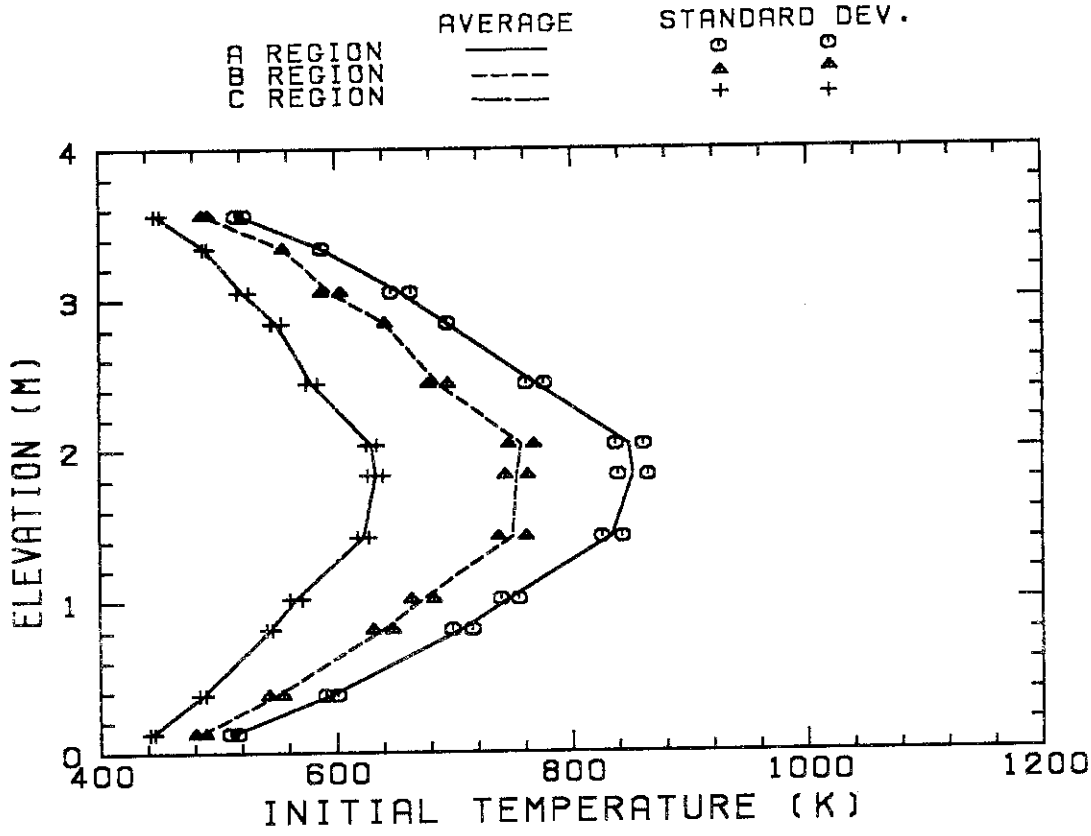

Fig. B.11 Initial clad surface temperature.

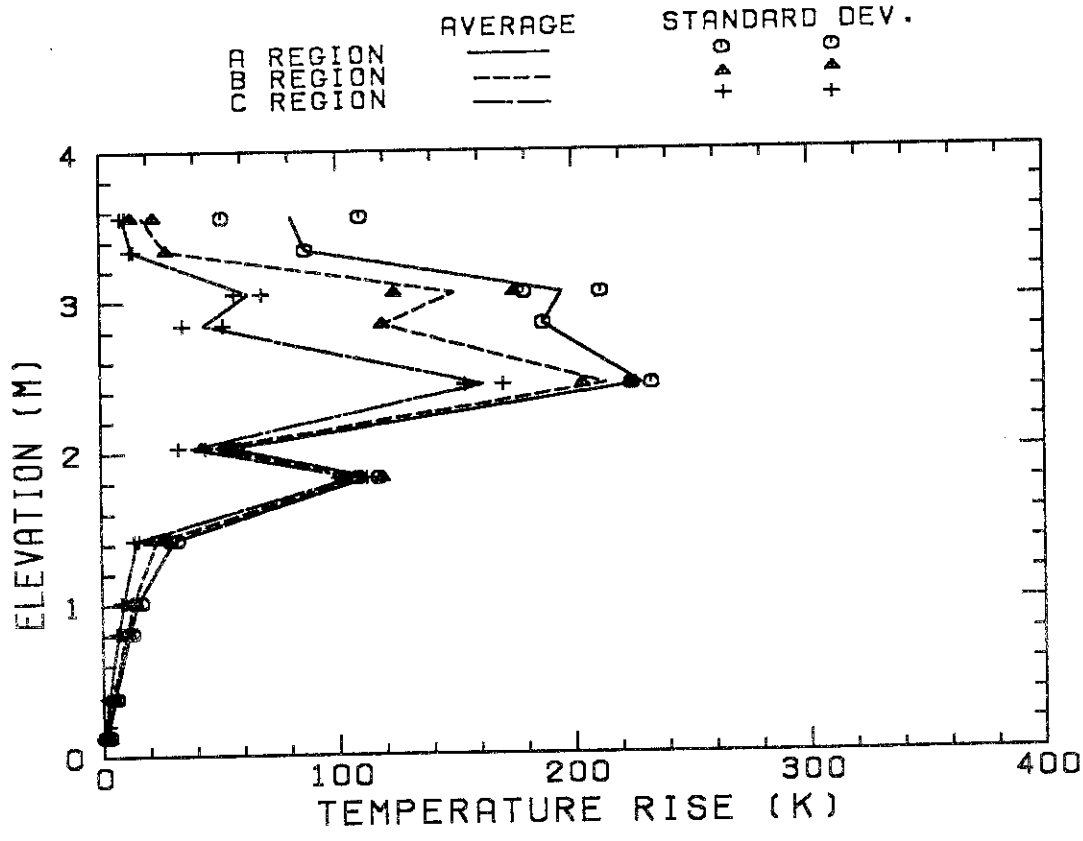

Fig. B.12 Temperature rise.

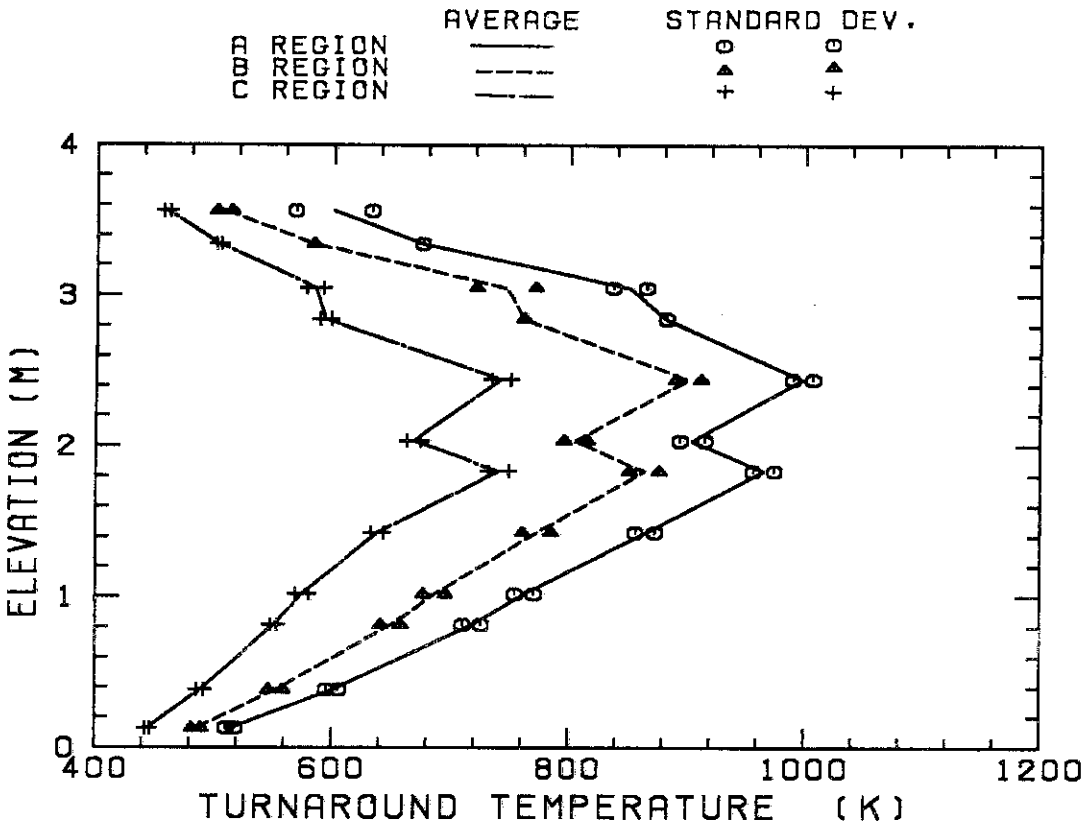

Fig. B.13 Turnaround temperature.

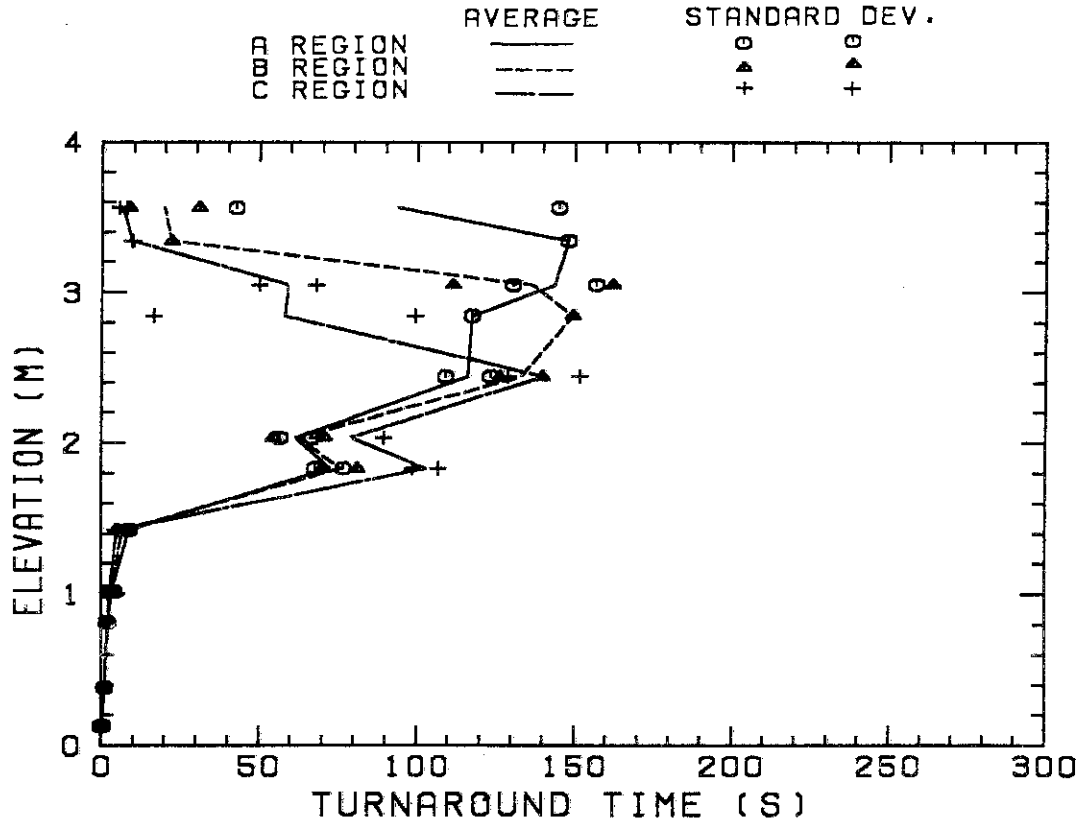

Fig. B.14 Turnaround time.

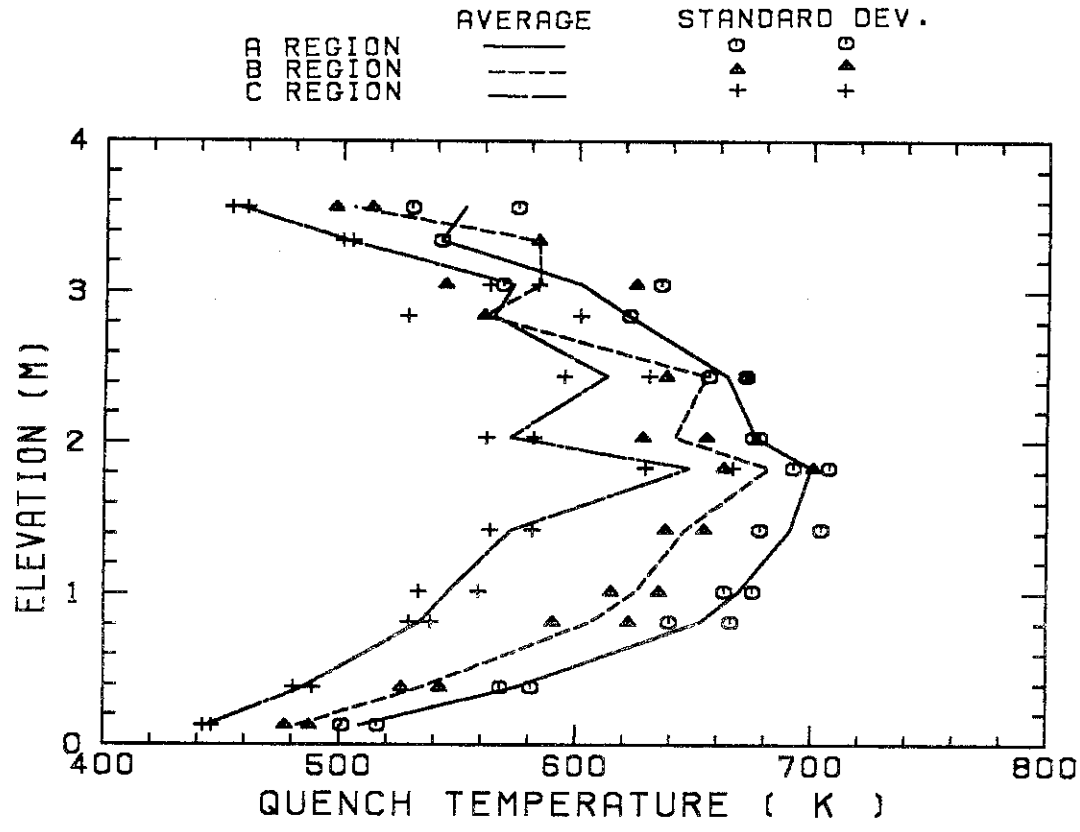

Fig. B.15 Quench temperature.

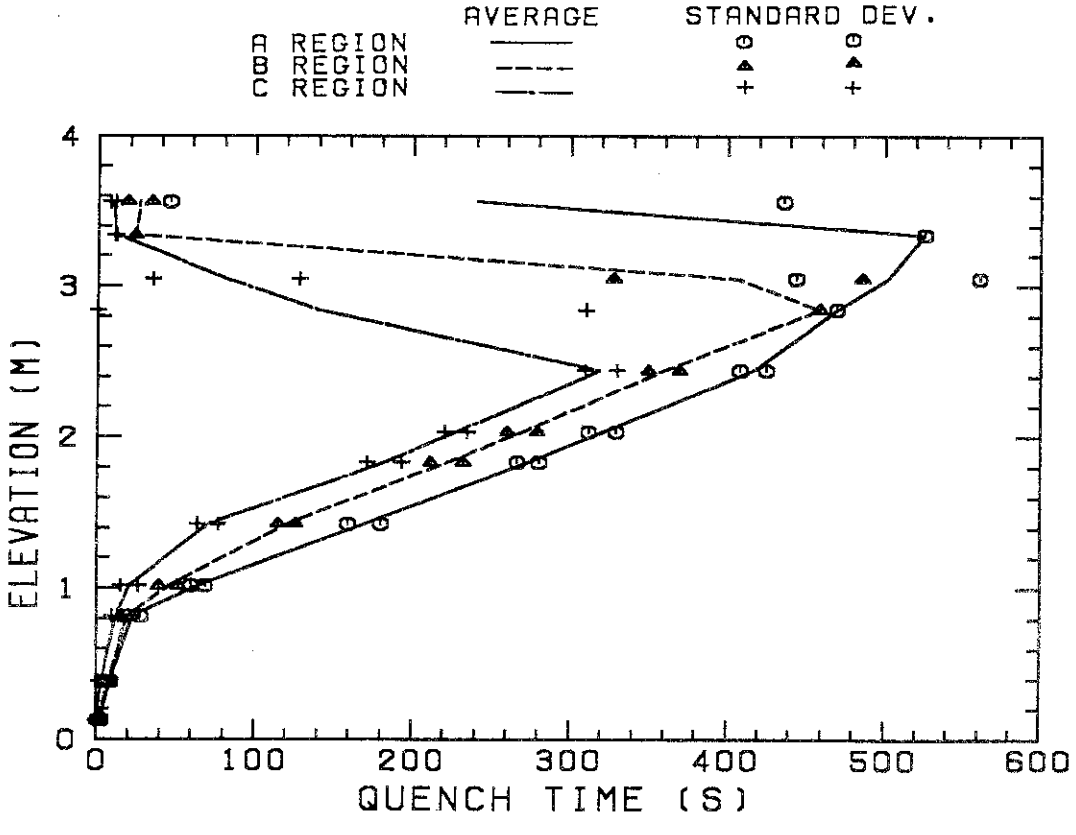

Fig. B.16 Quench time.

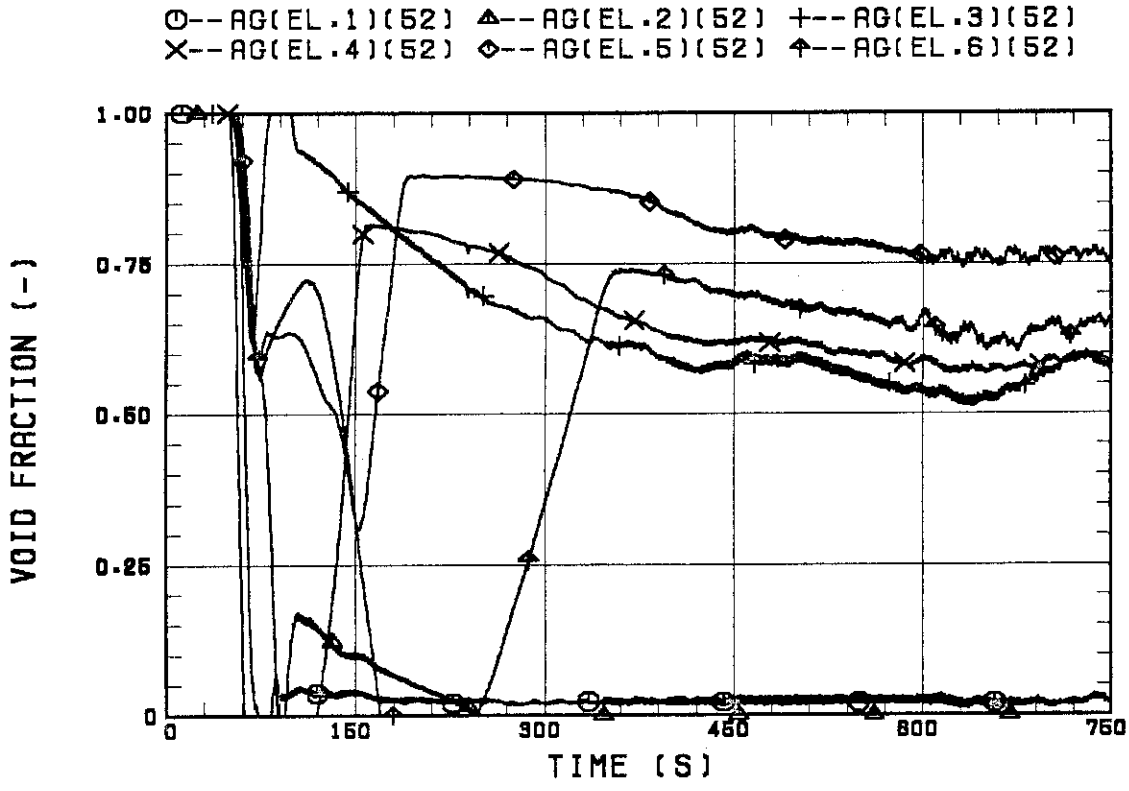

Fig. B.17 Void fraction in core.

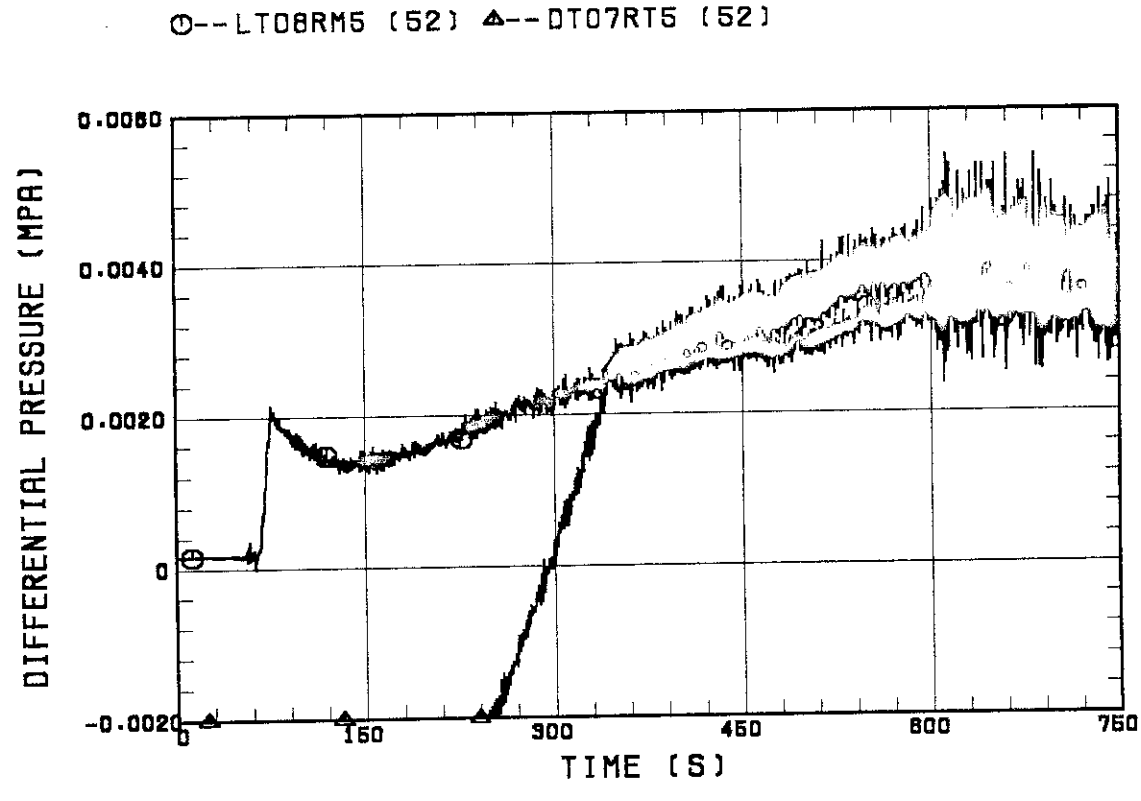

Fig. B.18 Differential pressure through upper plenum.

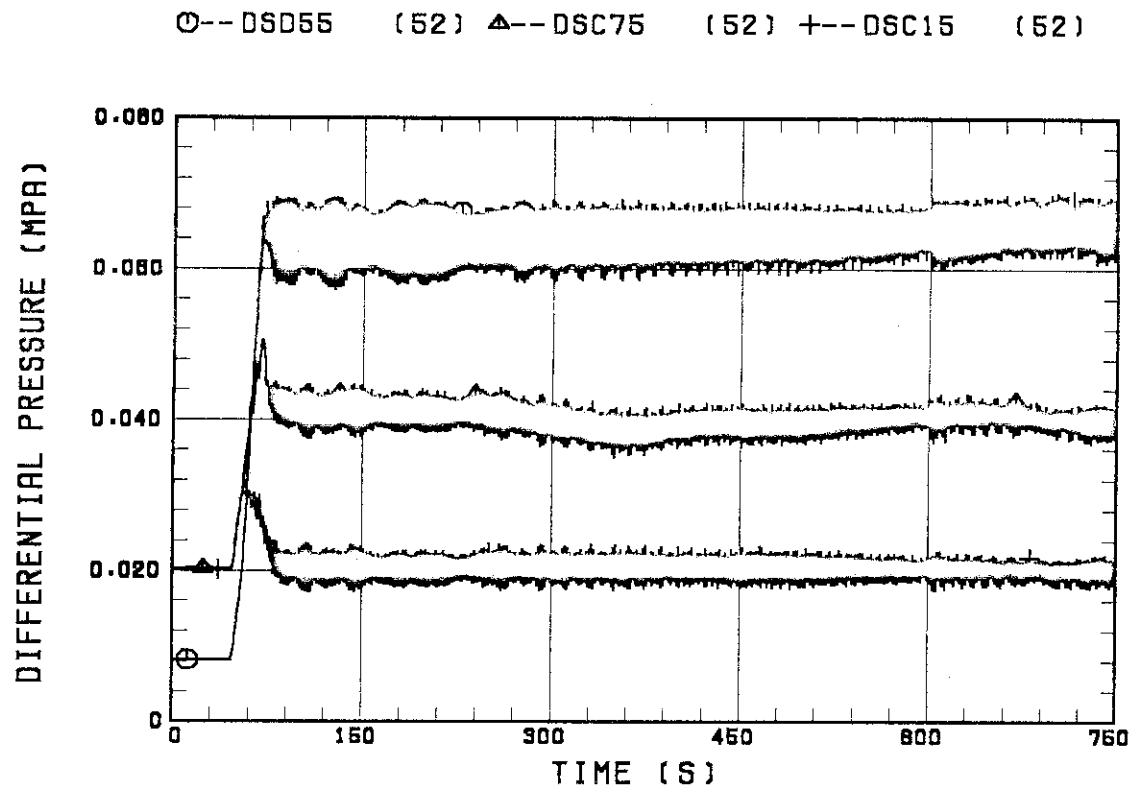

Fig. B.19 Differential pressure through downcomer, core, and lower plenum.

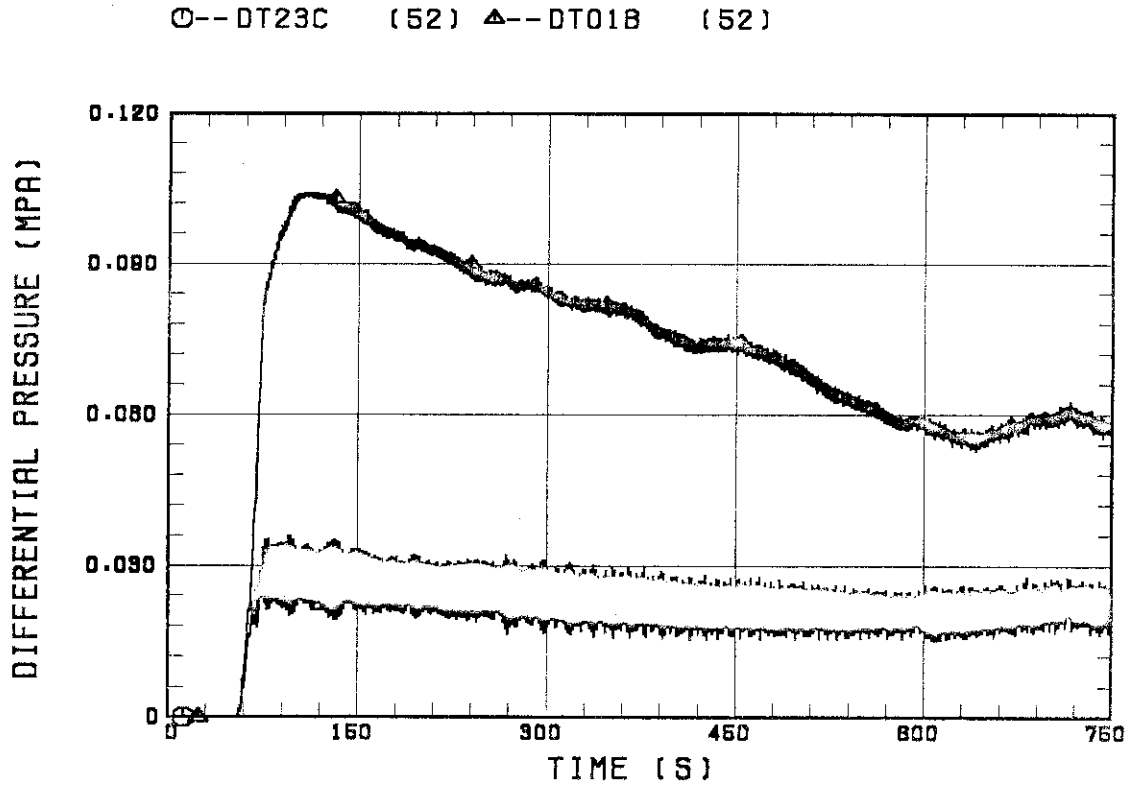

Fig. B.20 Differential pressure through intact and broken loops.

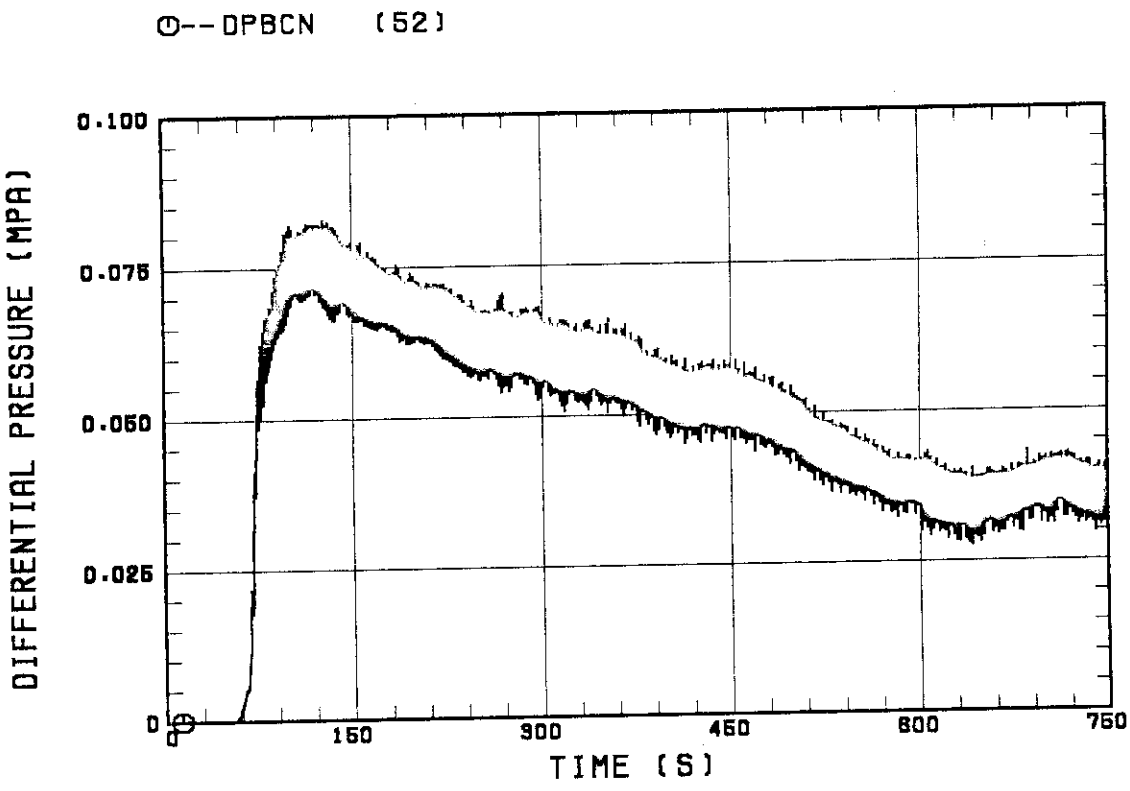

Fig. B.21 Differential pressure through broken cold leg nozzle.

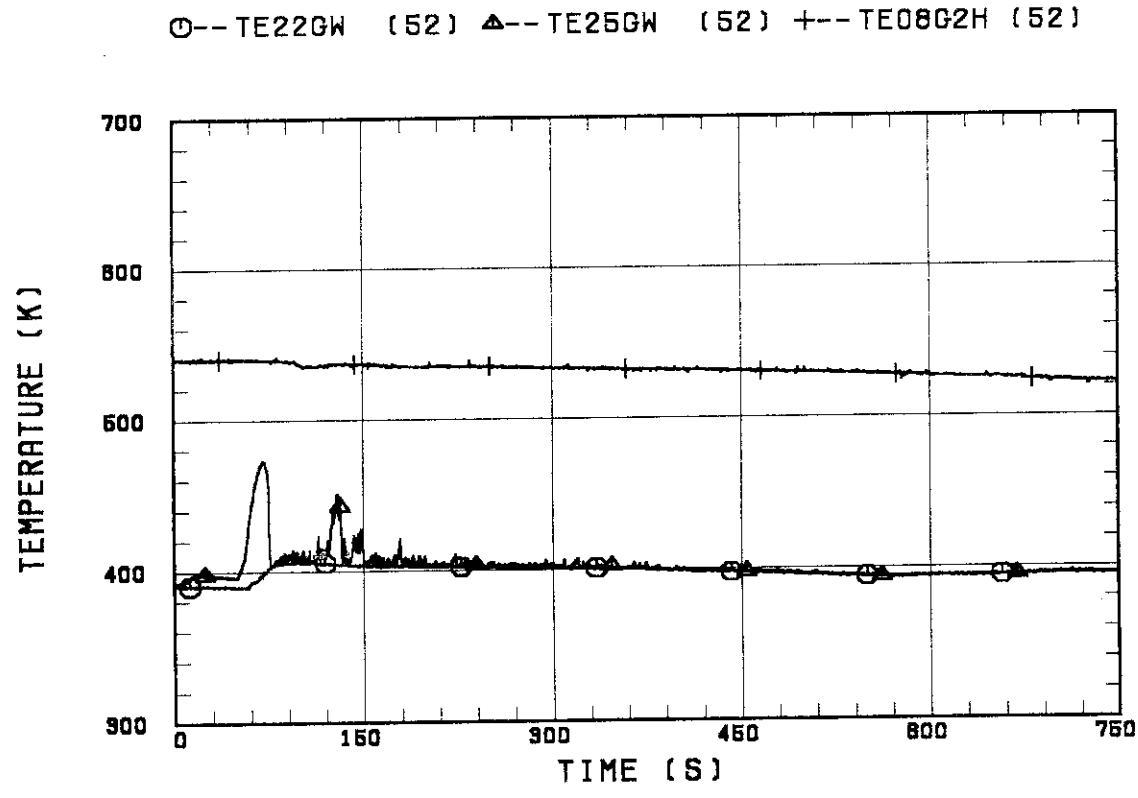

Fig. B.22 Fluid temperature in inlet plenum, outlet plenum, and secondary of steam generator 1.

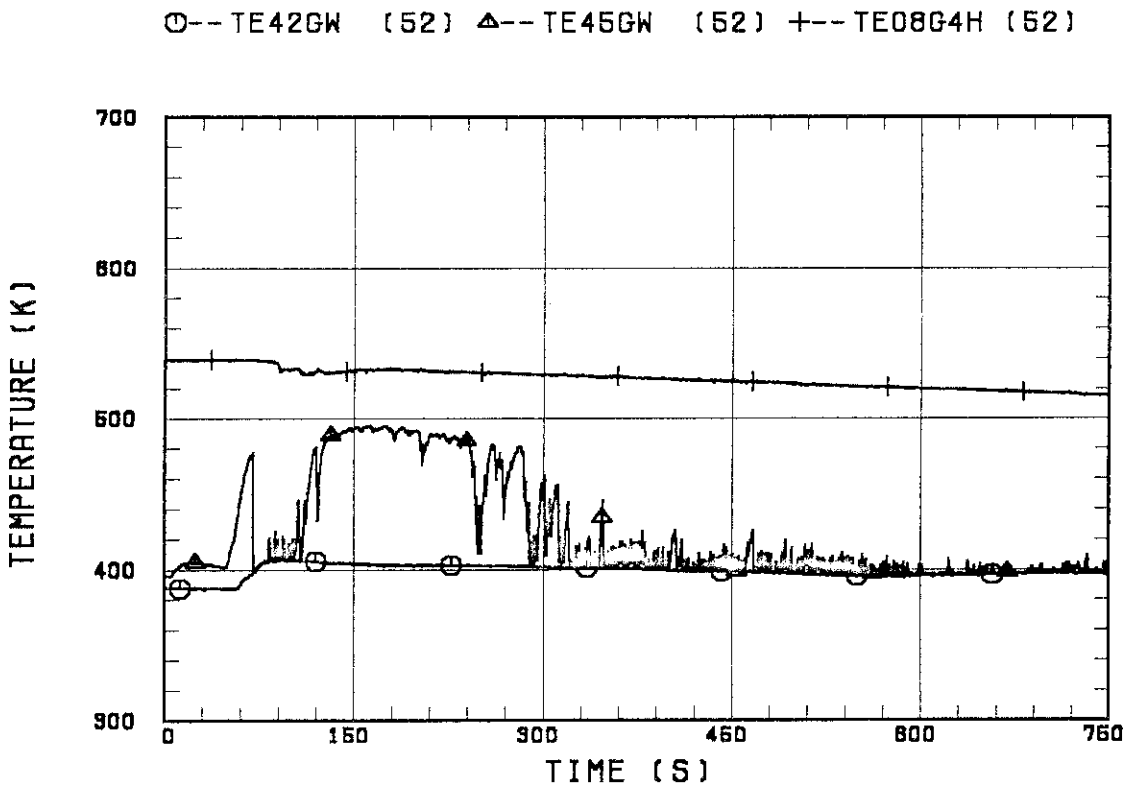

Fig. B.23 Fluid temperature in inlet plenum, outlet plenum, and secondary of steam generator 2.

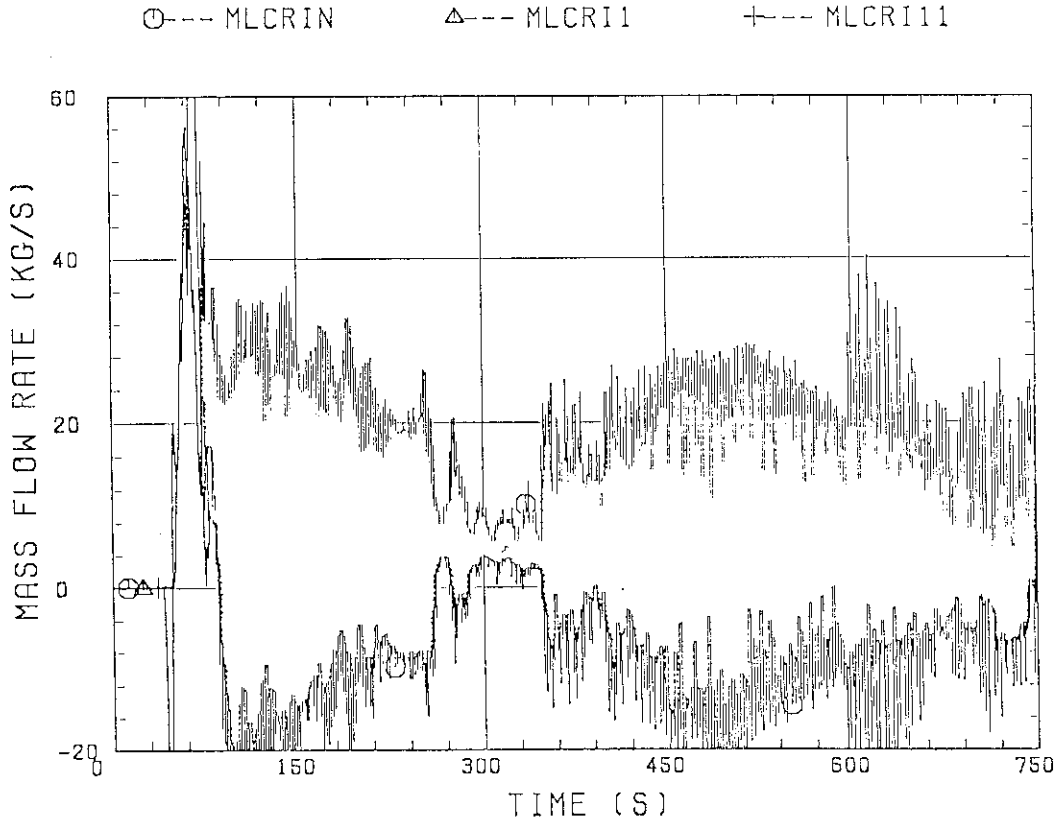

Fig. B.24 Core flooding mass flow rates evaluated with Eqs. (A.1) (A.2)

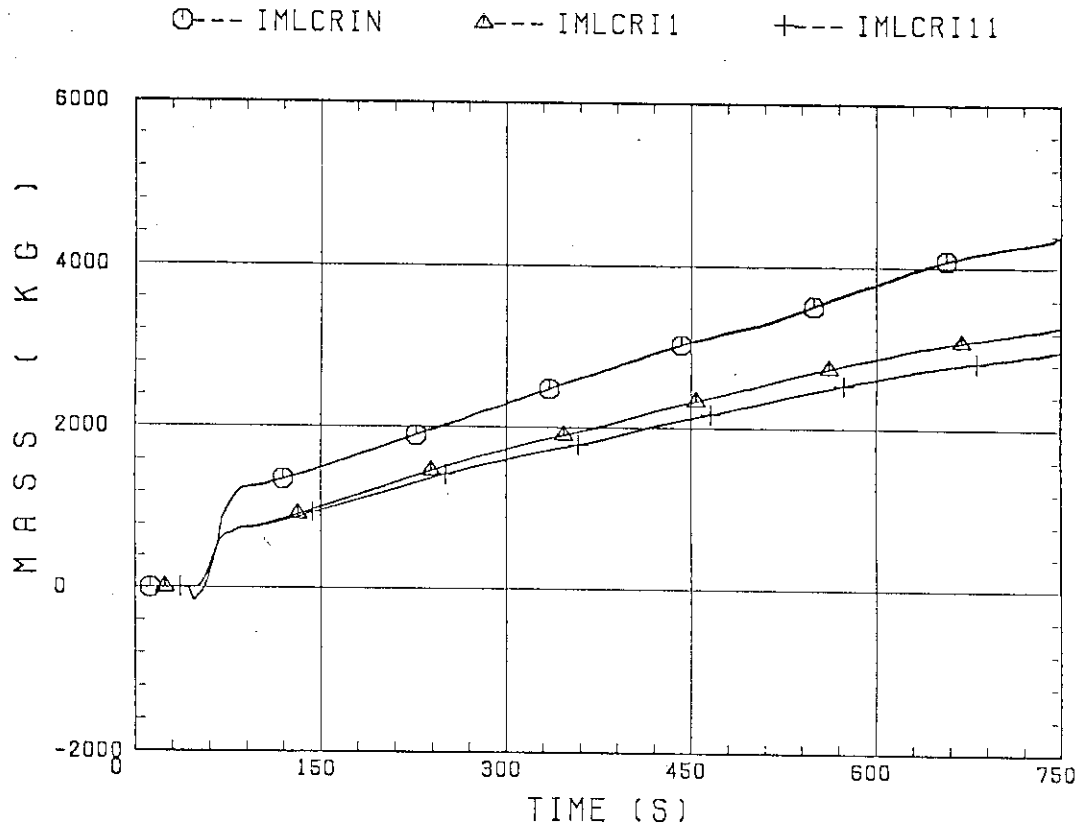

Fig. B.25 Time-integral mass flooded into core evaluated with Eqs. (A.1) and (A.2).

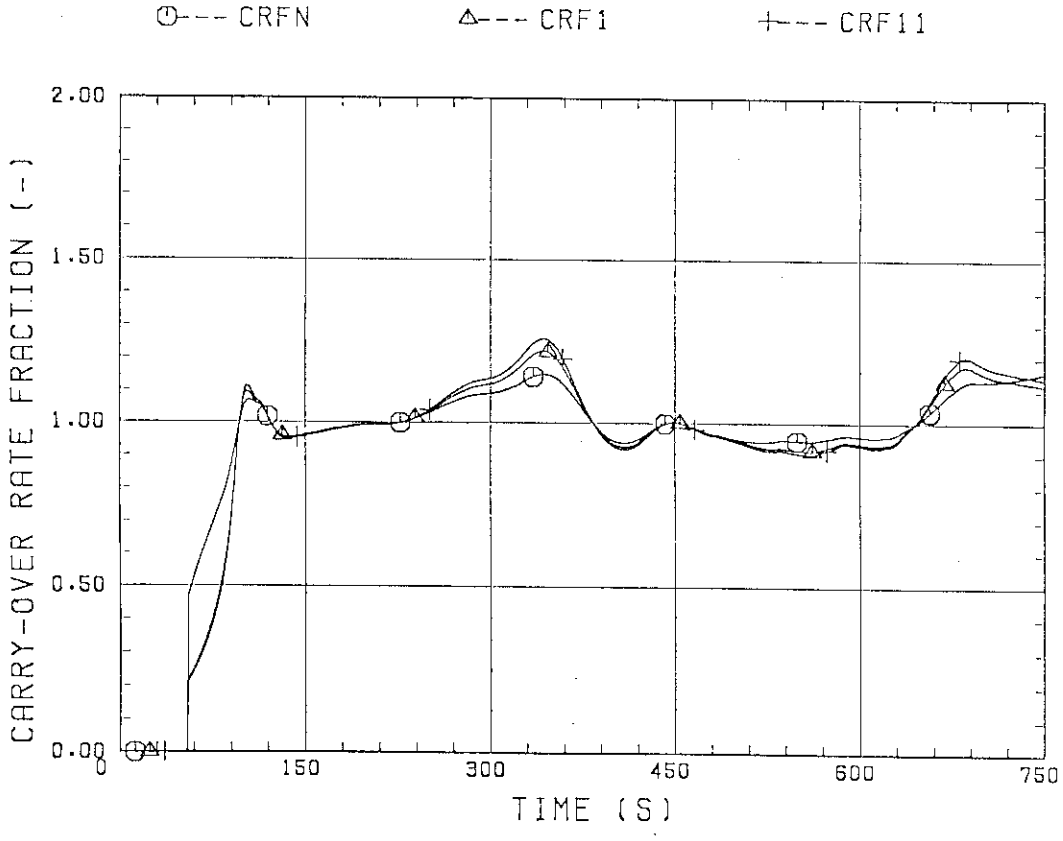

Fig. B.26 Carry-over rate fraction.

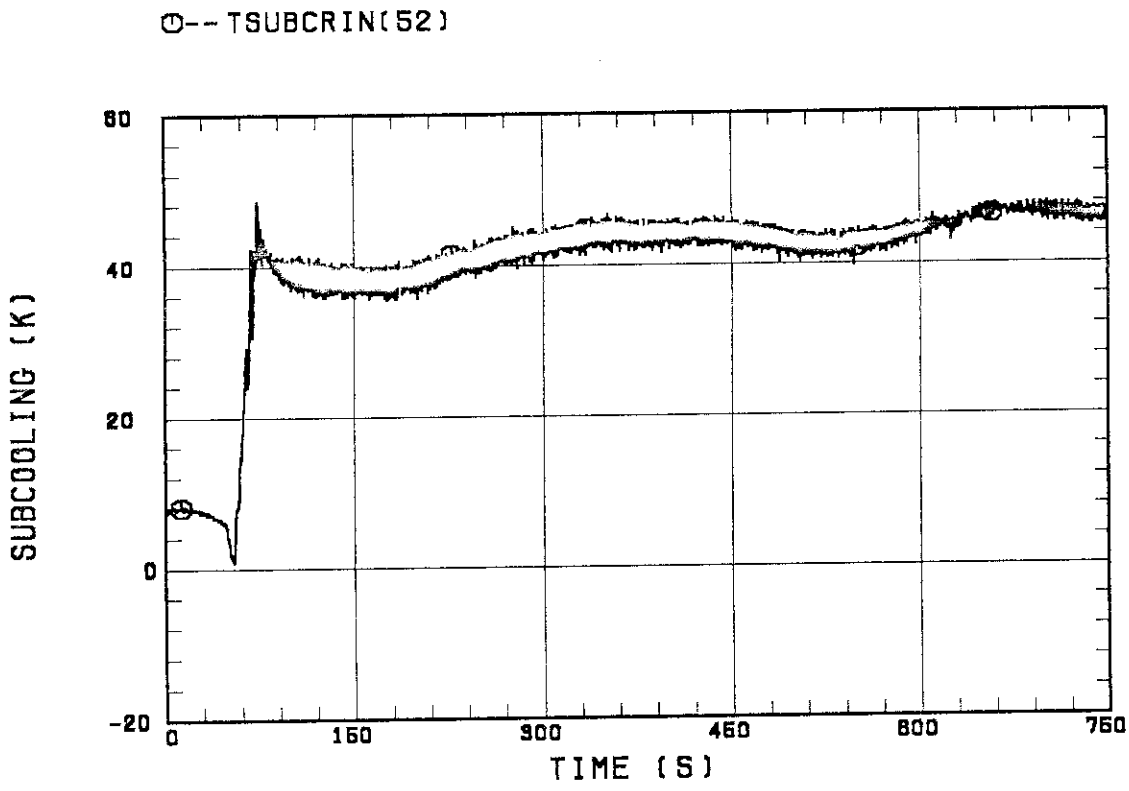

Fig. B.27 Core inlet subcooling.

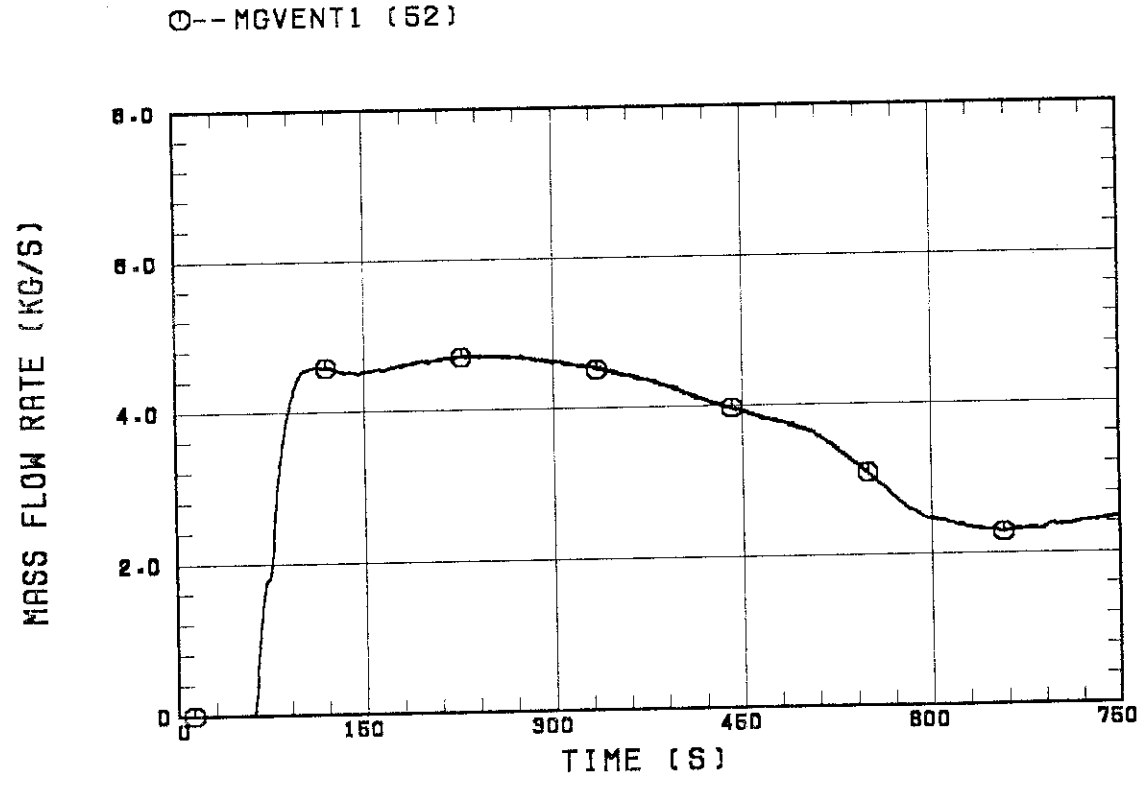

Fig. B.28 Exhausted mass flow rate from containment tank 2.